



**DEVELOPMENT OF TWO ANALYTICAL APPROACHES
BASED ON SOLUTION AND PAPER BASED SYSTEM FOR
CHLORPYRIFOS DETECTION USING GRAPHENE
QUANTUM DOT CAPPED GOLD NANOPARTICLES
FOR COLORIMETRIC ASSAY**

WARINPORN CHUNGCHAI

**A THESIS SUBMITTED IN PARTIAL FULFILLMENT OF
THE REQUIREMENTS FOR THE DEGREE OF MASTER
OF SCIENCE MAJOR IN CHEMISTRY
FACULTY OF SCIENCE
UBON RATCHATHANI UNIVERSITY
ACADEMIC YEAR 2019
COPYRIGHT OF UBON RATCHATHANI UNIVERSITY**



**DEVELOPMENT OF TWO ANALYTICAL APPROACHES
BASED ON SOLUTION AND PAPER BASED SYSTEM FOR
CHLORPYRIFOS DETECTION USING GRAPHENE
QUANTUM DOT CAPPED GOLD NANOPARTICLES
FOR COLORIMETRIC ASSAY**

WARINPORN CHUNGCHAI

**A THESIS SUBMITTED IN PARTIAL FULFILLMENT OF
THE REQUIREMENTS FOR THE DEGREE OF MASTER
OF SCIENCE MAJOR IN CHEMISTRY
FACULTY OF SCIENCE
UBON RATCHATHANI UNIVERSITY
ACADEMIC YEAR 2019
COPYRIGHT OF UBON RATCHATHANI UNIVERSITY**



UBON RATCHATHANI UNIVERSITY
THESIS APPROVAL
MASTER OF SCIENCE
MAJOR IN CHEMISTRY FACULTY OF SCIENCE

TITLE DEVELOPMENT OF TWO ANALYTICAL APPROACHES BASED ON
SOLUTION AND PAPER BASED SYSTEM FOR CHLORPYRIFOS
DETECTION USING GRAPHENE QUANTUM DOT CAPPED GOLD
NANOPARTICLES FOR COLORIMETRIC ASSAY

AUTHOR MISS WARINPORN CHUNGCHAI

EXAMINATION COMMITTEE

ASST. PROF. DR. NUANLAOR RATANAWIMARNWONG CHAIRPERSON

ASST. PROF. DR. MALIWAN AMATATONGCHAI MEMBER

ASST. PROF. DR. PURIM JARUJAMRUS MEMBER

DR. KETSARIN SEEBUNRUENG MEMBER

ADVISOR

..... *M. Amatongchai*

(ASST. PROF. DR. MALIWAN AMATATONGCHAI)

..... *Charida Pukahuta*

(ASST. PROF. DR. CHARIDA PUKAHUTA)

DEAN, FACULTY OF SCIENCE

..... *A. Pongrat*

(ASSOC. PROF. DR. ARIYAPORN PONGRAT)

VICE PRESIDENT FOR ACADEMIC AFFAIRS

ACKNOWLEDGEMENTS

I would like to thank my advisor, Asst. Prof. Dr. Maliwan Amatatongchai for her constant advice, guidance, insight, and for sharing her extensive chemistry knowledge. I wish to thank Asst. Prof. Dr. Purim Jarujamrus, Dr. Ketsarin Seebunrueng for comments and suggestions and Asst. Prof. Dr. Nuanlaor Ratanawimarnwong for her advice and criticism as the external examiner.

I also would like to thank the Center of Excellence for Innovation in Chemistry (PERCH-CIC) and Ubon Ratchathani University for financial support. My gratitude is extended to Department of Chemistry, Faculty of Science, Ubon Ratchathani University for providing all laboratory facilities.

Above all, my deepest gratitude is given to my beloved parents for their eternal love and care throughout my life.

Warinporn Chungchai
Researcher

บทคัดย่อ

- เรื่อง : การพัฒนาวิธีวิเคราะห์สองแบบในการตรวจวัดคลอโรไฟริฟอสด้วยระบบสารละลายและระบบที่ประดิษฐ์บนกระดาษโดยอาศัยการตรวจวัดทางสีของกราฟีนควอนตัมดอทที่เคลือบบนอนุภาคทองคำนาโน
- ผู้วิจัย : วารินทร์ ช่างชัย
- ชื่อปริญญา : วิทยาศาสตร์มหาบัณฑิต
- สาขาวิชา : เคมี
- อาจารย์ที่ปรึกษา : ผู้ช่วยศาสตราจารย์ ดร.มะลิวรรณ อมตรงไชย
- คำสำคัญ : กราฟีนควอนตัมดอท, อนุภาคทองคำนาโน, คลอโรไฟริฟอส, ระบบของไหลจุลภาคที่ประดิษฐ์มาจากกระดาษแบบสามมิติ, อะเซตทิลโคลินเอสเทอร์

วิทยานิพนธ์นี้เสนอการพัฒนาการตรวจวัดทางสีที่มีความไวและความจำเพาะสูง สำหรับตรวจวัดปริมาณสารกำจัดแมลงคลอโรไฟริฟอสในตัวอย่างผัก การตรวจวัดทางสีที่พัฒนาขึ้นจะอาศัยปฏิกิริยาของกราฟีนควอนตัมดอทที่เคลือบบนอนุภาคทองคำนาโน (GQDs-AuNPs) อนุภาคทองคำนาโนถูกสังเคราะห์ขึ้นโดยใช้กราฟีนควอนตัมดอททำหน้าที่เป็นทั้งตัวรีดิวซ์และตัวรักษาเสถียรภาพ หลักการของการตรวจวัดจะอาศัยเอนไซม์อะเซตทิลโคลินเอสเทอร์เร่งปฏิกิริยาไฮโดรไลซิสของอะเซตทิลไทโอโคลินทำให้เกิดไทโอโคลินที่มีหมู่ไทออล ไทโอโคลินมีผลทำให้เกิดการรวมตัวกันของกราฟีนควอนตัมดอทที่เคลือบบนอนุภาคทองคำนาโนและทำให้สีของผลิตภัณฑ์เปลี่ยนเป็นสีม่วง ในกรณีที่มีสารกำจัดแมลงคลอโรไฟริฟอสปฏิกิริยาไฮโดรไลซิสจะถูกยับยั้ง จึงไม่มีการรวมตัวกันของกราฟีนควอนตัมดอทที่เคลือบบนอนุภาคทองคำนาโนสารละลายที่ได้จึงมีสีแดง การพัฒนาการตรวจวัดทางสีสำหรับตรวจวัดความเข้มข้นของคลอโรไฟริฟอสแบ่งได้เป็นสองแนวทางคือ (i) ในระบบสารละลายตรวจวัดด้วยเทคนิคยูวี-วิสิเบิลสเปกโทรโฟโตมิเตอร์ (ii) ระบบของไหลจุลภาคที่ประดิษฐ์มาจากกระดาษแบบสามมิติตรวจวัดด้วยการถ่ายภาพร่วมกับโปรแกรมอิมเมจเจ (ImageJ)

ยูวี-วิสิเบิลสเปกโทรโฟโตมิเตอร์ จะถูกนำมาใช้ตรวจวัดการเปลี่ยนแปลงการดูดกลืนแสงในระหว่างการทำปฏิกิริยา คลอโรไฟริฟอสจะยับยั้งการทำงานของเอนไซม์โดยเข้าไปจับที่ตำแหน่งแอคทีฟไซต์ของเอนไซม์ การไฮโดรไลซิสของอะเซตทิลไทโอโคลินเกิดได้น้อยลงและปริมาณไทโอโคลินจึงน้อยลง โดยการเปลี่ยนแปลงสีของกราฟีนควอนตัมดอทที่เคลือบบนอนุภาคทองคำนาโนจากสีน้ำเงินเป็นสีแดงจะถูกตรวจวัดที่ความยาวคลื่นสูงสุดคือ 520 นาโนเมตร ภายใต้สภาวะที่เหมาะสมโดยใช้อะเซตทิลไทโอโคลินที่ความเข้มข้น 50 ไมโครโมลาร์ เอนไซม์อะเซตทิลโคลินเอสเทอร์ที่ความเข้มข้น

200 มิลลิลิตรต่อมิลลิลิตร สารละลายฟอสเฟตบัพเฟอร์ชาไลน์ความเข้มข้น 50 มิลลิโมลาร์ที่พีเอช 7.0 และเวลาในการทำปฏิกิริยา คือ 30 นาที การตรวจวัดทางสีที่พัฒนาขึ้นมีการตอบสนองแบบเป็นเส้นตรงในช่วง 0.1 ไมโครกรัมต่อมิลลิลิตร ถึง 50 ไมโครกรัมต่อมิลลิลิตร ค่าสัมประสิทธิ์สหสัมพันธ์ (r^2) เท่ากับ 0.996 ขีดจำกัดต่ำสุดในการตรวจวัดเท่ากับ 0.046 ไมโครกรัมต่อมิลลิลิตร วิธีการตรวจวัดทางสีจะให้ความแม่นยำ (% RSD) มีค่าเท่ากับร้อยละ 0.03 ของการตรวจวัดคลอโรไพริฟอส ซึ่งทำการวัดต่อเนื่อง 10 ครั้ง

การตรวจวัดด้วยระบบของไหลจุลภาคที่ประดิษฐ์มาจากกระดาษแบบสามมิติ เป็นเทคโนโลยีทางเลือกสำหรับการพัฒนาเครื่องมือที่ราคาไม่แพง พกพาง่าย ใช้งานง่ายและต้นทุนต่ำ ระบบของไหลจุลภาคที่ประดิษฐ์มาจากกระดาษแบบสามมิติถูกสร้างขึ้นโดยเทคนิคการสกรีนภายในขั้นตอนเดียว โดยใช้อย่างพารา ซึ่งเป็นสารที่ไม่ชอบน้ำ มีราคาถูกและใช้งานง่าย การออกแบบระบบของไหลจุลภาคที่ประดิษฐ์มาจากกระดาษแบบสามมิติในการตรวจวัดทางสีจะประกอบด้วยสองส่วน คือ (i) ส่วนของแผ่นทดสอบ ประกอบด้วย วงกลมสองวง วงกลมแรกคือโซนของการตรวจวัดใช้สำหรับหยดสารผสมของกราฟีนควอนตัมดอทที่เคลือบบนอนุภาคนาโนและเอนไซม์อะเซทิลโคลีนเอสเตอเรส และอีกหนึ่งวงคือพื้นที่สำหรับหยดสารละลายบัพเฟอร์ (ii) ส่วนสำหรับหยดสารตัวอย่าง ซึ่งถูกออกแบบให้มีลักษณะเป็นรูปดัมเบล วงกลมด้านล่างของรูปดัมเบลจะใช้สำหรับหยดสารผสมตัวอย่างหรือสารละลายมาตรฐาน (คลอโรไพริฟอส) และอะเซทิลไทโอโคลีน (ซัสเตรต) โดยในการตรวจวัดคลอโรไพริฟอส จะใช้กล้องดิจิทัลถ่ายภาพปฏิกิริยาที่เกิดขึ้นบน μ PAD ร่วมกับโปรแกรมคอมพิวเตอร์อิมเมจ ในการตรวจวัดจะให้ช่วงความเป็นเส้นตรงตั้งแต่ 0.001 ไมโครกรัมต่อมิลลิลิตร ถึง 1.0 ไมโครกรัมต่อมิลลิลิตร มีขีดจำกัดต่ำสุดในการตรวจวัดเท่ากับ 0.0007 ไมโครกรัมต่อมิลลิลิตร โดยไม่ต้องใช้เครื่องมือที่ซับซ้อน การพัฒนาระบบของไหลจุลภาคที่ประดิษฐ์มาจากกระดาษแบบสามมิติถูกนำมาใช้ในการตรวจวัดคลอโรไพริฟอสในตัวอย่างผักที่มีการเติมสารละลายมาตรฐานคลอโรไพริฟอสที่ทราบความเข้มข้นแน่นอนพบว่า มีร้อยละการได้กลับคืนมาในช่วง 93.0 เปอร์เซ็นต์ ถึง 104.6 เปอร์เซ็นต์ อุปกรณ์การตรวจวัดที่พัฒนาขึ้นให้ค่าความแม่นยำที่ดี โดยค่าร้อยละเบี่ยงเบนมาตรฐานสัมพัทธ์ในช่วง 0.3 ถึง 1.6 เมื่อนำมาคำนวณหาค่าความคลาดเคลื่อนสัมพัทธ์ที่เปลี่ยนไปเทียบกับเทคนิคมาตรฐานโครมาโทกราฟีของเหลวสมรรถนะสูง (HPLC) พบว่ามีค่าอยู่ในช่วงร้อยละตั้งแต่ 1.0 เปอร์เซ็นต์ ถึง 5.2 เปอร์เซ็นต์ แสดงให้เห็นถึงความถูกต้องในการตรวจวัดที่ดี ระบบของไหลจุลภาคที่ประดิษฐ์มาจากกระดาษแบบสามมิติมีข้อดีคือ มีความไว ความจำเพาะที่ดี ราคาถูกและรวดเร็ว ตรวจวัดสารกำจัดแมลงได้อย่างรวดเร็ว และสามารถนำไปใช้งานภาคสนามได้ดี

ABSTRACT

TITLE : DEVELOPMENT OF TWO ANALYTICAL APPROACHES
BASED ON SOLUTION AND PAPER BASED SYSTEM FOR
CHLORPYRIFOS DETECTION USING GRAPHENE QUANTUM
DOT CAPPED GOLD NANOPARTICLES FOR COLORIMETRIC
ASSAY

AUTHOR : WARINPORN CHUNGCHAI

DEGREE : MASTER OF SCIENCE

MAJOR : CHEMISTRY

ADVISOR : ASST. PROF. MALIWAN AMATONGCHAI, Ph.D.

KEYWORDS : GRAPHENE QUANTUM DOT, GOLD NANOPARTICLES,
CHLORPYRIFOS, THREE-DIMENSIONAL MICROFLUIDIC
PAPER-BASED ANALYTICAL DEVICE,
ACETYLCHOLINESTERASE

This thesis presents the development of a highly sensitive and selective colorimetric assay for chlorpyrifos pesticide in vegetable samples. Colorimetric assay was developed based on the reaction using graphene quantum dot capped with gold nanoparticles (GQDs-AuNPs) as reporter. AuNPs were synthesized using GQDs as a reducing agent

and stabilizing agent. The principle of assay was based on acetylcholinesterase (AChE) enzyme catalyzed hydrolysis of an acetylthiocholine (ATCh) substrate to produce thiol-bearing thiocholine. Thiocholine causes the aggregation of GQDs-AuNPs, to generate a purple-blue colored product. The hydrolysis step was inhibited in the presence of chlorpyrifos, resulting in anti-aggregation of red colored GQDs-AuNPs. Development of colorimetric assay for chlorpyrifos determination was carried out based on two approaches; (i) UV-Visible spectrophotometry for chlorpyrifos detection in solution, and (ii) three-dimensional microfluidic paper-based analytical device (3D- μ PAD) detected by image captured by digital camera compiled to ImageJ program.

UV-Visible spectrophotometry was used to monitor changes in absorbance during the reaction. Chlorpyrifos inhibited AChE by binding to the active site of an enzyme. This suppresses ATCh hydrolysis, thereby blocking the generation of thiocholine. The distinctive color change of GQDs-AuNPs, from red to blue, and the appearance of a maximum absorption wavelength at 520 nm. Optimal conditions were under, using ATCh and AChE concentrations of 50 μ M and 200 mU mL⁻¹, PBS solution (50 mM, pH 7.0), and 30 minutes of incubation time. The developed colorimetric in solution assay exhibits linear calibration over the range of 0.1-50 μ g mL⁻¹, with a linear correlation coefficient (r^2) of 0.996. The limit of detection (LOD) calculated based on [3 S.D.]/slope is 0.046 μ g mL⁻¹. The simple colorimetric method provides good precision (%RSD = 0.03) for chlorpyrifos detection with ten replicates.

Three-dimensional microfluidic paper-based analytical device (3D- μ PAD) is an alternative technology for development of affordable, portable, disposable and low-cost diagnostic tools. The 3D- μ PAD was fabricated by one-step polymer-screen-printing, using rubber latex (RL) waste as a hydrophobic reagent for low-cost and simple manufacture. 3D- μ PAD for colorimetric chlorpyrifos assay was designed by having two parts on paper. (i) the testing sheet, consisting of two circles; one circle forms the detection zone, for placing the GQDs-AuNPs and AChE-enzyme mixture, and the other circle is a buffer loading area, (ii) the sampling sheet in the shape of the dumbbell design, the bottom circle area of the dumbbell-shape was used to apply the mixing solution of sample/standard (chlorpyrifos) and ATCh (substrate). Chlorpyrifos was determined in the 3D- μ PAD using image captured by digital camera coupled by ImageJ software. The assay provided a linear range between 0.001 to 1.0 μ g mL⁻¹, with a detection limit of

0.0007 $\mu\text{g mL}^{-1}$, without sophisticated instrumentation. The developed 3D- μPAD was applied to detect chlorpyrifos in vegetable samples. Recovery study gave percent recoveries ranging from 93.0% to 104.6%. Our developed device provides good precision (%RSD ranges from 0.3 to 1.6). The calculated relative error comparison with HPLC ranges from 1.0% to 5.2%, indicating a high degree of accuracy. The 3D- μPAD exhibits good sensitivity and selectivity for a low-cost and rapid-screening test for the presence of insecticides, and might be useful for on-site applications.

CONTENTS

	PAGE
ACKNOWLEDGMENTS	I
THAI ABSTRACT	II
ENGLISH ABSTRACT	IV
CONTENTS	VI
LIST OF TABLES	VIII
LIST OF FIGURES	IX
LIST OF ABBREVIATIONS	XIII
CHAPTER 1 INTRODUCTION	
1.1 The importance and the source of the research	1
1.2 Objectives	5
1.3 Expected outcome	5
1.4 Scope of research	6
CHAPTER 2 LITERATURE REVIEWS	
2.1 Colorimetric detection	8
2.2 Microfluidic paper-based analytical device (μ PAD)	12
2.3 Nanocatalyst synthesis	15
2.4 Organophosphate pesticide detection	16
CHAPTER 3 METHODOLOGY	
3.1 Instrumentation	31
3.2 Chemical commercial product and materials	32
3.3 Preparation of standard stock solution	33
3.4 Synthesis of graphene quantum dot (GQDs)	34
3.5 Preparation of graphene quantum dot capped gold nanoparticles (GQDs-AuNPs)	35
3.6 Part I: Spectrophotometric method for chlorpyrifos determination	35
3.7 Part II: 3D- μ PAD for chlorpyrifos determination	40

CONTENTS (CONTINUED)

	PAGE
CHAPTER 4 RESULTS AND DISCUSSION	
4.1 Part I: Spectrophotometric method for chlorpyrifos determination	49
4.2 Part II: 3D- μ PAD for chlorpyrifos determination	66
CHAPTER 5 CONCLUSIONS	79
REFERNCES	82
APPENDICES	
A Part I: Spectrophotometric method for chlorpyrifos determination	96
B Part II: 3D- μ PAD for chlorpyrifos determination	103
C CONFERENCES	110
CURRICULUM VITAE	137

LIST OF TABLES

TABLE		PAGE
2.1	Comparison of advantages/drawbacks among fabrication techniques for μ PAD.	13
2.2	Comparison of the methods for organophosphate pesticides detection using various nanomaterials.	21
2.3	Comparison of PAD's analytical performance for the organophosphate pesticides determination.	29
3.1	Instrumentation for chlorpyrifos detection and characterizations	31
3.2	List of chemicals and materials.	32
3.3	The operating conditions of UV-Visible spectroscopy, fluorescence spectroscopy, TEM and FTIR.	36
3.4	The operating condition of photography with control light box system.	44
4.1	Comparison of the developed method analytical performance with other methods for the colorimetric detection of organophosphate pesticide.	63
4.2	Comparison of other method for the detection of organophosphate pesticide using μ PAD.	74
4.3	Comparison of chlorpyrifos determination in vegetables between the developed 3D- μ PAD and the reference HPLC method (n=3).	78

LIST OF FIGURES

FIGURE		PAGE
2.1	Schematic illustration of light transmission, surface reflection, and scattering in a liquid sample.	9
2.2	Schematic diagram of spectrophotometer.	10
2.3	RGB color model a) Combination of primary light colors generates the new color depending on RGB ration b).	11
2.4	Illustration of the test strip fabrication procedure(A). Photograph of the test strip (B) and illustration of the sandwich structure (C).	23
2.5	Photograph of TGA-capped CdTe QDs based lab on paper device for bi-enzyme assay with fluorescence detection in open and closed positions (a). Schematic illustration of the insecticide detection assay (b).	25
2.6	Schematics of the procedure for the pesticide detection. The blue arrows in the detecting procedure means the expected fluid flows on the microchannels of the paper device (A). The mechanism for the inhibition of AChE by a contaminated sample with pesticides, while reducing the color intensity in the outlet (B). The photographed image shows the fabricated paper-based analytic device with pesticide-positive (+) and negative (-) sample (C).	28
3.1	Diagram for the synthesis of GQDs.	34
3.2	Schematic show the formation of GQDs-AuNPs.	35
3.3	Schematic diagram of colorimetric assay for chlorpyrifos detection by using GQDs-AuNPs.	39
3.4	The designed 3D- μ PAD for chlorpyrifos detection using a foldable sheet consisting of two parts (top/bottom layer).	43

LIST OF FIGURES (CONTINUED)

FIGURE		PAGE
3.5	Fabrication of the chlorpyrifos 3D- μ PAD by using one-step polymer screen printing; Position a sheet of Whatman No.4 filter paper (1), Place the wooden-framed woven mesh screen (888.32 mesh (60T) nylon mesh) on the paper (2), Position the screen pattern to contact the paper surface (3), squeeze RL solution through the screen to penetrate to the bottom of the paper, creating a patterned hydrophobic barrier (4), remove paper from the screen, the patterned paper is ready for use (5), and Cut out individual fabricated devices piecewise (6).	42
3.6	Homemade control light box. An Image is captured by using a digital camera set to automatic mode.	42
3.7	The typical procedure for chlorpyrifos determination on 3D- μ PAD.	47
4.1	Absorbance spectra of GQDs (a), GQDs-AuNPs (b), and cit-AuNPs (c). Inset shows the respective images.	49
4.2	Fluorescence spectra of GQDs (a) and GQDs-AuNPs (b).	50
4.3	TEM images of well-dispersed GQDs-AuNPs nanocomposites. Inset is enlarged nanocomposite image.	51
4.4	FT-IR spectra of GQDs-AuNPs, GQDs, and Cit-AuNPs.	52
4.5	Absorption spectra of GQDs-AuNPs (a), GQDs-AuNPs after the addition of ATCh (50 μ M, pH 7.0 PBS) (b), GQDs-AuNPs after the addition of ATCh (50 μ M, pH 7.0 PBS) and AChE (200 mU mL ⁻¹) (c), GQDs-AuNPs after the addition of ATCh (50 μ M, pH 7.0 PBS), AChE (200 mU mL ⁻¹) and chlorpyrifos (5.0 μ g mL ⁻¹) (d). Incubation was performed at 25 °C for 30 min.	54
4.6	The proposed mechanism of chlorpyrifos colorimetric detection based on GQDs-AuNPs reaction.	54

LIST OF FIGURES (CONTINUED)

FIGURE		PAGE
4.7	The effect of pHs on the performance of the GQDs-AuNPs reactivity and AChE enzyme activity. Absorption spectra of the GQDs-AuNPs in various pHs (a) and the variation of absorption spectra of GQDs-AuNPs at 520 nm with pHs (b). The inset figure shows the color change of GQDs-AuNPs with the variation of pHs.	56
4.8	Variation of the absorbance at 520 nm versus time for GQDs-AuNPs in the presence of difference concentrations of ATCh (50, 100, 200, 300 and 500 μM) recorded every 5 min.	57
4.9	Variation of absorbance at 520 nm versus reaction time for GQDs-AuNPs in the presence of ATCh (50 μM , pH 7.0 PBS) having different concentrations of AChE (100, 200, 300, 400 and 500 mU mL^{-1}) recorded every 5 min.	59
4.10	Absorption spectra of GQDs-AuNPs after addition of ATCh (50 μM , pH 7.0 PBS) and AChE (200 mU mL^{-1}) recorded every 5 min (a) and the plots of absorbance at 520 nm and 650 nm versus the reaction time (b).	60
4.11	Absorption spectra of the reaction assay with different concentration of chlorpyrifos (0, 0.1, 0.5, 1.0, 5.0, 10, 20, 30, 40 and 50 $\mu\text{g mL}^{-1}$). The reaction composed of 0.9 mL of GQDs-AuNPs, 100 μL of ATCh (50 μM), 10 μL of AChE (200 mU mL^{-1}) and 290 μL of PBS (50 mM PBS, pH 7) (a). Inset is their respective images. The calibration plot between A/A_0 and the concentration of chlorpyrifos was constructed for the colorimetric detection of chlorpyrifos, where A and A_0 were the absorbance with and without chlorpyrifos ($n=3$) (b).	62

LIST OF FIGURES (CONTINUED)

FIGURE	PAGE
4.12 The selectivity of developed colorimetric method for chlorpyrifos detection, comparison between the absorbance band at 520 nm obtained from 20 $\mu\text{g mL}^{-1}$ of chlorpyrifos and the chlorpyrifos with interfering substances such as ions (Fe^{3+} , Zn^{2+} , Ni^{2+} , Mg^{2+} , NO_3^- , I^- , Ca^{2+} , K^+ , Na^+ , S^{2-} , and PO_4^{3-}) and compound molecules (fructose, maltose, glucose and ascorbic acid). Dotted marks the $\pm 5\%$ signal alteration range.	65
4.13 Photograph of the screen-printed 3D- μPAD : demonstration of hydrophilic and hydrophobic zones on the paper by applying a drop of colored food dye to the surface.	66
4.14 The color intensity (I_0-I) of the images was separated into red, green, blue and average grayscale $(R+G+B)/3$ intensity and plot versus concentration of chlorpyrifos ($n=3$).	67
4.15 The green color intensity of 3D- μPAD for chlorpyrifos detection in fixed concentration of 0.5 $\mu\text{g mL}^{-1}$ chlorpyrifos pesticide and various conditions; pH (a), volume of buffer (b), concentration of ATCh (c), concentration of AChE (d) and reaction time (e).	70
4.16 Calibration curve of chlorpyrifos using 3D- μPAD (plot between I_0-I of green intensity and the variation of chlorpyrifos concentrations; 0.001, 0.005, 0.01, 0.05, 0.1, 0.3, 0.5, 0.8 and 1.0 $\mu\text{g mL}^{-1}$) reaction conditions; GQDs-AuNPs, ATCh (0.5 mM) and AChE (5.0 U mL^{-1}). Error bar obtained from quintuplicate ($n=5$).	72
4.17 The selectivity of developed 3D- μPAD for chlorpyrifos detection, comparison between the color intensity obtained from 0.05 $\mu\text{g mL}^{-1}$ of chlorpyrifos and the chlorpyrifos with interfering substances such as ions (Fe^{3+} , Cu^{2+} , Zn^{2+} , Mg^{2+} , NO_3^- , I^- , Ca^{2+} , K^+ , Na^+ , S^{2-} , and PO_4^{3-}) and compound molecules (fructose, maltose, glucose and ascorbic acid), ($n=3$). Dotted mark the $\pm 5\%$ signal alteration range.	76

LIST OF ABBREVIATIONS

ABBREVIATION	DEFINITION
AuNPs	Gold nanoparticles
GQDs	Graphene quantum dots
ATCh	Acetylthiocholine
AChE	Acetylcholinesterase
Cit	tri-Sodium citrate
3D	Three dimensional
μ PAD	Microfluidic paper-based analytical device
mU	Milliunit
U	Unit
g	Gram
mg	Milligram
μ g	Microgram
ng	Nanogram
mL	Milliliter
L	Liter
μ L	Microliter
M	Molar
mM	Millimolar
μ M	Micromolar
nM	Nanomolar
cm	Centimeter
nm	Nanometer
mm	Millimeter
$^{\circ}$ C	Degree Celsius
min	Minutes
SD	Standard deviation
RSD	Relative standard deviation
LOD	Limit of detection

CHAPTER 1

INTRODUCTION

1.1 The important and the source of the research

Organophosphate pesticides (OPs) which consist of phosphate ester compound derivatives ($O=P(OR)_3$) are most widely used in environmental and agricultural pest-control applications. These compounds are highly toxic to humans and animals because they inhibit the activity of acetylcholinesterase (AChE) enzyme on the nervous system. High dose exposure of OPs can cause acute effects such as gastrointestinal upset, sweating, tearing, urination problems, bronchial spasms, muscle twitching, muscle weakness, bradycardia, and coma. For chronic exposure at low to moderately high doses, poisoning symptoms are including headache, dizziness, nausea, vomiting, abdominal pain, blurred vision, and chest tightness inhibit may cause. Moreover, there is evidence linking between OPs exposure and reproductive effects, non-Hodgkin's lymphoma, and cancer [1-3]. OPs are widely used in Thailand and Thai farmers are exposed to the OPs via multiple ways i.e., dermal absorption, inhalation, and unintentional ingestion [4, 5].

Chlorpyrifos (*O, O*-diethyl *O*-(3,5,6-trichloropyridin-2-yl-phosphorothioate)) is one of the most widely used OPs in many countries, including Thailand, Vietnam, China, and the United States, and is also common in other countries [6-8]. Chlorpyrifos is a white crystalline or irregularly flaked solid. It has a very faint mercaptan-type odor. It has low solubility in water and readily partitions from aqueous to organic phases in the environment, thus there is a significant hazard for human exposure. The Codex set the maximum residue limits (MRLs) for chlorpyrifos residues in/on several commodities ranged from 0.05 to 1 mg kg⁻¹ [9]. Thus, sensitive and selective methods for chlorpyrifos detection are highly desirable due to environmental protection requirements and concerns over the safety of human health.

Acetylcholinesterase (AChE) is a type-B carboxylesterase enzyme located primarily in the synaptic membrane of central and peripheral cholinergic synapses. This enzyme catalyzes the hydrolysis of the neurotransmitter acetylcholine into choline and

acetate at neuronal synapses, and neuromuscular junctions [10]. In the presence of pesticides, the inhibition of AChE was occurred, leading to decrease neurotransmitter degradation of acetylcholine and AChE overactivated in the synapses, so that levels of acetylcholine in the brains is significantly diminished. This enzyme inhibition results weakened neurotransmission, memory loss and other adverse effects such as Alzheimer's disease (AD) [11]. Therefore, it is important to develop highly sensitive and reliable for pesticides in complex samples. The conventional methods for determination of chlorpyrifos include high performance liquid chromatography (HPLC) [12, 13], liquid chromatography/ mass spectrometry (LC-MS) [14], gas chromatography/mass spectrometry (GC-MS) [15], enzyme linked immunosorbent assay (ELISAs) [16, 17], electrochemical [18, 19], chemiluminescence [20, 21], and fluorescence [22, 23]. Although these methods provide high performance for analysis such as high sensitivity, high selectivity and detection limits at the micromolar or nanomolar level. However, these aforementioned methods still require expensive instruments, long time analysis, the large amount of reagent or sample, and these drawbacks limited their practical applications in the remote place.

These problems can be improved by the recently developed microfluidic paper-based analytical device (μ PAD), since their original introduction by the Whitesides group in 2007 [24], which are known as an alternative method for medical diagnostic and chemical analysis [25], environmental analysis [26], and biochemical analysis [27]. The μ PAD has advantages including simple, inexpensive, lightweight, easy to fabricate, easy to use, disposable and provide timely results. Paper is white color that makes it's simple for colorimetric method. In addition, paper composed of hydrophilic cellulose fibers that make it a suitable platform for aqueous liquids to flow via capillary action. Design of flow channel on paper can be easily generated by creating hydrophobic barriers to confine the fluid flow within the desired section [28]. A number of fabrication techniques are established for μ PAD, including photolithography [24, 29], plotting [30], cutting [31], wax printing [32], inkjet printing [33] and screen printing [34]. Each method has its own advantages and drawbacks. Among the printing methods, the technique of screen printing has generally been the standard choice for μ PAD fabrication owing to its advantages such as high speed, simple operation, versatility, and cost effectiveness [34]. Specifically, a mass production of μ PAD can be fabricated in a

single batch using the technique of screen printing. Recently, the fabricated foldable sheet platforms have been published in the literature for pesticides detection [35, 36], which have the attention in the addition of a substrate reagent on paper for reducing multi operations. The most popular used detection system of μ PAD is colorimetric method which provide a simple and can be implemented in the real-life by even the naked eye. For the best of knowledge, there are only few reports using foldable sheets proposed for OPs detection using wax printing [35] and cutting technique covered with plastic sheet [36]. Moreover, these detection methods exploited the bienzymatic (AChE and Choline oxidase) based on thioglycolic acid-capped CdTe quantum dots reaction [35] and AChE based indoxyl acetate (IDA) reaction [36]. These methods somehow more expensive of use bi-enzymatic system and more toxic of using heavy metal as composition of the probe.

Gold nanoparticles (AuNPs) are one of the most widely used probe or reporter for colorimetric assay without the need for advanced instruments, due to unique size and distance dependent surface plasmon resonance (SPR) properties and ultrahigh molar extinction coefficients, which a molecular event can appear into color changes. The color changes are highly sensitive to the size, shape, capping agents and medium refractive index, causing the aggregation of AuNPs, which AuNPs has been universally used as a colorimetric assay for various analysts. The solutions of AuNPs well-dispersed present red color, while those the aggregates of AuNPs exhibited purple or blue color [37-39]. In general, tri-sodium citrate is the common reducing agent used in AuNPs synthesis. Since the ionization of trisodium citrate is quick in an aqueous medium. However, the synthesized AuNPs by tri-sodium citrate has disadvantages including easy to aggregation, unstable, low sensitivity and selectivity. To overcome these problems, modification of AuNPs with rhodamine B [37] or an amino acid namely cysteine [40] were reported to have much stronger interaction with the AuNPs surface. H. Li et al. [41] and W. Liu et al. [42] reported the citrate-coated AuNPs as colorimetric probe for rapid assay of OPs.

In recent years, graphene quantum dots (GQDs) have widely become the focus of attention in many research areas because of their good electronic and optical properties, non-toxicity, robust chemical inertness and excellent biocompatibility. GQDs are zero-dimensional materials a single or few layered graphene-like structures with the size

range of 3-20 nm, which is the structure consists of hydroxyl, carboxyl, and epoxy groups, with the sp^2 hybridized carbon atoms in inner and sp^3 hybridized carbon-oxygen bonds outside including hydroxyl and carboxylic group. Moreover, GQDs have the property as reducing and oxidizing agents. On the other hand, GQDs cannot be used for colorimetric assay applications because they show fluorescence only under UV light [43-45]. Therefore, GQDs were proposed as reducing and stabilizing agent in the synthesis of AuNPs for the colorimetric assay.

In this work, the development of a novel colorimetric assay, which is simple, rapid, sensitive and selective for the detection chlorpyrifos pesticides using two approaches of spectrophotometer and 3D- μ PAD. Colorimetric assay based on color changes of aggregated graphene quantum dots capped gold nanoparticles (GQDs-AuNPs) by interacting with thiocholine generated by AChE enzyme catalytic hydrolysis of acetylthiocholine (ATCh) substrate was exploited. AuNPs was firstly synthesized using GQDs as a reducing agent and capping agent. In the principle of chlorpyrifos assay, AChE catalyzes hydrolysis of ATCh to produce thiocholine with contains thiol group (-SH), caused the aggregation of GQDs-AuNPs and generates a purple blue-colored product. In the presence of chlorpyrifos pesticides, the inhibition of AChE was occurred, leading to anti-aggregation of GQDs-AuNPs and red-colored product. The proposed colorimetric method is simple and can be implemented in either detect by spectrophotometer or compact paper-based devices. Furthermore, a novel platform namely three-dimensional microfluidic paper-based analytical device (3D- μ PAD) was developed to simplify the process of chlorpyrifos detection. The developed 3D- μ PAD was fabricated and designed by one-step polymer screen printing (without the requirement of heat for baking the device) using rubber latex (RL) waste as eco-friendly hydrophobic reagent [46, 47] for a low-cost, rapid and simple fabrication to produce a foldable sheet composed of testing and sampling sheets. The testing sheet consists of two circles (the top circle as detection area for coating mixture solution of GQDs-AuNPs and AChE enzyme and the bottom circle as buffer loading area for analyte elution), while the sampling sheet consists of a dumbbell shape. The bottom circle area of the dumbbell shape was used as sample loading by applying the mixed solution of sample/standard (chlorpyrifos) and ATCh (substrate). To complete the 3D- μ PAD sheet, the testing sheet is folded up a sample preparation sheet. Quantification of chlorpyrifos

in 3D- μ PAD was carried out by detection of the red color produced by the reaction on the detection zone. The development of chlorpyrifos detection platform on the designed 3D- μ PAD platform has several advantages including simple, cost-effective, rapid, sensitive and selective for chlorpyrifos detection. This device could be extended as an effective tool for food quality control and on-site applications including environmental monitoring.

1.2 Objectives

1.2.1 To synthesize and characterize of GQDs-AuNPs nanocomposites by using UV-Visible spectrophotometry, Fluorescence spectroscopy, Infrared spectroscopy and Transmission electron microscope (TEM).

1.2.2 To optimize the of parameters used in the assay to enhance the sensitivity and selectivity of the colorimetric analysis of chlorpyrifos based on the reaction of GQDs-AuNPs with thiocholine generated from AChE enzyme and ATCh substrate using UV-Visible spectrophotometry.

1.2.3 To design and fabricate the three-dimensional microfluidic paper-based analytical device (3D- μ PAD) for colorimetric assay of chlorpyrifos.

1.2.4 To investigate the factors those effect on the sensitive and selective of chlorpyrifos detection implemented in the 3D- μ PAD.

1.2.5 To study the analytical features of the developed 3D- μ PAD on the quantitative analysis of chlorpyrifos.

1.2.6 To apply the developed 3D- μ PAD for chlorpyrifos determination in vegetable samples (cucumber, radish, lettuce, carrot, cabbage and tomato).

1.3 Expected outcomes

1.3.1 Sensitive and selective colorimetric method was developed based on GQDs-AuNPs for quantitative analysis of chlorpyrifos pesticide.

1.3.2 The developed 3D- μ PAD with a good performance for chlorpyrifos detection, which has advantages including a low-cost, rapid, simple to fabricate, easy to use, disposable and provide timely results.

1.4 Scope of Research

The development of colorimetric assay for highly sensitive and selective detection of chlorpyrifos pesticide was proposed. UV-Visible spectrophotometric method was used to test the possibility of the detection reaction and then implementation in the 3D- μ PAD for detection was investigated. Determination of chlorpyrifos was based on the aggregation of GQDs-AuNPs when reacted with thiocholine generated from enzymatic hydrolysis of ATCh by AChE. In the presence of chlorpyrifos, the inhibition of enzymatic hydrolysis of AChE was occurred, leading to anti-aggregation of GQDs-AuNPs. In addition, the 3D- μ PAD was newly designed as a foldable sheet included testing sheet and buffer loading sheet.

1.4.1 Part I: Spectrophotometric method for chlorpyrifos determination

1.4.1.1 Synthesis of graphene quantum dot (GQDs)

1.4.1.2 Synthesis of graphene quantum dot capped with gold nanoparticles (GQDs-AuNPs)

1.4.1.3 Characterization of the nanomaterials

1) Characterization by UV-Visible spectroscopy, Fluorescence spectroscopy, Transmission Electron Microscopy (TEM) and Fourier-transform infrared spectroscopy (FTIR).

1.4.1.4 Parameters that effect the sensitivity of the chlorpyrifos determination

- 1) Optimization of pH of 50 mM phosphate buffer saline
- 2) Optimization of ATCh concentrations
- 3) Optimization of AChE enzyme concentrations
- 4) Optimization of reaction times

1.4.1.5 Colorimetric method for chlorpyrifos determination

- 1) Linear concentration range of chlorpyrifos pesticide
- 2) Limit of detection (LOD) for chlorpyrifos pesticide

1.4.1.6 Interference study

1.4.2 Part II: 3D- μ PAD for chlorpyrifos determination

1.4.2.1 Parameters that effect the sensitivity of the chlorpyrifos detection

- 1) Optimization of pH of 50 mM phosphate buffer saline
- 2) Optimization of the volume of buffer
- 3) Optimization of the ATCh concentrations
- 4) Optimization of the AChE enzyme concentrations
- 5) Optimization of the reaction time
- 6) Optimization of the color intensity

1.4.2.2 Colorimetric method for chlorpyrifos detection

- 1) Linear concentration range of chlorpyrifos pesticide
- 2) Limit of detection (LOD) for chlorpyrifos pesticide

1.4.2.3 Interference study

1.4.2.4 Detection of chlorpyrifos in real samples

CHAPTER 2

LITERATURE REVIEWS

2.1 Colorimetric detection

Colorimetry is the technique used to determine the concentration of colored analyte in solution, which can be used to identify the molecules depending on their absorption and emission properties. The color intensity measured by this technique relates to the concentration of the analyte in samples. Colorless molecule can make to the colored compound by a chemical reaction in order to make compound can be apply to this technique. When radiation interacts with matter, a number of process can occur, including reflection, scattering and absorption (Figure 2.1) can occur. The total potential energy of a molecule generally is represented as the sum of its electronic, vibrational and rotational energies. The concentration of a sample can be calculated from the intensity of light before and after it passes through the sample by using the Beer-Lambert law [48, 49].

The Beer-Lambert law (or Beer's law) is the linear relationship between absorbance and concentration of an absorbing species. The law is only true for monochromatic light, which is light of a single wavelength or narrow band of wavelength, and provided that the physical or chemical state of the substance does not change with concentration. When monochromatic radiation passes through a homogeneous solution n the cell. The intensity of the emitted radiation is directly proportional to path length and concentration of solution [48, 49]. The absorbance (A) of the sample is related to I and I_0 according to the following equation (2.1):

$$A = \log \frac{I_0}{I} = -\log T = \epsilon bc \quad (2.1)$$

Where, I_0 and I are intensity of light of reference cell (I_0) and the sample cell (I), respectively.

T is transmittance.

ϵ is the molar extinction ($\text{dm}^3 \text{mol}^{-1} \text{cm}^{-1}$).

b is the path length, i.e. dimension of the cell or cuvette (cm).

c is the concentration of solution (mol dm^{-3}).

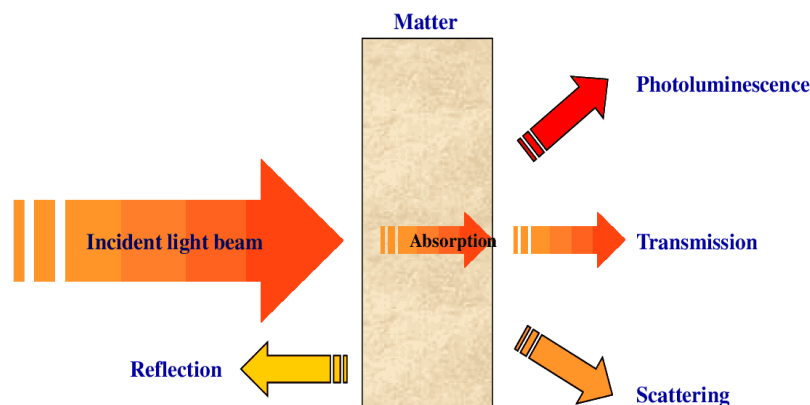


Figure 2.1 Schematic illustration of light transmission, surface reflection, and scattering in a liquid sample. [49]

UV-visible spectrometers can be used to measure the absorbance of ultra violet or visible light by a sample, either at a single wavelength or perform a scan over a range in the spectrum. The UV region ranges from 190 to 400 nm and the visible region from 400 to 800 nm. The technique can be used both quantitatively and qualitatively. Figure 2.2 shows diagram of a spectrophotometer which is the instruments used in measure concentration of a solution by measuring its absorbance of a specific wavelength of light. The light source (a combination of tungsten, halogen and deuterium lamps) provides a visible and near ultraviolet radiation covering the 200-800 nm. The output from the light source is focused onto the diffraction grating which splits the incoming light into its component colors of different wavelength, like a prism but more efficiently. For liquids the samples were contain in sample cell or cuvette. The reference cell or

cuvette contains the solvent in which the sample is dissolved and this is commonly referred to as the blank. The detector converts the incoming light into a current, then the record signal as an absorbance against wavelength (nm) in the UV and visible section of the electromagnetic spectrum. The wavelength that corresponds to the highest absorption is usually referred to as “lambda-max” (λ_{\max}) [48, 49].

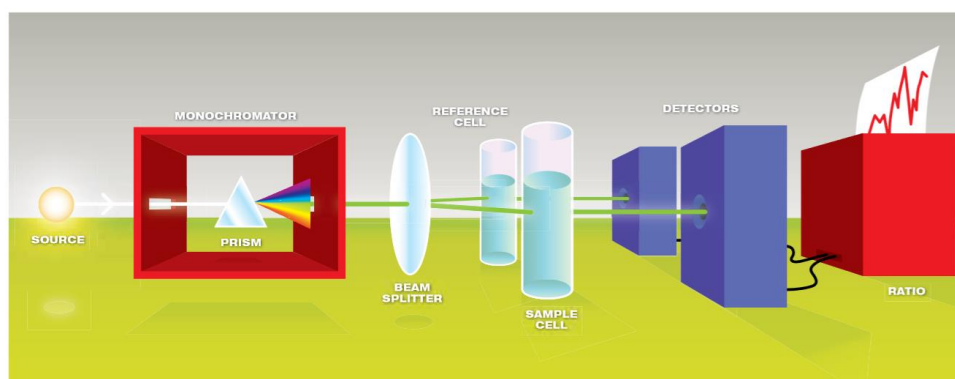


Figure 2.2 Schematic diagram of spectrophotometer. [48]

2.1.1 The chromatic analysis based on RGB color system

The chromatic analysis based on RGB color system has attracted interest as an alternative method due to its simplicity, rapidity, low cost and practicality in on-site analysis and high sample throughput, which can be described based on the light spectrum theory and any visible light in the RGB system. In general, the RGB system consists of three primary components of red (R), green (G) and blue (B) as illustrated in Figure 2.3a. The combination of primary light colors generates a new color rely on a RGB intensity ratio. For the RGB system applied in 8-bit digital images, there are 256 different level of colors (0-255). Each color of a pixel in a digital image is explained by the intensity of each primary color represented by the (R, G, B) coordinate which is informed by image analysis software (Figure 2.3b). The coordinates of white and black light colors are (255, 255, 255) and (0, 0, 0), respectively. The total color intensity is calculated from the equation $R + 255G + 255^2B$ [50, 51]. The gray scale system is the two-tone system of white and black colors which can be calculated from an RGB coordinate by using a white filter (255, 255, 255). Each RGB coordinate is planned on to the direction of a line passing through the black and white coordinates. This results

in a new coordinate with the same RGB intensity values ($R = G = B$) and the gray scale also consists of 256 levels within the range of 0-255 of the 8-bit image as that in the RGB system. The ideal average grayscale is calculated by $(R + G + B)/3$. However, this is not the true value in the grayscale system. Moreover, actual luminosity and human perception of each light color are different. Humans perceive red and green light brighter than blue light. Luminance factors are thus added in to the grayscale (grayscale with luminosity) calculation for each light color as $0.299R + 0.587G + 0.114B$. Moreover, an RGB color must be transformed in to the grayscale in each color channel before use for calculation of the ideal average grayscale and grayscale with luminosity [52]. Image J is a image processing software based on the RGB system, that applied to analyze the light color of detection zones through the grayscale system. As a consequence, all of the color intensities were examined in the grayscale with different channels of red (G_R), green (G_G) and blue (G_B), respectively. Application of Image J allows all color to be converted into the grayscale for the chromatic analysis (Figure 2.3b). It is noteworthy that the colors gained from the three channels (RGB) are subtractive colors and selectively absorb certain wavelengths of light (i.e. blue, green, and red light as the wavelength ranges of 400-500, 500-580 and 580-700 nm, respectively), thus affecting the observed colors [53-59]. Humans perceive the converse of the color component that is primarily absorbed [58] such as the bright yellow were expected to reflect red and green light (slight alter) and absorb blue light (significant alter) [60]. The relationship between the subtractive color and wavelength selectivity to light absorption was described in the previous studies [53-55].

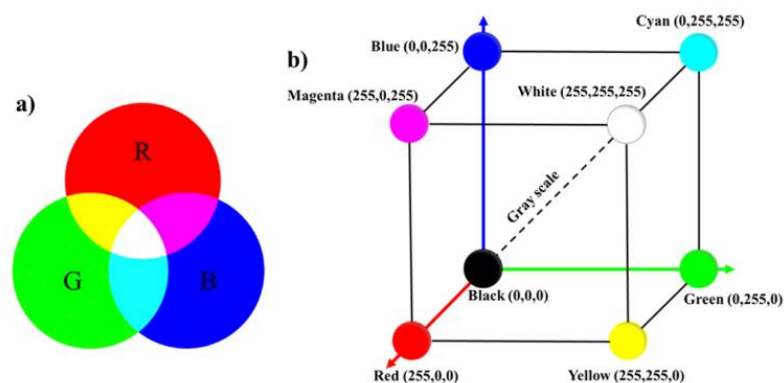


Figure 2.3 RGB color model a) Combination of primary light colors generates the new color depending on RGB ration b). [47]

2.2 Microfluidic paper-based analytical device (μ PAD)

Microfluidic paper-based analytical device (μ PAD) is an alternative technology for development of affordable, portable, disposable and low-cost diagnostic tools for improving point of care testing and disease screening [61]. The development of μ PAD began in 2007 by Whitesides group from Harvard University [24]. Subsequently, μ PAD has become of growing interest specifically in various applications. By patterning the hydrophobic channel structure on the hydrophilic paper, an aqueous solution is able to wick through the porous paper structure while being directed by the hydrophobic barrier. μ PAD displays many advantages as a tool for rapid and easy-to-perform detection that requires small amounts of reagents with little to no external supporting equipment or power. For these reasons making the μ PAD is suitable for point-of-need detection that may not even desire trained personnel to perform the measurement. An ideal fabrication method for μ PAD would be (i) inexpensive instrumentation and materials, (ii) allow a rapid fabrication for mass production, (iii) simple and does not require the hydrophilic region to be exposed to solvent during fabrication. Various techniques in the literature for fabrication of μ PAD such as (1) wax printing, (2) inkjet printing, (3) photolithography, (4) flexographic printing, (5) plasma treatment, (6) laser treatment, (7) wet etching, (8) screen printing, and (9) wax screen-printing were reported. The advantages/disadvantages for different techniques of μ PAD fabrication were summarized in Table 2.1.

Table 2.1 Comparison of advantages/drawbacks among fabrication techniques for μ PAD.

Fabrication techniques	Patterning agent	Size of hydrophobic barrier	Stored time	Advantages	Drawbacks	Ref.
Wax printing	Wax	0.1 mm	3 months	Simple and rapid fabrication process, environmentally friendly	Requires expensive wax printers and an extra heating step	[62-64]
Inkjet printing	Permanent marker ink: hexadecenoyl succinic anhydride	0.55 mm	At least 6 months when stored at room temperature	Can be scaled up, inexpensive thermal inkjet printers; print high resolution and conductive patterns	Print head is less durable, prone to clogging and damage the nozzle of ink tank	[65-67]
Photolithography	Photoresist	0.5 mm	-	Rapid (15 min), high resolution of microfluidic channels	Requires organic solvents, expensive photoresists (SU-8)	[34, 68]
Flexographic printing	Polystyrene	At least 0.4 mm	-	Thin fluidic channels and small sample volumes	Requires two prints of polystyrene solution and requires different printing plates	[69, 70]
Plasma Treatment	Alkyl ketene dimer	<1.5 mm	-	Cheap patterning agent	The substrate under a mask is often over etching	[71]

Table 2.1 Comparison of advantages/drawbacks among fabrication techniques for μ PAD (Continued).

Fabrication techniques	Patterning agent	Size of hydrophobic barrier	Stored time	Advantages	Drawbacks	Ref.
Laser treatment	Any paper with a hydrophobic surface coating	0.12 – 0.15 mm	-	Versatile, easy controlled and selectively modify the surface structure	It is not well suited for a scale up to very high throughput mass production of devices	[72-74]
Wet etching	Trimethoxyoctadecylsilan			No expensive facilities and materials are used	The printing apparatus must be customized	[75, 76]
Screen printing	Varnish paint solution, roof sealant	0.5 mm	-	Produces devices with simple process	Low resolution of channels	[70, 77]
Wax screen-printing	Wax	Diameter of 6 mm/1.3 mm	At 4 °C (sealed) for at least 5 weeks	Cheap, environmentally friendly, it requires only a common hot plate	Patterned mesh is necessary, making it inadequate for prototyping	[70, 78]

2.3 Nanocatalyst synthesis

2.3.1 Gold nanoparticles (AuNPs)

Gold nanoparticles (AuNPs) [37-39] are widely used in many fields due to their unique optical and biological properties. They could be used for highly sensitive diagnostic assays, thermal ablation and radiotherapy enhancement as well as for drug and gene delivery. The main method for AuNPs preparation is by chemical reduction that is contained of two steps: (i) the use of reducing agents such as borohydrides, citric and oxalic acids, polyols, hydrogen peroxide, sulfites, among many others. They provide electrons to reduce the gold ions, Au^{3+} (auric) to Au^0 which is the electric state for nanoparticles. (ii) the use of stabilizing agents such as trisodium citrate dihydrate, sulfur ligands (mostly thiolates), phosphorus ligands, polymers, surfactants (in particular cetyltrimethylammonium bromide; CTAB), and others [79-81]. They stabilize nanoparticles against aggregation by imparting a repulsive force that control growth of the nanoparticles in terms of rate, final size or geometric shape. It is possible that stabilizing agent is the same molecule that acts as the reduction agent. So, the major step involving the synthesis of AuNPs is reducing Au^{3+} to Au^0 by adding an electron donor (reducing agent) in the reaction. The precursor of choice for the majority of researchers is chloroauric acid (HAuCl_4) [82, 83].

AuNPs exhibit interaction of light at specific wavelength cause strong optical absorption and scattering on nanoparticles surface, that known as the surface plasmon resonance (SPR) band due to the collective oscillations of the conduction electrons coupled with incident light. This property is dependent on the size and shape of AuNPs. Hence, colloidal gold has red (for particles $<100\text{nm}$) or dark yellowish color (for larger particles). The maximum absorption wavelength of 10 nm AuNPs is around 520 nm [37-39].

2.3.2 Graphene quantum dot (GQDs)

Graphene quantum dot (GQDs) have gained significant interest in recent years due to their potential for biomedical applications, owing to their distinctive and tunable photoluminescence properties, remarkable physicochemical properties and high photostability, good biocompatibility. GQDs are semiconductor nanoparticles or nanocrystals, usually in the range of 2-10 nm (10-50 atoms) in size. GQDs have been classified as carbon nanodots (C-dots). However, it is differ in some respect such as C-

dots are quasi-spherical NPs less than 10 nm in diameter, possessing photoluminescence properties, while GQDs are graphene nanosheets in the form of one, two or more layers all less than 10 nm thick and 100 nm in lateral size; also, the GQDs contain of functional groups (carboxyl, hydroxyl, carbonyl, epoxide) at their edges that can act as reaction sites and alter photoluminescence emission from the dots by changing their electron density [84]. Previous methods of GQD synthesis involved high-cost materials such as graphene or photonic crystals and fairly low-yield and expensive methods such as laser ablation, electron beam lithography, or electrochemical synthesis [85]. These factors made GQDs practically unavailable for commercial applications. Recently, the preparation of GQD from fairly inexpensive organic sources such as citric acid and urea was reported and gained in the widely attention because of the product cost reduction and simple application [44, 45, 86].

2.4 Organophosphate pesticide detection

2.4.1 Spectrophotometric method

UV-visible spectroscopy is the most widely used method for diagnostics of the optical properties and electronic structure of nanoparticles, as the absorption bands are related to the diameter and aspect ratio of metal nanoparticles. It has been further suggested that the spectroscopic properties of nanoparticles can provide an indicator of their size distribution by fitting the position of the SPR to a simple wavelength function [88, 89].

In 2011, H. Li et al. [41] presented the citrate-coated AuNPs as a colorimetric probe for rapid assay of organophosphorus pesticides (OPs). The colorimetric analysis of mathamidophos organophosphorus insecticide was performed as followed: 0.9 mL of AuNPs and 0.1 mL of 15 μ M ATCh (pH 8.0 phosphate buffer saline; PBS) were added into centrifuge tubes with different concentrations of methamidophos (50 μ L), followed by the addition of 10 μ L of 500 mU mL⁻¹ AChE. The mixtures were incubated at 25 °C for 30 min. The absorption spectra of the reacted solutions were recorded at 522 nm (A_{522}). The assay principle was based on catalytic hydrolysis of ATCh to thiocholine (TCh) by AChE, which induces the aggregation of AuNPs and the color change from claret-red to purple or even grey. The original plasmon absorption of AuNPs at 522 nm decreases, and simultaneously, a new absorption band appears at 675

nm. The irreversible inhibition of OPs on AChE prevents aggregation of AuNPs. Under optimum conditions, the absorbance at 522 nm of AuNPs is related linearly to the concentration of mathamidophos in the range of 0.02–1.42 $\mu\text{g mL}^{-1}$ with a detection limit of 1.40 ng mL^{-1} .

In 2011, J. Sun et al. [90] proposed lipoic acid (LA) capped AuNPs for the detection of OPs nerve agents. A negatively charge of LA could provide protection of AuNPs and the aggregation-induced change in the color associated with TCh, which is generated through AChE/ATCh hydrolysis reaction approach. In the presence of OPs, the production of TCh could be suppressed and the color change of LA-AuNPs is gradually diminished according to different concentrations of OPs. Inhibition assay for AChE activity by OPs was then determined, OPs of various concentrations (2.0 μL) were added to 200 μL of aqueous solution containing 4.95×10^{-2} units/mL AChE and 10 mM Tris-HCl at pH 7.6. The resulting mixtures were incubated under 37 °C for 2.5 h, followed by addition of 2.0 μL of 1.0 mM ATCh and incubated at 37 °C for 30 min. After subsequent addition of 200 μL of 7.5 nM LA-AuNPs, the solution was measured by UV–visible spectrophotometer. The development biosensor provided a linear range between 4.52×10^4 – 4.95×10^5 pM and limit of detection was 4.52×10^4 pM for paraoxon pesticides.

In 2012, D. Liu et al. [37] presented a highly sensitive, rhodamine B-covered AuNPs (RB-AuNPs)-based assay with dual readouts (colorimetric and fluorometric) for detection OPs and carbamate pesticides in complex solutions. The RB-AuNPs was negatively charged because of the carboxyl group capped on RB. The charge of aggregated RB-AuNPs was neutralized by the presence of TCh derived from AChE catalyzed hydrolysis of ATCh, which turned the RB-AuNPs solutions to blue and unquenched the fluorescence of RB simultaneously. In the present of pesticides, the inhibition of enzymatic hydrolysis of AChE was occurred. The color of the RB-AuNPs solution remained red and the fluorescence of RB was quenched. In the pesticide detection, 10 mU mL^{-1} AChE solution was added various concentrations of carbaryl solutions with (final concentrations were set to be 0, 0.1, 0.3, 0.6, 1.0, 3.0, 6.0, 10, and 100 $\mu\text{g L}^{-1}$). 0.5 mL of 5 nM RB-AuNPs was added into each mixture and then aliquot of 20 μM of ATCh was finally added into the mixtures. The resulting mixtures were kept in the dark for 5 min, UV–visible absorption and fluorescence were measured

respectively. By the use of this dual-readout assay, the lowest detectable concentration for several kinds of pesticides including carbaryl, diazinon, malathion, and phorate were 0.1, 0.1, 0.3, and 1 $\mu\text{g L}^{-1}$, respectively. All of the lowest detectable concentration of pesticides in this work are much lower than the maximum residue limits (MRL) as reported in the European Union pesticides database as well as those from the U.S. Department Agriculture (USDA).

In 2015, R. Bala et al. [40] reported a simple, rapid and sensitive method using cysteine capped gold nanoparticles (cys-AuNPs) as a key material for ethyl parathion detection. The detection was based on the aggregation of cys-AuNPs leading to a visible color change from red to blue as a consequence of the generation of TCh. The hydrolytic reaction of ATCh by the enzyme AChE affects the production of TCh. Presence of ethyl parathion leads to suppression of TCh resulting in no color change whereas its absence leads to a visible color change from red to blue. Detection of this work performed by adding was as followed, 50 μL of different concentration of ethyl parathion to 10 μL of 200 mU mL^{-1} and the solution was incubated for 2.5 h at room temperature. Then, 100 μL of 15 μM ATCh was added to the mixture solution and incubated again for 30 min. Finally, 0.9 mL of 5 nM cys-AuNPs was added and the absorption was measured by UV-visible spectrophotometer. The development assay provided a linear range between 0.02-0.20 ng mL^{-1} and limit of detection was 0.081 ng mL^{-1} for pesticides. The proposed method can be employed for the on-site monitoring of OPs owing to its low cost, simple instrumentation and rapid nature.

In 2015, N. Li et al. [91] developed a novel fluorometric method based on graphene quantum dots (GQDs) for highly sensitive, highly selective, label-free, and one-step detection of AChE and its inhibitors. The assay 'mix-and-detect' strategy was based on quenching of GQD photoluminescence (PL). First, 0.5 mg mL^{-1} of GQDs solution was modified by 10 mM of ATCh molecules via simple electrostatic interaction. Subsequently, addition of 117 nM of AChE to quickly hydrolyzes ATCh molecules into thiocholine (TCh) molecules whose thiol group (-SH) catalyzes the growth of gold nanoparticles (AuNP) on GQD by potently reducing Au^{3+} ions was performed. Consequently, GQD PL is quenched by AuNP due to Förster resonance energy transfer (FRET). Furthermore, Au-S covalent bonding between the unreacted -SH groups and formed AuNPs on neighboring GQDs causes aggregation of GQDs,

thereby leading to further PL quenching. The optical sensor can serve as a universal platform to detect a trace amount of AChE inhibitors such as nerve gases, pesticides and therapeutic drugs. Paraoxon was chosen for the proof-of concept demonstration and a half maximal inhibitory concentration (IC_{50}) of paraoxon was estimated to be 19.86 nM. This report also demonstrates the great potential of GQDs for the development of optical sensor.

In 2017, J. Ling et al. [92] studied an assay with turn-on fluorescence for monitoring cerebrospinal acetylcholinesterase (AChE) fluctuation as a biomarker for organophosphorus pesticides poisoning and management based on single layer MnO_2 nanosheets with GQDs as signal readout. Initially, the fluorescence of GQDs was quenched by MnO_2 nanosheets mainly due to the inner filter effect (IFE). However, with the presence of reductive TCh, the enzymatic product, hydrolyzed from ATCh by AChE, the redox between MnO_2 and TCh occurred, leading to the destruction of the MnO_2 nanosheets, and thereby IFE was diminished gradually. As a result, the turn-on fluorescence of GQDs with the changes in the spectrum of the dispersion constituted a new mechanism for sensing of cerebrospinal AChE. With the method developed here, they could monitor cerebrospinal AChE fluctuation of rats exposed to organophosphorus pesticides before and after therapy, and could thereby open up the pathway to a new sensing platform for better understanding the mechanism of brain dysfunctions associate with organophosphorus pesticides poisoning.

In 2017, N. Chen et al. [93] presented a new colorimetric sensor based on citrate-stabilized gold nanoparticles for the rapid pesticide residue detection of both terbutylazine (TBA) and dimethoate (DMT). The preparation of citrate-stabilized AgNPs was performed as followed: 5 mL of 5 mM $HAuCl_4$ was added to Milli-Q water and stirring. After that 2 mL of 10 mg mL^{-1} sodium citrate dihydrate ($Na_3Ct \cdot 2H_2O$) was added until color change from yellow to red and kept in the refrigerator. For the colorimetric detection of TBA and DMT, 100 μL of TBA and DMT with various concentration were mixed with 20 μL of 1.0 M NaOH. The mixture was then added the obtained 0.85 mL of 0.25 mM AuNPs and kept at room temperature. The detection mechanism has been verified via fourier transform infrared (FT-IR) spectroscopy, UV-visible spectrophotometer, zeta potential, transmission electron microscopy (TEM) and dynamic light scattering (DLS). Under the optimized experimental conditions, 30 kinds

of potential environmental pollutants have no interference on the TBA or DMT detection indicating the high selectivity of the AuNP-based colorimetric sensor. The limits of detection of TBA and DMT by eye vision were respectively 0.3 μM and 20 nM, respectively and LOD based on calculated (3SD) 0.02 μM and 6.2 nM, respectively. The linear relationships of the UV-visible spectrometry demonstrate that AuNP-based colorimetric sensor can be used for the quantitative analysis of TBA in the range of 0.1-0.9 μM , and DMT in the range of 1-40 nM. Finally, the developed AuNP-based colorimetric sensor is also verified to in the real environmental samples.

In 2018, H. Li et al. [94] developed the colorimetric and fluorometric detection. The fluorescent carbon dot (CDs) was synthesized by using one-step hydrothermal treatment of folic acid and p-phenylenediamine. Principle of the assay was based on 50 μL of 2.0 $\mu\text{g mL}^{-1}$ AChE enzyme catalyze the hydrolysis of 50 μL of ATCh to TCh, which specifically reacted with 150 μL of 200 $\mu\text{g mL}^{-1}$ 5,5-ditiobis (2-nitrobenzoic acid) (DTNB) to form yellow-colored 5- thio-2-nitrobenzoic acid (TNBA) with the absorption peak around 412 nm. The fluorescence intensity of CDs quench by TNBA, which the TNBA was positively charged while CDs were negatively charged. There exists intensive electrostatic attraction between CDs and TNBA. Upon the addition of different concentration of paraoxon, the activity of enzyme was blocked, leading to the increased fluorescence signal and the decrease of absorbance intensity at 412 nm with color variation. The dual-mode assay provided good sensitivity of paraoxon detection in the range between 0.0-0.5 $\mu\text{g mL}^{-1}$ and 0.001-1.0 $\mu\text{g mL}^{-1}$ for colorimetry and fluorometry, respective.

Table 2.2 Comparison of the methods for organophosphate pesticides detection using various nanomaterials.

Materials	Enzyme	Method	Analytes	Concentration range	LOD	Ref.
Citrate coated AuNPs	AChE	Colorimetric	Methamidophos	0.02-1.42 $\mu\text{g mL}^{-1}$	1.40 ng mL^{-1}	[41]
LA-AuNPs	AChE	Colorimetric	Paraoxon	4.52×10^4 - 4.95×10^5 pM	4.52×10^4 pM	[89]
RB-AuNPs	AChE	Colorimetric	Carbaryl	0.1-100 $\mu\text{g mL}^{-1}$	0.1 $\mu\text{g mL}^{-1}$	[37]
		Colorimetric	Diazinon	0.1-100 $\mu\text{g mL}^{-1}$	0.1 $\mu\text{g mL}^{-1}$	
		Fluorometric	Malathion	0.1-100 $\mu\text{g mL}^{-1}$	0.3 $\mu\text{g mL}^{-1}$	
Cys-AuNPs	AChE	Colorimetric	Phorate	0.01-1000 $\mu\text{g mL}^{-1}$	1.0 ng mL^{-1}	[40]
			Ethyl parathion	0.02-0.2 ng mL^{-1}	0.081 ng mL^{-1}	
ATCh-GQDs	AChE	Fluorometric	Paraoxon	-	2.0 nM	[91]
			Tacrine	-	6.2 nM	
GQDs-MnO ₂	AChE	Fluorometric	Parathion	1.0-40 ng mL^{-1}	-	[92]
Citrate stabilized AuNPs	-	Colorimetric	Terbuthylazine	0.1-0.9 μM	0.02 μM	[93]
			Dimethoate	1.0-40 nM	6.2 nM	
CDs-DTNB	AChE	Colorimetric	Paraoxon	0.0-0.5 $\mu\text{g mL}^{-1}$	0.4 ng mL^{-1}	[94]
		Fluorometric				

LA = lipoic acid, AuNPs = gold nanoparticles, RB = rhodamine B, Cys = cysteine, GQDs = graphene quantum dot, MnO₂ = Manganese (IV) oxide nanosheet, CDs = carbon nanodot, DTNB = 5,5-dithio-bis-(2-nitrobenzoic acid)

2.4.2 Microfluidic paper-based analytical device (μ PAD)

In 2009, S.M. Z. Hossain et al. [95] developed a reagentless bioactive paper-based solid-phase biosensor for detection of OPs pesticides. The assay strip was composed of a paper support (1×10 cm), onto which AChE and a chromogenic substrate, indophenyl acetate (IPA), were entrapped using biocompatible sol-gel derived silica inks in two different zones (e.g., sensing and substrate zones). The principle of assay was based on AChE hydrolysis the red-yellow color of IPA substrate to blue-purple color of indophenoxide anion (IDO^-). In the present of pesticides, the inhibition of enzymatic hydrolysis of AChE was occurred. As a result, the decreased of blue-purple color. The development of reagent less lateral flow sensor provides the detection limits (bendiocarb ~ 1 nM; carbaryl ~ 10 nM; paraoxon ~ 1 nM; malathion ~ 10 nM) and rapid response times (~ 5 min). The sensor showed negligible matrix effects in detection of pesticides in spiked milk and apple juice samples.

In 2014, E. I. Mohamed. et al. [96] developed a bioactive paper-based sensor for detection of OPs and carbamate pesticides. Based on the Ellman colorimetric assay, the assay strip was composed of a paper support (1×10 cm), onto which a biopolymer chitosan gel immobilized in crosslinking by glutaraldehyde with AChE and 5,5'-dithiobis(2-nitrobenzoic) acid (DTNB) and used acetylthiocholine iodide (ATChI) as an outside reagent. The assay protocol involves introducing the sample to sensing zone via dipping of a pesticide-containing solution. The assay protocol involved introducing the sample to sensing zone via dipping of a pesticide-containing solution. Following an incubation period, the paper was placed into ATChI solution to initiate enzyme catalyzed hydrolysis of the substrate, causing a yellow color change. The absence or decrease of the yellow color indicated the levels of the AChE inhibitors. The biosensor was able to detect organophosphate and carbamate pesticides with good detection limits (methomyl = 6.16×10^{-4} mM and profenofos = 0.27 mM) and rapid response times (~ 5 min). The results show that the paper-based biosensor was rapid, sensitive, inexpensive, portable, disposable, and easy-to-use.

In 2015, Q. Liu et al. [2] presented the test strip for OPs detection. The test strip was designed to have a sandwich structure with the middle layer as a detector and the out layers as protectors (as shown in Figure 2.4C). The size of the test strip was $100 \times 10 \times 0.5$ mm³. The center detector layer had a gel matrix structure to entrap AuNPs.

The substrate (thiocholine, generated from ATC catalyzed by AChE) was able to pass through the gel matrix to react with the Au NPs. The gel matrix was also designed to have a transparent structure, so the color changes of the Au NPs could be observed directly by naked eyes. The strip was further validated by various pesticide samples. Its detection limit was demonstrated to meet the maximum residue limits (MRL) reported in the European Union pesticides database. The developed strip also showed its good sensitivity and high reliability on testing river water samples, which suggested its great potential in environmental analysis.

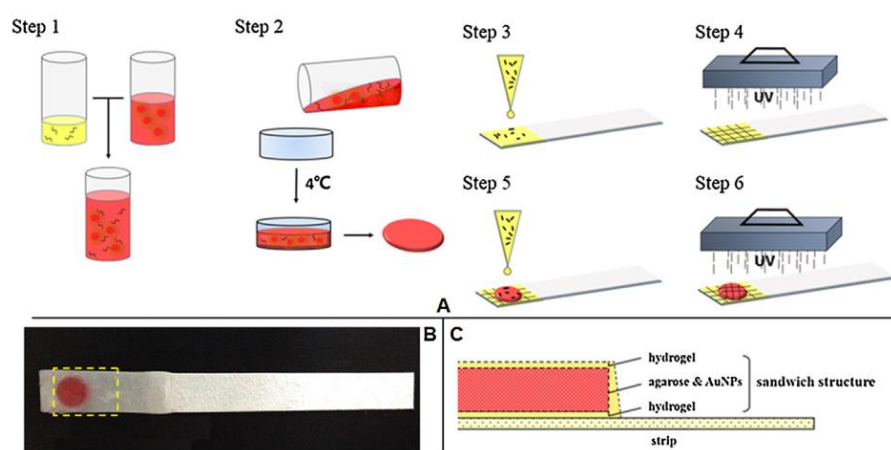
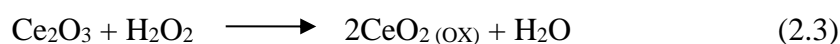


Figure 2.4 Illustration of the test strip fabrication procedure(A). Photograph of the test strip (B) and illustration of the sandwich structure (C). [2]

In 2016, S. Nouanthavong et al. [97] reported the first use of a paper-based device coated with nanoceria as a simple, low-cost and rapid detection platform for OPs detection, methyl-paraoxon (MPO) and chlorpyrifos-oxon (CPO). The paper-based device was fabricated using polymer screen-printing method. Briefly, polystyrene solution (25% w/v in toluene) was applied onto a patterned screen placed on top of a Whatman no. 4 filter paper, which the solution passed through the paper to create a hydrophobic barrier with a cycle detection zone of a 5 mm diameter. The patterned paper devices were then coated with nanoceria by depositing 5 μL of 3% w/v colloidal nanoceria solution onto detection zones and dried at room temperature. Moreover, 5 μL of 10 mg mL^{-1} polyethylene glycol (PEG) solute ion was added onto the device for increases hydrophilic of the detection zone. After drying, the nanoceria-coated paper-

based devices were ready for MPO and CPO determination. In general, the assay was based on the enzyme inhibition of AChE by the pesticides using nanoceria as a colorimetric agent as described in (2.1) through (2.3). Acetylcholine (ATC) is catalyzed by AChE to form choline (2.1), which is then oxidized by choline oxidase (ChOX) to generate hydrogen peroxide (H_2O_2) (2.2). The amount of H_2O_2 produced is measured calorimetrically by nanoceria, when Ce^{3+} is oxidized to Ce^{4+} in the presence of H_2O_2 resulting in the color change from colorless to yellow (2.3). In the presence of OPs, the activity of AChE is inhibited leading to a decrease in the yellow intensity for the nanoceria.



The assay was able to analyze OPs without the use of complicated instruments and gives detection limits of 18 ng mL^{-1} and 5.3 ng mL^{-1} for MPO and CPO, respectively.

In 2016, A. Apillux et al. [35] presented the development of thioglycolic acid capped cadmium telluride quantum dot (TGA-capped CdTe QDs) lab on paper device for practical detection of OPs and carbamate (CM) insecticides. The pattern device was created on Whatman No.1 paper using a wax printing method with a printer. The designed wax printed paper was placed on hot plate at $75 \text{ }^\circ\text{C}$ for 2 min to melt the wax to create the hydrophobic barrier on paper. A device was designed as shown in Figure 2.5, the foldable sheet included detection zone and the buffer solution loading channel to simplify the multi-step reaction of bi-enzyme (AChE and ChOX enzyme) assay (Figure 2.5). The first part is a testing sheet and another is a buffer loading sheet as shown in Figure 2.5 (a) (left). The center of testing sheet contains a hydrophilic circular detection area with diameter of 0.6 mm for pre-spotting of bi-enzyme (AChE-ChOX) and TGA-capped CdTe QDs. The buffer loading sheet was designed as a dumbbell shaped which contained two hydrophilic circular areas with diameter of 0.6 mm. The hydrophilic circular area located at the top of the channel was coated by ATCh substrate, while the hydrophilic circular area located at the end of the channel was prepared for

the buffer loading. To complete the device, the testing sheet will be folded up a buffer loading sheet as shown in Figure 2.5(a) (right) using double adhesive tape. To prepare TGA-capped CdTe QDs paper-based device, 2 μL of standard (2500 U mL^{-1} AChE, 5000 U mL^{-1} ChOX and 240 mg mL^{-1} TGA-capped CdTe QDs)/samples, which were coated at the detection zone, while 2 μL of 10 mM ATCh substrate was coated at the buffer loading sheet and incubated for 10 min. After closing the device, 15 μL of 20 mM PBS, pH 7.4 was added onto buffer loading area to mix well and signal enhancement. Hydrolysis of ATCh was catalyzed by AChE followed by ChOX which leads to yield H_2O_2 which can quench the TGA-capped CdTe QDs fluorescence. In the presence of OPs and CM insecticides, the AChE activity was inhibited, resulting in decreased quenching of TGA-capped CdTe QDs. The change in TGA-capped CdTe QDs fluorescence intensity can be observed by naked eye under UV-black light (Figure 2.5 (b)). Under the optimized conditions, the limit of detection of pirimicarb, dichlorvos and carbaryl were found to be 0.05, 0.01 and 0.01 $\mu\text{g mL}^{-1}$, respectively by visual measurement. The developed device showed good selectivity and sensitivity for screening test of insecticides and could be useful for on-site applications.

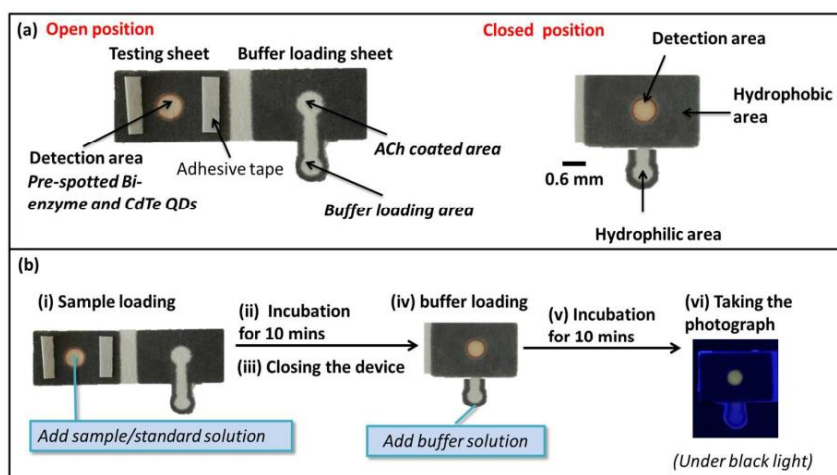
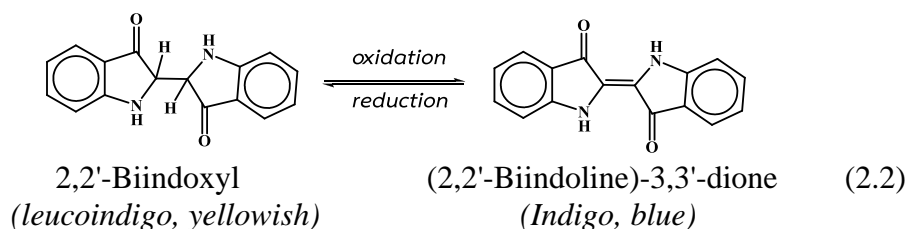
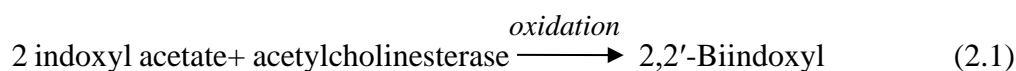


Figure 2.5 Photograph of TGA-capped CdTe QDs based lab on paper device for bi-enzyme assay with fluorescence detection in open and closed positions (a). Schematic illustration of the insecticide detection assay (b). [35]

In 2017, S. Wu et al. [98] presented a colorimetric method based on the AChE hydrolysis reaction and dissolution of AuNPs in Au³⁺-cetyltrimethylammonium bromide (Au³⁺-CTAB) solution for the highly sensitive detection of OPs. The detection principle was based on AChE hydrolysis the substrate of ATCh to produce a large amount of TCh reducing agent, which reduces Au³⁺ in the reaction system and slightly promote the growth of AuNPs, thus changing the color of the solution to dark red. In the presence of OPs, the activity of AChE was inhibited, which could only produce a small amount of TCh. Then, the large amount of residual Au³⁺ would oxidize the AuNPs with the assistance of CTAB and lead to the formation of a colorless Au⁺-CTAB complex, thus leading to an obvious red-to-colorless color change. Under optimal conditions, the colorimetric method could indicate the presence of OPs, with the concentration down to 0.7 ppb. After loading AuNPs on a cellulose paper, an AuNPs-coated dipstick was developed for the detection of OPs, which was highly sensitive with an observable limit of detection of 35 ppb.

In 2018, Q. Luo et al. [99] presented a three-dimensionally printed self-propelled mini-motor (SPM) for the detection of carbaryl. The device uses highly sensitive metal nanoparticles for colorimetric monitoring. Gold nanoparticles covered with Rhodamine B (RB-AuNPs) were prepared, based on established colorimetric and fluorometric approaches for detecting pesticides. The detection mechanism monitors the inhibition of the activity of AChE by the pesticide, in which the production of thiocholine from the hydrolysis of ATCh catalyzed by AChE was reduced. As a result, the color of the RB-AuNP solution remains red, and the fluorescence of RB remains quenched. Under the optimized conditions, excellent reproducibility (with a relative standard deviation of 5.8%) and low sensitivity limits, ranging from 0.4 to 3.0 $\mu\text{g L}^{-1}$ were achieved. The limit of quantity (LOQ) was 0.3 $\mu\text{g L}^{-1}$, and LOD was 0.23 $\mu\text{g L}^{-1}$ which was much lower than the maximum residue limits reported in the European Union pesticide database. With the aid of 3D-printed SPMs and nano-colorimetry, both qualitative and quantitative analyses can be performed for pesticide detection in river water.

In 2018 H. J. Kim et al. [100] reported the paper device consists of three paper layers (sample injection, reagent storage, and observation of color) for chlorpyrifos detection. The fabrication multilayered paper device was designed with Clewin (ver. 4) and Illustrator (CS 4, Adobe). The top and bottom layers included a circle 3 mm in diameter in the center and off-center of the layer. In the middle layer, two circles and a pathway (4 mm long and 1.5 mm wide) were designed for flow and mixing reagents. The designed layers were printed on a sheet of filter paper with a commercial wax printer. The patterned paper was heated at 120°C for 105 s to melt the wax ink and let it permeate into the paper matrix, thus forming a hydrophobic barrier. Then, 3 μL of each chemical reagent (0.8 unit mL^{-1} of AChE and 40 mM of IDA) was dropped on the two circles of the middle layer, where it dried. All the layers were collected and adhered to each other using adhesive tapes (Figure 2.6A). In colorimetric quantification of pesticides, the blue color produced by the interaction between acetylcholinesterase and indoxyl acetate was inhibited by the pesticide molecules present in the sample solutions. The reaction process was as followed:



A single indoxyl radical produced by AChE was oxidized and make a coupling with another indoxyl radical to 2,2'-Biindoxyl (yellow) which was an intermediate form of the whole reaction. this intermediate was reversibly converted to (2,2'-Biindoline)-3,3'-dione, so called Indigo dye (blue). The procedure for the pesticide detection was show in Figure 2.6A. the buffer solution contains pesticides, the analyte binds to the AChE molecules, inhibiting the conversion of indoxyl acetate (IDA) to indigo dye. In the absence of chlorpyrifos in the buffer, the chromogenic precursor was activated by AChE, resulting in development of blue color (Figure 2.6B, 2.6C). These color changes were observable at the bottom of the paper device. Under optimum conditions, the pesticide was sensitively detected (LOD =8.60 ppm) within 5 min.

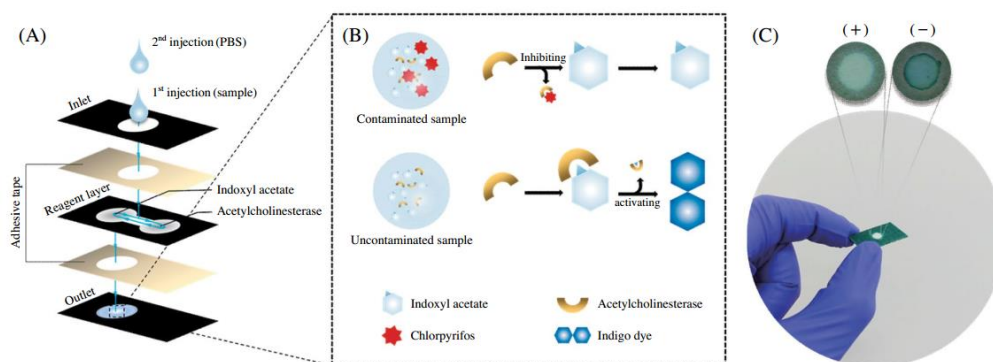


Figure 2.6 Schematics of the procedure for the pesticide detection. The blue arrows in the detecting procedure means the expected fluid flows on the microchannels of the paper device (A). The mechanism for the inhibition of AChE by a contaminated sample with pesticides, while reducing the color intensity in the outlet (B). The photographed image shows the fabricated paper-based analytic device with pesticide-positive (+) and negative (-) sample (C). [100]

Table 2.3 Comparison of PAD's analytical performance for the organophosphate pesticides determination.

Fabrication technique	Patterning agent	Materials coated on μPAD	Response time	Pesticides	Concentration range	LOD	Ref.
Cutting	-	IPA/AChE	5 min	Bendiocarb	0.0-1.0 μ M	1.0 nM	[95]
				Carbaryl		10 nM	
				Paraoxon		1.0 nM	
				Malathion		10 nM	
Cutting	-	Chitosan/DTNB/AChE-hydrogel	5 min	Methomyl	0.1-0.2 μ M	0.616 μ M	[96]
				Profenofos	0.01-0.12 mM	0.27 mM	
Cutting	-	RB-AuNPs/hydrogel/AChE	2 h	Chlorpyrifos	5.0-500 ng mL ⁻¹	-	[2]
Screen printing	Polystyrene	CeO ₂ /AChE/ChOX	15 min	Methyl-paraoxon	0.0-0.1 μ g mL ⁻¹	18 ng mL ⁻¹	[97]
				Chlorpyrifos-oxon	0-60 ng mL ⁻¹	5.3 ng mL ⁻¹	
Wax printing	Wax	TGA capped CdTe QDs/AChE/ChOX	10 min	Pirimicarb Carbaryl	0.01-10 μ g mL ⁻¹	50 ng mL ⁻¹ 10 ng mL ⁻¹	[35]

Table 2.3 Comparison of PAD's analytical performance for the organophosphate pesticides determination (Continued).

Fabrication technique	Patterning agent	Materials coated on μPAD	Response time	Pesticides	Concentration range	LOD	Ref.
Wax film	Wax	Au ³⁺ -CTAB/AuNPs/AChE	10 min	Parathion	0-1.0 $\mu\text{g mL}^{-1}$	35 ng mL^{-1}	[98]
Printing	Resin	RB-AuNPs/IDA	2 h	Carbaryl	0.4-3.0 $\mu\text{g L}^{-1}$	0.23 $\mu\text{g L}^{-1}$	[99]
Wax printing	Wax	IDA/AChE	5 min	Chlorpyrifos	0.0-25 $\mu\text{g mL}^{-1}$	8.6 $\mu\text{g mL}^{-1}$	[100]

IPA = indophenyl acetate, AChE = acetylcholinesterase enzyme, DTNB = 5,5-dithio-bis-(2-nitrobenzoic acid), RB = rhodamine-B, AuNPs = gold nanoparticles, ChOX = Choline oxidase, TGA = thioglycolic acid, CdTe QDs = cadmium telluride quantum dot, CTAB = Cetyltrimethylammonium bromide and IDA = indoxyl acetate.

CHAPTER 3

METHODOLOGY

3.1 Instrumentation

Equipments used in this work were listed in Table 3.1.

Table 3.1 Instrumentation for chlorpyrifos detection and characterizations.

Instrument and device	Model	Company
Digital camera	IXUS 105	Canon
UV-Visible spectrophotometer	UV-2600	Shimadzu, Japan
Fluorescence spectrophotometer	LS-55	PerkinElmer, USA
Transmission electron microscope, (TEM)	JEM 1230	JEOL, Japan
Fourier transformed infrared spectrometer, (FTIR)	Spectrum RX-I	Perkin Elmer, USA
High Performance liquid chromatography, (HPLC)	CTO-10AC	Shimadzu, Japan

3.2 Chemical commercial product and materials

All chemicals and materials used in this work were analytical grade summarized in Table 3.2.

Table 3.2 List of chemicals and materials.

Chemical	Grade	Supplier
Hydrogen tetrachloroauric (III) acid trihydrate (HAuCl ₄ ·3H ₂ O)	AR	Acros Organic
Citric acid (C ₆ H ₈ O ₄)	AR	Carlo Erba
Sodium hydroxide (NaOH)	AR	Carlo Erba
Tri-sodium citrate dihydrate	AR	Sigma-Aldrich
Acetylcholinesterase (AChE, ≥1000 units mg ⁻¹ protein)	AR	Sigma-Aldrich
Acetylthiocholine chloride (ATCh)	AR	Sigma-Aldrich
Chlorpyrifos (C ₉ H ₁₁ Cl ₃ NO ₃ PS)	AR	Sigma-Aldrich
Iron (III) chloride (FeCl ₃)	ACS	Sigma-Aldrich
Nickel (II) sulfate (NiSO ₄)	ACS	Sigma-Aldrich
Copper (II) sulfate pentahydrate (CuSO ₄ ·5H ₂ O)	AR	Carlo Erba
Zinc sulfate heptahydrate (ZnSO ₄ ·7H ₂ O)	AR	Carlo Erba
Magnesium sulfate heptahydrate (MgSO ₄ ·7H ₂ O)	AR	Carlo Erba
Sodium chloride (NaCl)	AR	Carlo Erba
Sodium nitrate (NaNO ₃)	AR	Carlo Erba
Potassium chloride (KCl)	ACS	Carlo Erba
Potassium iodide (KI)	ACS	Carlo Erba
Sodium sulfide nonahydrate (Na ₂ S·9H ₂ O)	ACS	Carlo Erba
di-Sodium hydrogen phosphate (Na ₂ HPO ₄)	Analysis	Carlo Erba
Sodium phosphate monobasic dihydrate (NaH ₂ PO ₄ ·H ₂ O)	Analysis	Carlo Erba
β-D-glucose (C ₆ H ₁₂ O ₆)	ACS	Sigma-Aldrich

Table 3.2 List of chemicals and materials (Continued).

Chemical	Grade	Supplier
Maltose (C ₁₂ H ₂₂ O ₁₁)	ACS	Sigma-Aldrich
Fructose (C ₆ H ₁₂ O ₆)	ACS	Sigma-Aldrich
Ascorbic acid	ACS	Sigma-Aldrich
Methanol (CH ₃ OH)	ACS	Carlo Erba
Acetonitrile (CH ₃ CN)	AR	Carlo Erba
Nitric acid (HNO ₃ , 65% w/w)	AR	Carlo Erba
Hydrochloric acid (HCl, 37% w/w)	AR	Carlo Erba
Gasoline	95% pure -grade 4	PTT Public Company Limited
Filter paper	-thickness 205 μm -pore size (20-25 μm)	Whatman International Ltd.

3.3 Preparation of standard stock solution

Hydrogen tetrachloroaurate (III) hydrate (HAuCl₄·3H₂O) solution (0.4 mM)

A stock of H₂AuCl₄ solution (0.4 mM) was prepared by dissolving approximately 0.015 g of H₂AuCl₄·3H₂O in 100 mL of deionized water.

Sodium hydroxide (NaOH) solution (0.25 M)

1.0 g of NaOH was dissolved and diluted with deionized water to 100 mL in a beaker to give a 0.25 M of NaOH solution.

Chlorpyrifos pesticide (C₉H₁₁Cl₃NO₃PS) solution (5.0 mg mL⁻¹)

Chlorpyrifos pesticide (5.0 mg) was initially dissolved in methanol (1.0 mL) to prepare stock solution (5.0 mg mL⁻¹) and then stored in the dark at 4 °C. Different concentration of chlorpyrifos were diluted with phosphate buffer saline (PBS) and used for further experiments.

Acetylcholinesterase (AChE) enzyme (100 Unit mL⁻¹)

1,000 Unit of AChE enzyme was dissolved in 10.0 mL the PBS and this stock solution was kept at -20 °C.

Acetylthiocholine (ATCh) solution (50 mM)

A stock solution of 50 mM ATCh was prepared immediately before used by dissolving approximately 0.25 g of acetylthiocholine chloride in 25 mL deionized water. The solution was used not for more than 3 h after preparation to minimize possible hydrolysis.

Di-sodium hydrogen phosphate (Na_2HPO_4) solution (50 mM)

1.774 ± 0.0005 g of $\text{Na}_2\text{HPO}_4 \cdot \text{H}_2\text{O}$ was dissolved and diluted with deionized water to 250 mL in a volumetric flask to give a 50 mM $\text{Na}_2\text{HPO}_4 \cdot \text{H}_2\text{O}$ solution.

Sodium dihydrogen phosphate monobasic ($\text{NaH}_2\text{PO}_4 \cdot \text{H}_2\text{O}$) solution (50 mM) and potassium chloride (KCl) solution (5.0 mM)

1.950 ± 0.0005 g of $\text{NaH}_2\text{PO}_4 \cdot \text{H}_2\text{O}$ and 0.059 ± 0.005 g of KCl were dissolved and diluted with deionized water to 250 mL in a volumetric flask to give NaH_2PO_4 -KCl solution.

Phosphate buffer saline (PBS) solution pH 7.0 (50 mM)

50 mM phosphate buffer saline pH 7.0 was prepared by mixing 58.7 mL of 50 mM Na_2HPO_4 and 41.3 mL of 50 mM NaH_2PO_4 -KCl, then the mixture was adjusted to pH 7.0.

3.4 Synthesis of graphene quantum dot (GQDs)

GQDs were synthesized by a pyrolyzing method adopted from Sinduja et al [44]. 2.0 g of citric acid was heated to 200 °C on a magnetic stirrer-hotplate for 30 min. The solution color changed from yellow to orange. The resulting orange liquid (1.0 g) was added dropwise to a 0.25 M NaOH solution (100 mL) under continuous stirring, to provide the GQDs product (10 mg mL^{-1}) as a yellow solution. The reaction mechanism is as shown in Figure 3.1.

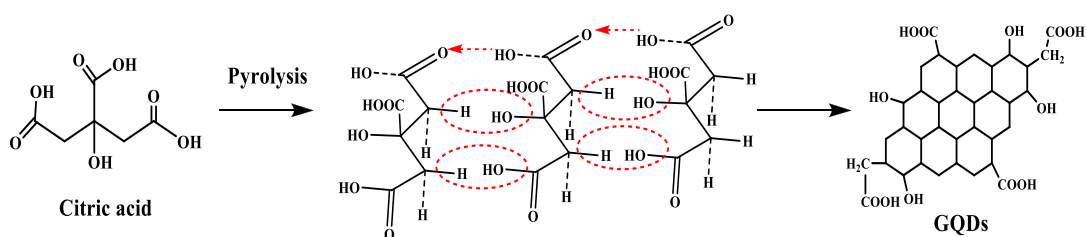


Figure 3.1 Diagram for the synthesis of GQDs.

3.5 Preparation of graphene quantum dot capped gold nanoparticles (GQDs-AuNPs)

The preparation of GQDs-AuNPs was carried out by mixing HAuCl_4 (10 mL, 0.4 mM), GQDs (10 mL 0.4 mg mL^{-1}), and deionized water (5 mL) in a 250-mL round-bottomed flask and heating to $100 \text{ }^\circ\text{C}$ under continuous stirring. Stirring was continued a further 30 min until the colorless solution had turned red. Stirring continued for 1 h to ensure completion of the reaction. After cooling, the GQDs-AuNPs were separated by centrifugation at 10,000 rpm for 30 min. The prepared GQDs-AuNPs were then re-dispersed in deionized water and stored at $4 \text{ }^\circ\text{C}$, ready for use. Figure 3.2 illustrates the preparation of GQDs-AuNPs.

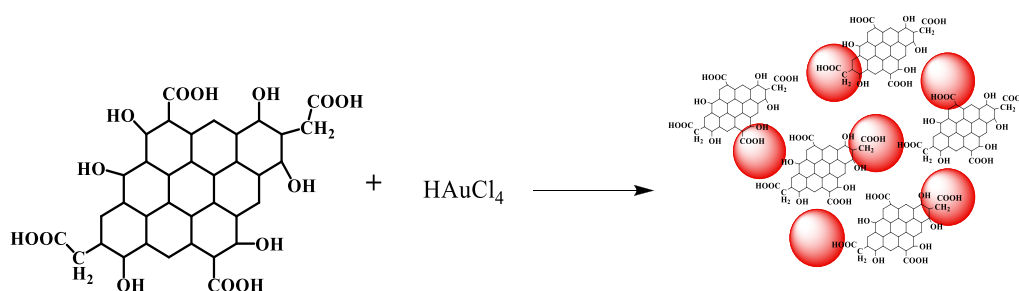


Figure 3.2 Schematic show the formation of GQDs-AuNPs.

3.6 Part I: Spectrophotometric method for chlorpyrifos determination

3.6.1 Characterizations of nanomaterials

3.6.1.1 UV-Visible spectroscopy

UV-visible spectroscopy was used to measure the absorption capabilities of certain compounds with reference to wavelengths of light in the ultraviolet and visible light ranges. The absorbance spectra of the GQDs, GQDs-AuNPs and cit-AuNPs were collected using a double beam, UV-2600 spectrophotometer, Shimadzu Company in Japan and the spectral range of 400-800 nm. The operating conditions of UV-Visible spectroscopy parameters are listed in table 3.3.

3.6.1.2 Fluorescence spectroscopy

Fluorescence spectroscopy is used to determine the concentration of an analyte in solution on the basis of its fluorescence properties. Fluorescence spectra of GQDs and GQDs-AuNPs were assessed with a LS-55 spectrofluorometer, PerkinElmer

Ltd Company in United State of America (USA) and the spectral range of 190-800 nm. The operating conditions of fluorescence spectroscopy parameter listed in table 3.3.

3.6.1.3 Transmission Electron Microscopy (TEM)

Transmission Electron Microscopy (TEM) model: a JEM-1230; JEOL from Japan was used to observe the morphology and size characterized of GQDs-AuNPs. The GQDs-AuNPs was transferred to 200 mesh of Cu grid and detect at an accelerating voltage of 200 kV. The operating conditions of TEM parameter listed in table 3.3.

3.6.1.4 Fourier Transform Infrared (FT-IR) spectroscopy

Fourier Transform Infrared (FT-IR) spectroscopy is an important technique for investigation nanoparticle structure and composition. GQDs, GQDs-AuNPs and AuNPs were characterized by using attenuated total reflection (ATR) mode, spectrum II FT-IR spectrometer equipped with a diamond ATR cell from PerkinElmer Ltd Company in USA. The transmission spectra were measured at room temperature in the wavenumber range of 400 to 4000 cm^{-1} for colloids solution of nanoparticles. The operating conditions of ATR-FTIR parameter listed in table 3.3.

Table 3.3 The operating conditions of UV-Visible spectroscopy, fluorescence spectroscopy, TEM and FTIR.

UV-Visible spectroscopy operating conditions	
Slit width (nm)	1.0
Scan range (nm)	400-800
Scan speed	medium
Sample interval (nm)	0.5
Fluorescence spectroscopy operating conditions	
Excitation wavelength (nm)	393
Emission wavelength (nm)	486
excitation and emission slit width (nm)	10

Table 3.3 The operating conditions of UV-Visible spectroscopy, Fluorescence spectroscopy, TEM and FTIR (Continued).

Fluorescence spectroscopy operating conditions	
photomultiplier tube voltage (V)	auto
Scan speed (nm/min)	500
Spectral range (nm)	200-600
TEM operating conditions	
Acceleration voltage (kV)	200
Time scan(s)	300
Temperature (°C)	25
FTIR operating conditions	
Spectral range (cm ⁻¹)	400-4000
Resolution (cm ⁻¹)	4
Temperature (°C)	25

3.6.2 Parameters that effect the sensitivity of the chlorpyrifos detection

3.6.2.1 Effect of buffer pH (50 mM PBS)

The effect of pHs on the performance of the GQDs-AuNPs reactivity and enzyme activity for detection of chlorpyrifos pesticide was studied by varying the solution pH at 4, 5, 6, 7, 8, 9 and 10 using 0.5 mM PBS. An aliquot of 0.6 mL PBS with different pHs and 0.9 mL of GQDs-AuNPs were added into micro-centrifuge tube and incubated for 30 min at 25 °C. The mixture solution was investigated by UV-visible spectrophotometer. UV-visible absorption spectra and color change of GQDs-AuNPs according to pH variation were recorded. The results are presented in Section 4.1.3.1.

3.6.2.2 Effect of ATCh concentration

Effect of ATCh concentration on the performance of colorimetric assay was investigated from 50 to 500 µM. Firstly, 0.1 mL of different concentration of ATCh (50, 100, 200, 300 and 500 µM) was added into micro-centrifuge tube and incubated for 30 min at 25 °C. Next, 0.9 mL of GQDs-AuNPs was added into the solution and the final volume of 1.5 mL was adjusted by pH 7.0 of 50 mM PBS. Finally, the resulting solution was investigated by UV-Visible spectrophotometer. Variation of

absorbance at 520 nm versus reaction time was also recorded every 5 min with the variation of ATCh concentrations. The results shown in Section 4.1.3.2.

3.6.2.3 Effect of AChE enzyme concentrations

The effect of AChE concentration on the assay response was investigated in the range of 100 to 500 mU mL⁻¹ by using UV-Visible spectrophotometer. Experimentally, 0.2 mL of the various concentration of AChE (100, 200, 300, 400 and 500 μ M) was reacted with fixed volume of 50 μ M ATCh at 0.1 mL in micro-centrifuge tube. The resulting solution was incubated for 30 min at 25 °C. Then, 0.9 mL of GQDs-AuNPs was added to the mixture solution and the final volume of 1.5 mL was adjusted by pH 7.0 of 50 mM PBS. The final solution was examined by UV-visible spectrophotometer to find the most sensitive condition for chlorpyrifos detection and absorbance was recorded every 5 min for 1 h. The results illustrate in Section 4.1.3.3.

3.6.2.4 Effect of reaction time

The effect of reaction time in the range of 0 to 60 min for colorimetric assay was investigated. 0.2 mL of 200 mU mL⁻¹ AChE and 0.1 mL of 50 μ M ATCh were added into micro-centrifuge tube and incubated for 30 min at 25 °C. Then, 0.9 mL of GQDs-AuNPs was added to the mixture solution and the final volume of 1.5 mL was adjusted by pH 7.0 of 50 mM PBS. The incubation times was varied at 0, 5, 10, 15, 20, 25, 30, 35, 40, 45, 50, 55 and 60 min. The final solution was examined by UV-visible spectrophotometer to find the most suitable reaction time for chlorpyrifos detection. The results shown in Section 4.1.3.4.

3.6.3 Colorimetric method for chlorpyrifos detection

3.6.3.1 Colorimetric method study of chlorpyrifos

Colorimetric method for chlorpyrifos assay illustrates in Figure 3.3. Chlorpyrifos determination was performed as follows: (i) 10 μ L of AChE (200 mU mL⁻¹) and 100 μ L of ATCh (50 μ M) were added into a 2 mL centrifuge tube. (ii) 200 μ L of chlorpyrifos standard was added to the mixture and the resulting solution was incubated for 30 min at 25 °C. (iii) 0.9 mL of GQDs AuNPs and 290 μ L of PBS (50 mM, pH 7.0) was added to make the final volume as 1.5 mL and then the solution was incubated from 30 min. The final reaction solution was monitored by UV-Visible spectrophotometer. Figure 3.3 shows diagram of colorimetric method for chlorpyrifos detection.

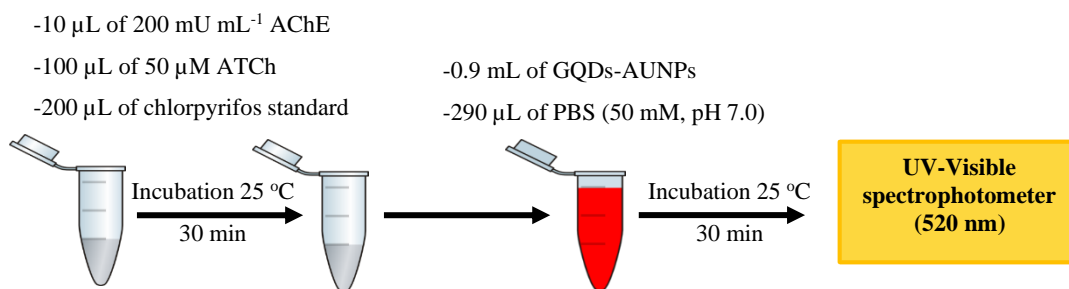


Figure 3.3 Schematic diagram of colorimetric assay for chlorpyrifos detection by using GQDs-AuNPs.

3.6.3.2 Linear concentration range of chlorpyrifos

Difference standard solutions of chlorpyrifos were prepared by diluting the appropriate amount of chlorpyrifos with PBS to give working solutions in the range of 0 to 50 µg mL⁻¹. The resulting calibration solution were prepared and measured triplicate. The reaction solution was based on AChE-enzyme catalyzed hydrolysis of an ATCh substrate to produce thiol-bearing thiocholine, which causes the aggregation of GQDs-AuNPs, to generate a purple-blue colored product. The hydrolysis reaction is inhibited in the presence of chlorpyrifos, resulting in anti-aggregation of GQDs-AuNPs, a red-colored product. The absorbance response of GQDs-AuNPs was recorded at 520 nm by UV-Visible spectrophotometer. The results present in Section 4.1.4.1.

3.6.3.3 Limit of detection (LOD) of chlorpyrifos

In this study, the limit of detection (LOD) for chlorpyrifos was examined by using measuring absorption spectra of blank solution of chlorpyrifos (0.0 µg mL⁻¹) with the ten replicates. The LOD was calculated on the basic of 3-fold of standard deviation per slope ($3S.D._{\text{blank}}/\text{slope}$) where S.D. is standard deviation of absorbance GQDs-AuNPs at 520 nm for blank signal and slope is the slope of calibration curve. The results were shown in Section 4.1.4.2.

3.6.4 Interference study

The effect of potential interferences that are likely present in vegetable samples, including cations (K⁺, Na⁺, Fe³⁺, Ca²⁺, Zn²⁺, Ni²⁺ and Mg²⁺), anions (NO³⁻, I⁻, S²⁻, and PO₄³⁻) and compound molecules (fructose, maltose, glucose and ascorbic acid) were investigated. The interference effect was evaluated by adding different amounts of

competing substance into $20 \mu\text{g mL}^{-1}$ of chlorpyrifos standard solution, and comparing the intensity response to that for the initial chlorpyrifos measurement. The concentration of the interferent specie that provided absorbance change greater than $\pm 5\%$ was considered as the tolerance limit. The results were discussed in Section 4.1.5.

3.7 Part II: The three-dimensional microfluidic paper-based analytical device (3D- μ PAD) for chlorpyrifos determination

3.7.1 Design of 3D- μ PAD

3D- μ PAD for colorimetric chlorpyrifos assay was designed by having two parts on paper in one sheet. The top-layer or test sheet, consisting of two 5 mm circles; one circle forms the detection zone, for placing the GQDs-AuNPs and AChE-enzyme mixture, and the other is a loading area, for adding buffer for analyte elution. When folded, the detection zone and loading area align with a hydrophilic dumbbell-shape printed on the bottom-layer sampling sheet. The dumbbell shape features two 5 mm circles connected by a straight 2×8 mm channel. The bottom circle area of the dumbbell-shape was used as sample loading by applying the mixed solution of sample/standard (chlorpyrifos) and ATCh (substrate). After loading the 3D- μ PAD, the test sheet is folded so that the circles in the upper and lower layers align. Sample then elutes from the loading area and into the detection zone, where reaction with GQDs-AuNPs occurs. As shown in Figure 3.4.

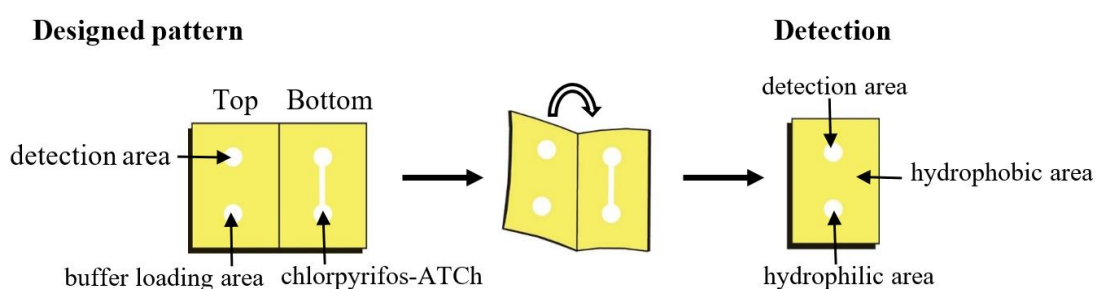


Figure 3.4 The designed 3D- μ PAD for chlorpyrifos detection using a foldable sheet consisting of two parts (top/bottom layer).

3.7.2 Fabrication of 3D- μ PAD for assay using GQDs-AuNPs reactions

The chlorpyrifos 3D- μ PAD was fabricated by using a paper sheet, folded to form upper and lower layers. The pattern on the chlorpyrifos 3D- μ PAD was fabricated by one-step polymer-screen printing, using rubber latex (RL) waste as the hydrophobic barrier [47]. Finely chopped RL (3.8 g) was placed in a 250 mL glass-beaker. Toluene (200 mL) was added and mixed to form a homogeneous RL solution. The solution was incubated at room temperature overnight. The resulting solution (80 mL) was added into gasoline (20 mL) using RL solution and gasoline in a 4:1 volume ratio. The mixture was shaken until homogeneous (~5 min) and the resulting solution screened on Whatman No.4 filter paper under a wooden-framed woven mesh screen (888.32 mesh, 60T), which was designed and patterned as shown in Figure 3.5. First, the patterned screen was placed directly on a sheet of No. 4 Whatman paper, and the RL solution was forced through the screen by using a squeegee. The RL solution created a patterned hydrophobic barrier as it penetrated to the bottom of the paper. The patterned paper was ready for use after removal from the screen. Finally, the fabricated device was cut out from the patterned sheet. The results were discussed in Section 4.2.1.

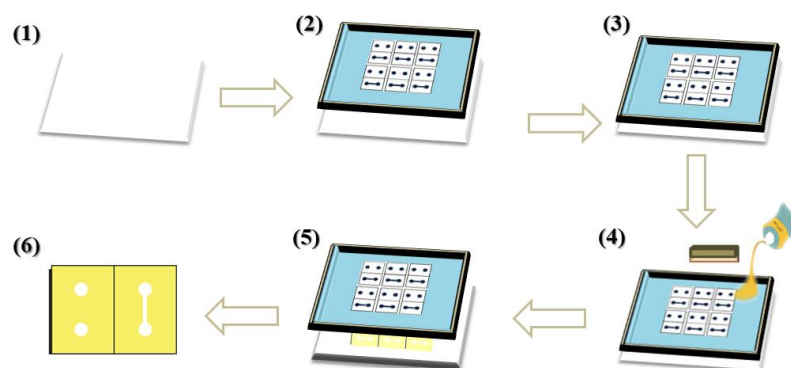


Figure 3.5 Fabrication of the chlorpyrifos 3D- μ PAD by using one-step polymer screen printing; Position a sheet of Whatman No.4 filter paper (1), Place the wooden-framed woven mesh screen (888.32 mesh (60T) nylon mesh) on the paper (2), Position the screen pattern to contact the paper surface (3), squeeze RL solution through the screen to penetrate to the bottom of the paper, creating a patterned hydrophobic barrier (4), remove paper from the screen, the patterned paper is ready for use (5), and Cut out individual fabricated devices piecewise (6).

Analysis in this μ PAD study was carried out in a homemade control light box consisting of top turbidity plastic cover and control light box as illustrated in Figure 3.6. The box was employed to minimize interference from the luminosity. The operating conditions of photography with control light box system were listed in Table 3.4.

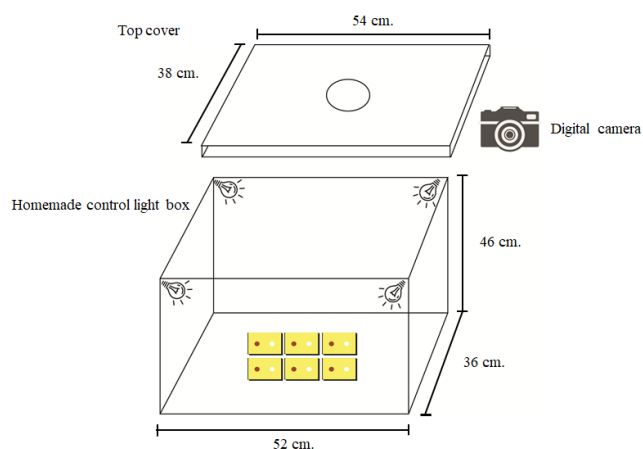


Figure 3.6 Homemade control light box. An Image is captured by using a digital camera set to automatic mode.

Table 3.4 The operating conditions of photography with control light box system.

Homemade control light box system	
Dimension (wide (cm) x long (cm) x high (cm))	36 x 52 x 46
Illuminance (lx)	2400
Digital camera	
ISO rating	400
Digital zoom	1.5x
Auto focus type	TTL
Resolution (pixels)	4000 x 3000
Image ratio	4 : 3

3.7.3 Parameters that effect the sensitivity of the chlorpyrifos detection

3.7.3.1 Optimization of the color intensity values

To optimize the color intensity values in the RGB system (R (red), G (green), B (blue)) obtained from the measurement using our proposed 3D- μ PAD in the presence of chlorpyrifos was performed. Resulting reaction using difference standard solution of chlorpyrifos (0.0, 0.1, 0.3, 0.5, 0.8 and 1.0 $\mu\text{g mL}^{-1}$) in the detection zone was captured in the homemade control light box by using digital camera. An image of the detection zone was measured by ImageJ program (<https://imagej.nih.gov/ij/>). Then, the original image was separated in four color intensity values (being gray in red channel, gray in green channel, gray in blue channel and filter average gray) and the calibration curves were plotted in OriginPro 8. Calibration graphs were constructed by measuring the change between the intensity of color upon the sensor reacting with different concentration of standard chlorpyrifos and that of the blank. The results were discussed in Section 4.2.2.1.

3.7.3.2 Effect of buffer pH (50 mM PBS)

To measure chlorpyrifos using our developed 3D- μ PAD, 0.5 mL of GQDs-AuNPs and 0.5 mL of AChE (5.0 U mL^{-1}) solutions were added to a 1 mL micro-centrifuge tube and mixed using a vortex mixer for 2 min. $5.0 \mu\text{L}$ of the resulting mixture was applied to the detection zone. After combining 0.4 mL of ATCh (0.5 mM), 0.2 mL of chlorpyrifos standard, and 0.4 mL of PBS (pH 7.0) in a 1 mL micro-centrifugal tube. $8.0 \mu\text{L}$ of the ATCh-chlorpyrifos mixture was applied to the loading area at one end of the dumbbell, and incubated for 5 min at room temperature. The upper and lower layers were folded together and the 3D- μ PAD was placed on an acrylic block to perfectly align the top and the bottom layers, and so clip them together. Finally, $8.0 \mu\text{L}$ of difference pHs (pH 6.0, 6.5, 7.0, 7.5, 8.0, 8.5 and 9.0) of PBS was dropped onto the loading area. The PBS buffer eluted the chlorpyrifos-ATCh mixture along the channel and gather to the detection area. The elution process was allowed to proceed for 15 min at room temperature. Images of the detection zone were then captured in a homemade light box (Figure 3.6) by using a digital camera set to automatic mode. The color changes in the detection area were analyzed by using ImageJ software. The results were discussed in Section 4.2.2.2.

3.7.3.3 Effect of buffer volume

The effect of buffer volume for elution of chlorpyrifos-ATCh from the loading area to the detection zone was investigated. The volume of buffer was varied at 4.0, 6.0, 8.0 and $10.0 \mu\text{L}$ (50 mM PBS, pH 7.0). $5.0 \mu\text{L}$ of mixture (GQDs-AuNPs and of AChE (15 U mL^{-1})) solution was applied to the detection zone. Then, $8.0 \mu\text{L}$ of chlorpyrifos-ATCh mixture solution (0.2, 0.4 and 0.4 mL at concentration of chlorpyrifos ($0.5 \mu\text{g mL}^{-1}$), ATCh (5.0 mM) and PBS (pH 7.0), respectively) was applied to the loading area, and incubated for 5 min at room temperature. The upper and lower layers were folded together and the 3D- μ PAD was placed on an acrylic block to perfectly align the top and the bottom layers, and so clip them together. Finally, the various buffer volume at 4.0, 6.0, 8.0 and $10.0 \mu\text{L}$ was dropped onto the buffer loading area and incubated for 30 min at room temperature. The color changes in the detection area captured from digital camera are analyzed by using ImageJ software. The results are presented in Section 4.2.2.3.

3.7.3.4 Effect of ATCh concentrations

To optimize concentration for ATCh within the range of 0.1 to 10 mM was investigated. Experimentally, 5.0 μL of mixture (GQDs-AuNPs and of AChE (15 U mL^{-1})) solution was applied to the detection zone. Next, difference concentration of ATCh (0.0, 0.1, 0.3, 0.5, 1.0, 5.0 and 10 mM) was reacted with fixed volume of 0.5 $\mu\text{g mL}^{-1}$ chlorpyrifos at 0.2 mL and the final volume of 1.0 mL was adjusted by pH 7.0 PBS. 8.0 μL of the ATCh-chlorpyrifos mixture was applied to the loading area, and incubated for 5 min at room temperature. The upper and lower layers were folded together and the 3D- μPAD was placed on an acrylic block to perfectly align the top and the bottom layers, and so clip them together. Finally, 8.0 μL of PBS (50 mM, pH 7.0) was dropped onto the buffer loading area and incubated for 30 min at room temperature. The color intensities of reaction captured from digital camera were recorded based on RGB system calculated by ImageJ. The results present in Section 4.2.2.4.

3.7.3.5 Effect of AChE enzyme concentrations

The activity and concentration of AChE on the response of the assay was investigated in the range of 0.5 to 20 U mL^{-1} . Experimentally, 0.5 mL of the various concentration of AChE (0.0, 0.5, 1.0, 5.0, 10, 15 and 20 U mL^{-1}) in fixed 0.5 mL of GQDs-AuNPs was examined to find the most condition for chlorpyrifos detection. 5.0 μL of the resulting mixture was applied to the detection zone. Then, 8.0 μL of chlorpyrifos-ATCh mixture solution (0.2, 0.4 and 0.4 mL at concentration of chlorpyrifos ($0.5 \mu\text{g mL}^{-1}$), ATCh (5.0 mM) and PBS (pH 7.0), respectively) was applied to the loading area, and incubated for 5 min at room temperature. The upper and lower layers were folded together and the 3D- μPAD was placed on an acrylic block to perfectly align the top and the bottom layers, and so clip them together. Finally, 8.0 μL of PBS (50 mM, pH 7.0) was dropped onto the buffer loading area and incubated for 30 min at room temperature. The color intensities of reaction captured from digital camera were recorded based on RGB system calculated by ImageJ. The results present in Section 4.2.2.5.

3.7.3.6 Effect of reaction time

The effect of reaction time in the range of 0 to 60 min for chlorpyrifos detection was studied. Firstly, 5.0 μL of mixture (GQDs-AuNPs and AChE (5.0 U mL^{-1})) solution was applied to the detection zone. Then, 8.0 μL of chlorpyrifos-ATCh mixture solution (0.2, 0.4 and 0.4 mL at concentration of chlorpyrifos (0.5 $\mu\text{g mL}^{-1}$), ATCh (5.0 mM) and PBS (pH 7.0), respectively) was applied to the loading area, and incubated for 5 min at room temperature. The upper and lower layers were folded together and the 3D- μPAD was placed on an acrylic block to perfectly align the top and the bottom layers, and so clip them together. Finally, 8.0 μL of PBS (50 mM, pH 7.0) was dropped onto the buffer loading area. The reaction time was varied at 0.0, 5.0, 10, 15, 20, 30 and 40 min. The color intensities of reaction were recorded based on RGB system calculated by ImageJ. The results present in Section 4.2.2.6.

3.7.4 Colorimetric method for chlorpyrifos detection

3.7.4.1 Colorimetric method study of chlorpyrifos

To measure chlorpyrifos using developed 3D- μPAD , 0.5 mL of GQDs-AuNPs and 0.5 mL of AChE solutions (5.0 U mL^{-1}) were added to a 1.0 mL micro-centrifuge tube and mixed using a vortex mixer for 2 min. 5.0 μL of the resulting mixture is applied to the detection zone. After combining 0.4 mL of ATCh (0.5 mM), 0.2 mL of chlorpyrifos standard, and 0.4 mL of PBS (50 mM, pH 7.0) in a 1 mL micro-centrifugal tube. 8.0 μL of the ATCh-chlorpyrifos mixture was applied to the loading area at one end of the dumbbell, and incubated for 5 min at room temperature. The upper and lower layers were folded together and the 3D- μPAD was placed on an acrylic block to perfectly align the top and the bottom layers, and so clip them together. Finally, 8.0 μL of PBS was dropped onto the loading area. The PBS buffer elutes the chlorpyrifos-ATCh mixture along the channel and gather to the detection area. The elution process is allowed to proceed for 15 min at room temperature. Images of the detection zone are then captured in a homemade light box by using a digital camera set to automatic mode. The color changes in the detection area are analyzed by using ImageJ software. Figure 3.7 shows the diagram of colorimetric assay for chlorpyrifos detection.

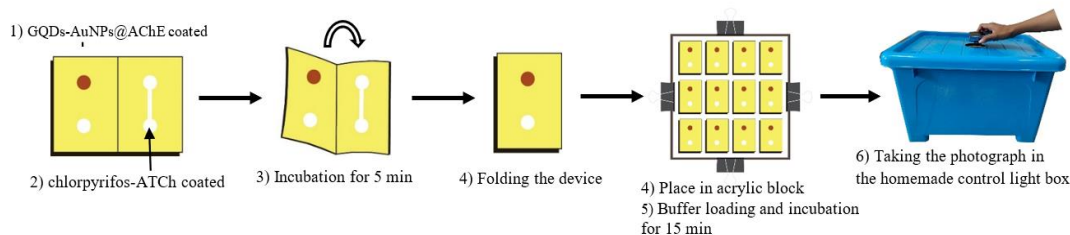


Figure 3.7 The typical procedure for chlorpyrifos determination on 3D- μ PAD.

3.7.4.2 Linear range of chlorpyrifos

Calibration curve of chlorpyrifos was examined by using the developed 3D- μ PAD. Difference chlorpyrifos standard solutions were prepared by diluting the appropriate amount of chlorpyrifos with PBS to give the working solutions in the range of 0.001 to 1.0 $\mu\text{g mL}^{-1}$. The resulting calibration were prepared and measured quintuple. Detection of chlorpyrifos was based on inhibition of AChE-enzyme catalyzed hydrolysis of ATCh, resulting in anti-aggregation of GQDs-AuNPs and the formation of a colored product. The color changes in the detection area captured by digital camera were analyzed by using ImageJ software. The results shown in Section 4.2.3.1.

3.7.4.3 Limit of detection (LOD) of chlorpyrifos

In this study, the LOD for chlorpyrifos was examined by using measuring green intensity of blank of chlorpyrifos ($0.0 \mu\text{g mL}^{-1}$) on detection zone with the ten replicates. The LOD was calculated on the basic of 3-fold of standard deviation per slope ($3S.D.\text{blank}/\text{slope}$) where S.D. is standard deviation of color intensity GQDs-AuNPs for blank signal ($n=10$) and slope is the slope of calibration curve. The results shown in Section 4.3.3.2.

3.7.5 Interference study

The effect of potential interferences that are likely present in vegetable samples were investigated. The interested ions and compounds molecule were selected as the interferences by using the developed 3D- μ PAD for detection. The interference effect was evaluated by adding different amounts of competing substance into 0.05 $\mu\text{g mL}^{-1}$ chlorpyrifos standard, and comparing the intensity response to that for the initial chlorpyrifos measurement. The concentration of the interferent species that provide color intensity change greater than $\pm 5\%$ was considered as the tolerance limit. The results were discussed in Section 4.2.4.

3.7.6 Samples preparation

To evaluate the practical applicability of the designed 3D- μ PAD, vegetable samples were assayed using a spiked recovery experiment. Cucumber, radish, lettuce, carrot, cabbage, and tomato were purchased from a local market in Ubon Ratchathani Province, Thailand. Samples were prepared following an extraction method described by Harshit et al [101]. Briefly, finely cut and chopped 25 g samples of various vegetables were weighed, and 50 mL of acetonitrile was added to each sample. Samples were homogenized in a blender for 3 min, then centrifuged at 4000 rpm for 10 min, and supernatants from the centrifuge tubes were collected. Finally, solution samples were filtered through a PTFE syringe filter (33 x 0.22 μm) prior to chlorpyrifos determination.

3.7.7 Method validation

Chlorpyrifos concentration results obtained the proposed 3D- μ PAD were compared to those obtained from a standard HPLC method [101]. Analysis was performed in triplicate using HPLC equipment, model CTO-10AC (Shimadzu, Japan), coupled to a SPD-20A UV/Vis detector. Separation was performed using a separation column; C-18 (VertiSepTM UPS, 4.6 x 250 mm, 5.0 μm), isocratic elution with an acetonitrile: water mobile phase (90 : 10 v/v), 1.0 mL min^{-1} flow rate, 20 μL injection volume, detection at 219 nm absorbance and column temperature of 25 $^{\circ}\text{C}$. Experimentally, 0.5 mL of the difference concentration of chlorpyrifos (0.0, 0.03 and 0.1 $\mu\text{g mL}^{-1}$) was reacted with fixed volume of each samples solution at 0.2 mL in microcentrifuge tube and the final volume of 1.0 mL was adjusted by mobile phase. The resulting solution was examined by HPLC to detect chlorpyrifos in spiked vegetable samples. The results were discussed in Section 4.2.5.

CHAPTER 4

RESULTS AND DISCUSSION

4.1 Part I: Spectrophotometric method for determination of chlorpyrifos

4.1.1 Characterizations of nanomaterials

4.1.1.1 UV-Visible spectroscopy

UV-Visible spectroscopy was used to investigate the absorption spectra of GQDs, GQDs-AuNPs, and cit-AuNPs nanocomposite materials. As shown in Figure 4.1, GQDs prepared by pyrolysis (curve (a), yellow product) did not show absorption band. Whereas AuNPs prepared using tri-sodium citrate and GQDs as reducing agents (cit-AuNPs and GQDs-AuNPs) show a unique surface plasmon bands at 520 nm, attributed to monodispersed particles (curves b and c). The red color and the maximum absorbance (λ_{\max}) at 520 nm obtained from GQDs-AuNPs indicates their effectiveness as reducing agent and stabilizer.

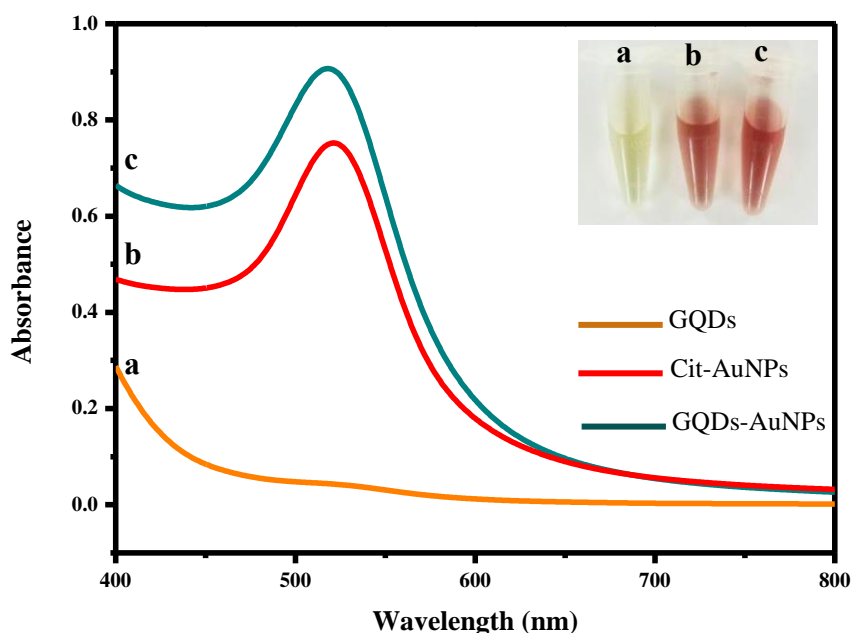


Figure 4.1 Absorbance spectra of GQDs (a), GQDs-AuNPs (b), and cit-AuNPs (c).

Inset shows the respective images.

4.1.1.2 Fluorescence spectroscopy

Fluorescence spectra were investigated to further explore the optical properties of GQDs and GQDs-AuNPs. As displayed in Figure 4.2a, the GQDs in aqueous solution shows strong fluorescence intensity with an emission maximum (λ_{em}) at 486 nm and excitation (λ_{ex}) at 393 nm. This observation is similar to the result reported by J. Shi et al [45] that the GQDs emitted intense blue light with the λ_{em} around 460 nm (λ_{ex} = 365 nm). On the other hand, the GQDs-AuNPs exhibited weak fluorescence intensity due to the AuNPs can act as electron acceptor to quench fluorescence in the photoinduced electron transfer (PET) process and the fluorescence intensity of GQDs-AuNPs shows λ_{em} at 458 nm (λ_{ex} = 343 nm) (Figure 4.2 b).

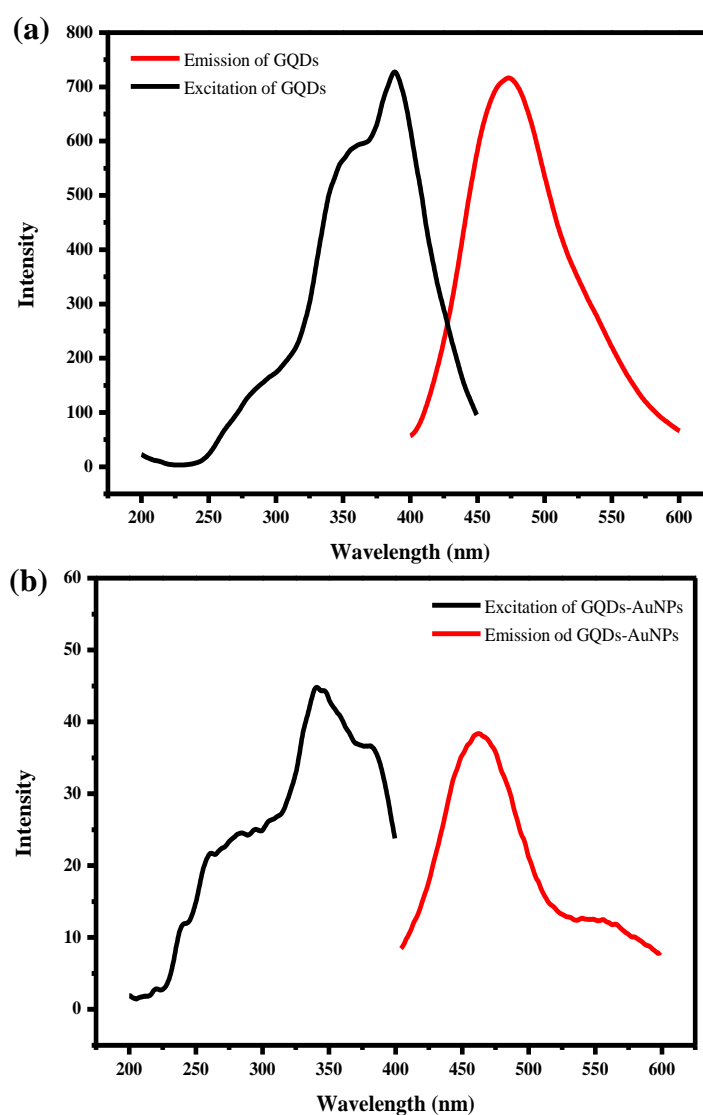


Figure 4.2 Fluorescence spectra of GQDs (a) and GQDs-AuNPs (b).

4.1.1.3 Transmission Electron Microscopy (TEM)

TEM analysis was performed in order to investigate the morphology and size of as prepared GQDs-AuNPs. TEM images from Figure 4.3 show that GQDs-AuNPs have round shapes and uniform sizes, with an average diameter of 12 ± 0.26 nm ($n = 20$). The inset figure shows that large AuNPs were surrounded by many smaller GQDs, forming a satellite type structure. TEM images also show that the well-dispersed GQDs had diameters of approximately 3 nm. This results were in good agreement with a previous report [45] that AuNPs synthesized by using citrate as the reducing agent had diameters of approximately 15 nm and GQDs synthesized by pyrolysis had smaller average diameters of 3 ± 1 nm. In this work, GQDs were used as a reducing agent and as a stabilizer by capping on the AuNPs surface.

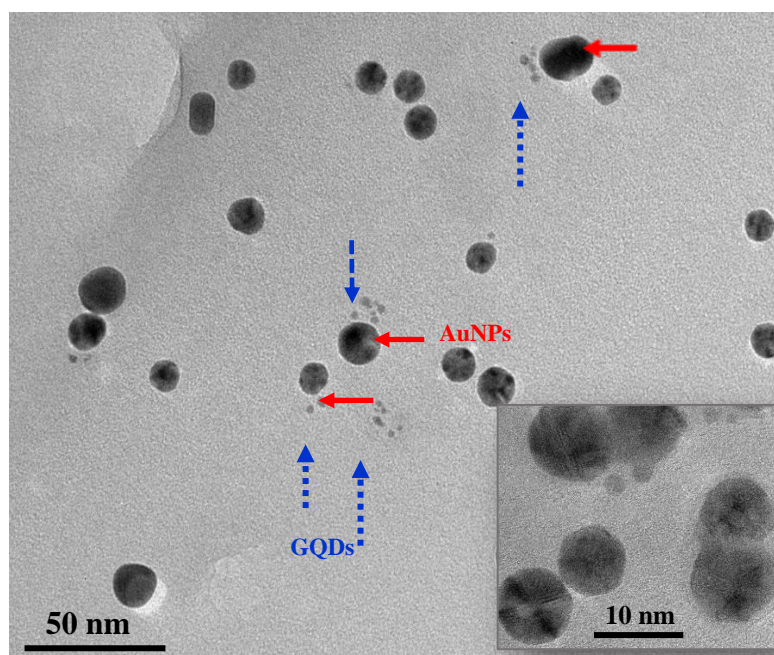


Figure 4.3 TEM images of well-dispersed GQDs-AuNPs nanocomposites. Inset is enlarged nanocomposite image.

4.1.1.4 Fourier-transform infrared spectroscopy (FTIR)

FT-IR spectra of the as-prepared nanocomposites are shown in Figure 4.4. Citrate-stabilized AuNPs spectrum (curve a) shows absorption bands at 1690 cm^{-1} and 3542 cm^{-1} which attributed to citrate carboxylate ion (COO^-) and $-\text{OH}$ stretching, respectively. GQDs spectrum (curve b) shows $-\text{OH}$ and COO^- absorption bands at 1690 and 1386 cm^{-1} due to bending vibrations and an $-\text{OH}$ stretching absorption at 3427 cm^{-1} . Spectrum of GQDs-AuNPs (curve c) exhibits all three characteristic GQDs bands, together with the characteristic of AuNPs absorption bands. These results indicate the successful preparation of GQDs-AuNPs. The confirmation data of GQDs-AuNPs formation is consistent with previous report from J. Shi et al. [45].

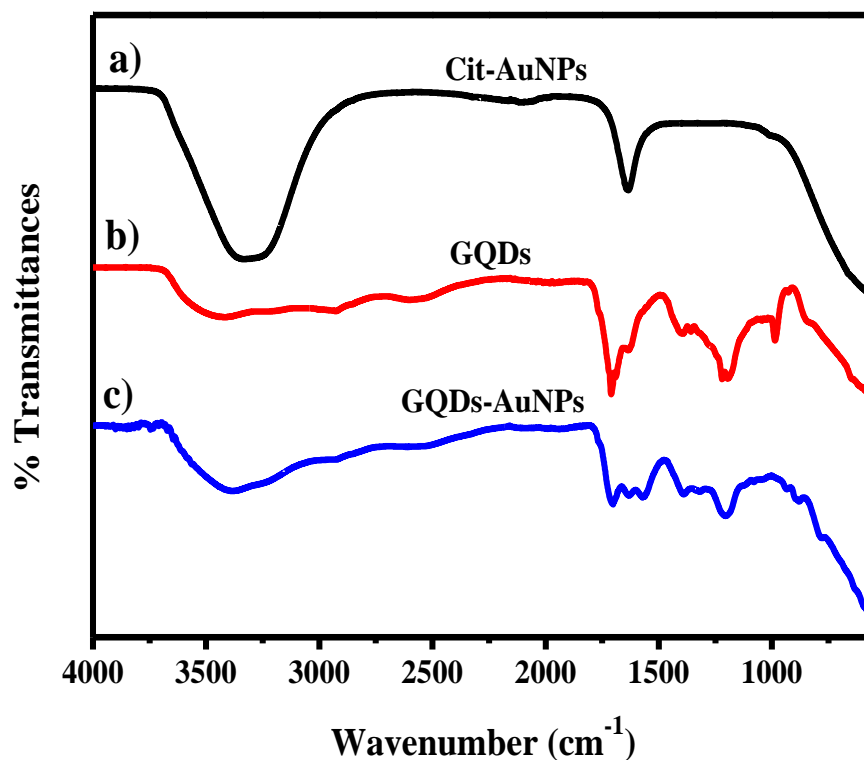


Figure 4.4 FT-IR spectra of GQDs-AuNPs, GQDs, and Cit-AuNPs.

4.1.2 Detection mechanism of the colorimetric method for chlorpyrifos detection

GQDs-AuNPs was used as a color probe for colorimetric assay due to easy preparation, biocompatibility, stability and high extinction coefficients. The solution of GQDs-AuNPs well-dispersed present red color, while those the aggregates of GQDs-AuNPs exhibited blue color. Chlorpyrifos is known to inhibit AChE activity by binding to the active site of an enzyme. This result suppresses ATCh hydrolysis, thereby blocking the generation of thiocholine [35]. In this study, detection of chlorpyrifos was based on competitive inhibition between chlorpyrifos and the GQDs-AuNPs-AChE-ATCh reagent. UV-Visible spectrophotometer was used to monitor changes in absorbance to investigate the reaction mechanism. As shown in Figure 4.5, GQDs-AuNPs absorption spectrum exhibits a characteristic peak at 520 nm (curve a). Addition of 50 μM ATCh (pH 7.0 PBS) does not show any color change (curve b). This result reveals that ATCh does not affect the absorption properties of the reaction solution. After addition of AChE (200 mU mL^{-1}) to the reaction solution and incubating for 30 min, the peak at 520 nm decreases and a new absorbance band appears at 650 nm (curve c). The color of solution changes from red to purple-blue, which is clearly visible to the naked eye (inset, Figure 4.5). Enzymatic hydrolysis of ATCh by AChE releases thiocholine. The thiol group in thiocholine interacts with the AuNPs to cause aggregation of the nanoparticles, and this produce of the color change [40, 41]. Addition of chlorpyrifos (curve d) inhibits AChE hydrolysis of ATCh, leading to anti-aggregation of GQDs-AuNPs. The detection mechanism of the proposed assay illustrates in detail in Figure 4.6.

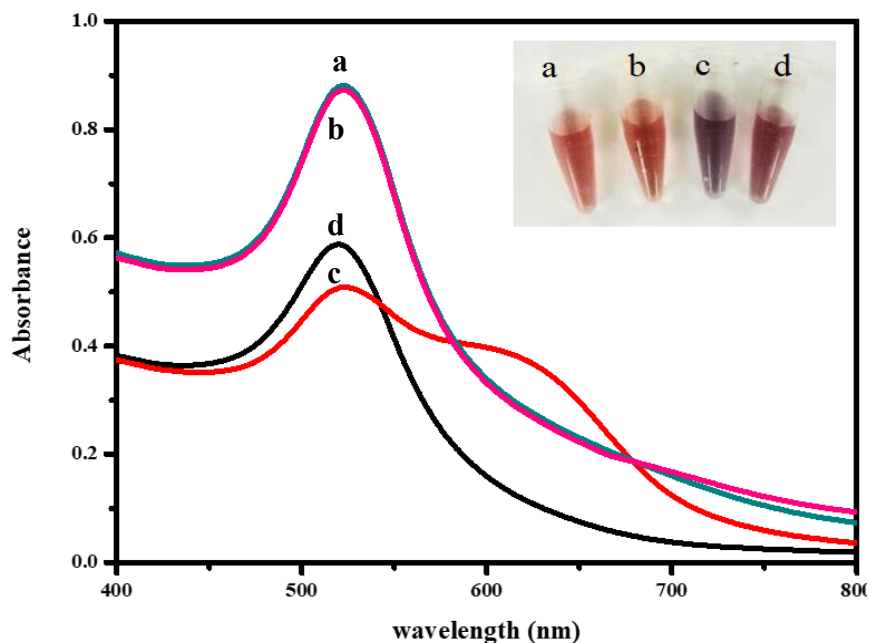


Figure 4.5 Absorption spectra of GQDs-AuNPs (a), GQDs-AuNPs after the addition of ATCh (50 μM , pH 7.0 PBS) (b), GQDs-AuNPs after the addition of ATCh (50 μM , pH 7.0 PBS) and AChE (200 mU mL^{-1}) (c), GQDs-AuNPs after the addition of ATCh (50 μM , pH 7.0 PBS), AChE (200 mU mL^{-1}) and chlorpyrifos (5.0 $\mu\text{g mL}^{-1}$) (d). Incubation was performed at 25 $^{\circ}\text{C}$ for 30 min.

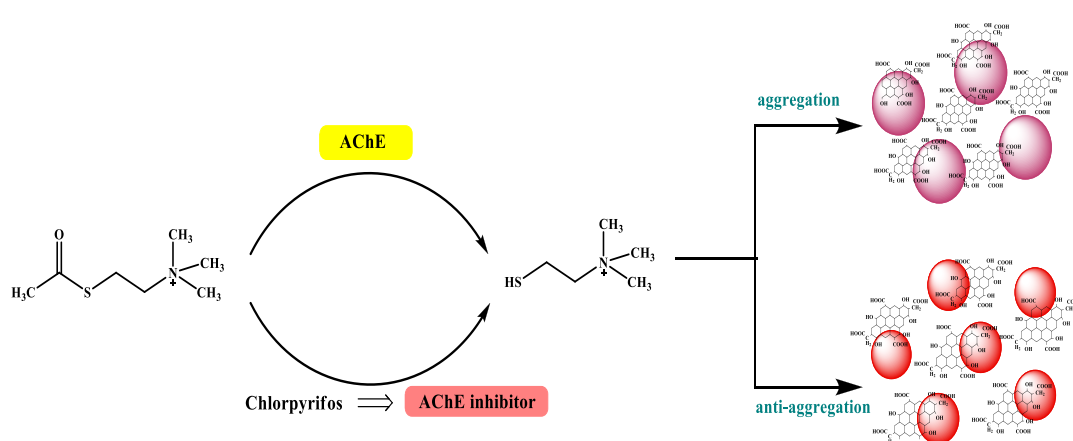


Figure 4.6 The proposed mechanism of chlorpyrifos colorimetric detection based on GQDs-AuNPs reaction.

4.1.3 Parameters that effect the sensitivity of the chlorpyrifos detection

4.1.3.1 Effect of pH of phosphate buffer saline

The pH of solution could influence the performance of the GQDs-AuNPs. It has considerable effect on morphology, size, surface area and color change of GQDs-AuNPs. Hence, the effect of pH value for the absorption and color of solution was investigated over the range of pH 4 to 10 using 50 mM PBS. As shown in Figure 4.7, the absorption spectra of GQDs-AuNPs increased with pH and reached a maximum at pH 7.0. Further increasing of pH resulted in weaker absorption spectra. At the lower pH below 7.0 the aggregation was caused and the color of GQDs-AuNPs was changed due to electrostatic interaction between the negatively charge of GQDs on the AuNPs surface and acidic (H^+). At the higher pH above 7.0 slightly aggregation of GQDs-AuNPs was found because the solution presents OH^- (base), leading to the electrostatic repulsion and made them move in the opposite directions. The inset figure shows that the color of GQDs-AuNPs change with different pHs. The result shows that natural pH at 7.0 almost has no influence on the color change of GQDs-AuNPs, whereas the other pH could induce the aggregation and color change of GQDs-AuNPs. In addition, the un neutral pH could induce the AChE denature and result in lower activity of the enzymes. Therefore, the pH at 7.0 (50 mM PBS) was selected as the optimum detection medium in further experiments. The pH used in this work was similar to the result reported by Y. Shen et al [102], that the pH of solution at pH 7.4 was the optimum value. They were reported that the optimum pH values for preparation of nanoparticle and AChE was pH 7.0-8.0.

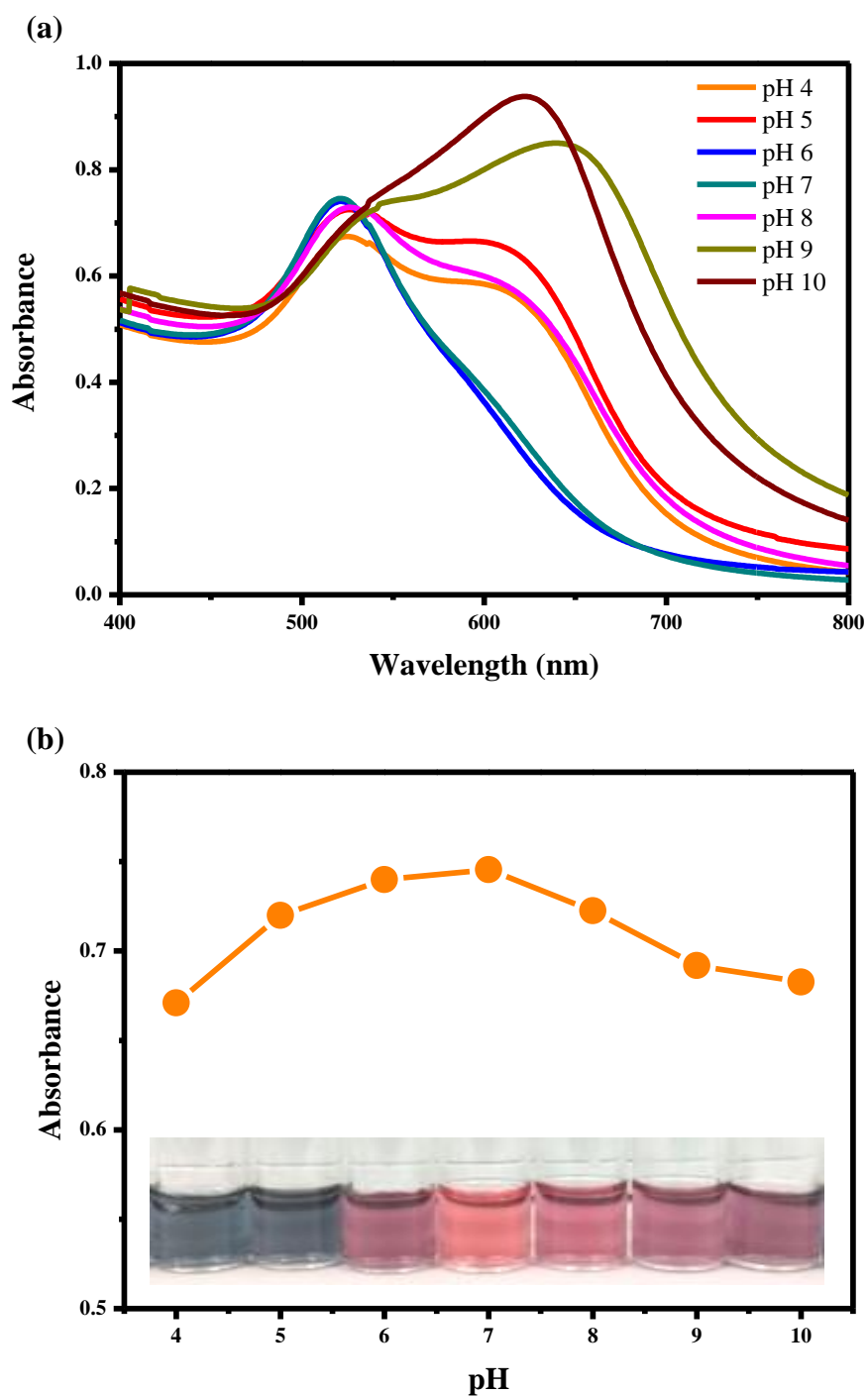


Figure 4.7 The effect of pHs on the performance of the GQDs-AuNPs reactivity and AChE enzyme activity. Absorption spectra of the GQDs-AuNPs in various pHs (a) and the variation of absorption spectra of GQDs-AuNPs at 520 nm with pHs (b). The inset figure shows the color change of GQDs-AuNPs with the variation of pHs.

4.1.3.2 Effect of the ATCh concentrations

The effect of ATCh concentration on the performance of GQDs-AuNPs was investigated from 50 to 500 μM and the corresponding absorbances were recorded every 5 min for 1 h. It was found that extreme ATCh concentration could result in the aggregation and spectral change of GQDs-AuNPs due to electrostatic interactions between positively charged ATCh and negatively charged of GQDs on surface of AuNPs. Figure 4.8 shows the plots of absorbance at 520 nm versus the reaction time for different concentrations of ATCh. As evident from UV-visible data, the absorbance at 520 nm for 50 μM of ATCh almost has no influence in aggregation of GQDs-AuNPs within the tested time (60 min). However, given ATCh concentration more than 100 μM , the absorbance at 520 nm decreased with increasing ATCh concentration. In consequence, 50 μM of ATCh was used as the optimum for colorimetric analysis in the following experiments.

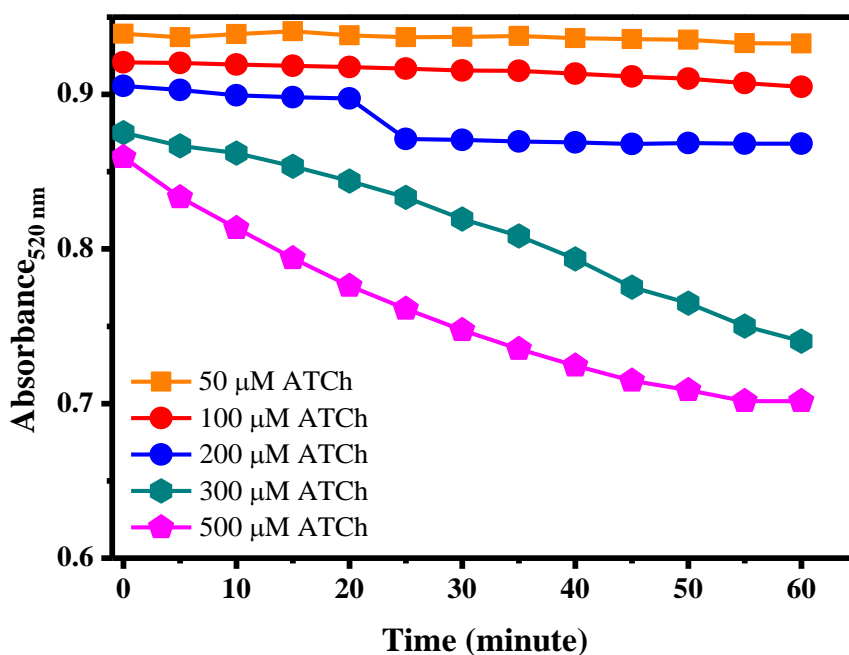


Figure 4.8 Variation of the absorbance at 520 nm versus time for GQDs-AuNPs in the presence of difference concentrations of ATCh (50, 100, 200, 300 and 500 μM) recorded every 5 min.

4.1.3.3 Effect of the AChE enzyme concentrations

The activity or concentration of AChE have a great impact on the conversion of ATCh to thiocholine and therefore effect on the performance of colorimetric analysis. The effect of AChE concentration on the response of chlorpyrifos analysis was examined in the range of 100 to 500 mU mL⁻¹ and the absorption spectra of solution in each case was measured every 5 min for 1 h. As shown in Figure 4.9, the absorbance at 520 nm decreased gradually with the reaction time due to AChE-enzyme catalysed hydrolysis of an ATCh substrate to produce thiocholine, which caused the aggregation of GQDs-AuNPs. Additionally, the decline of absorbance at 520 nm was more remarkable for the ensemble solution with a higher concentration of AChE. Given the higher concentration of AChE, the hydrolysis reaction could be completed within a shorter time. Therefore, the experimental result indicated that the concentration of 200 mU mL⁻¹ AChE was used for colorimetric analysis due to it was able to catalyze the hydrolysis faster and provide the highest absorbance band. This optimum of AChE concentration at 200 mU mL⁻¹ from our work was lower than the value of 400 mU mL⁻¹ and 500 mU mL⁻¹ AChE concentration, reported by R. Bala et al [40] and H. Li et al [41], respectively.

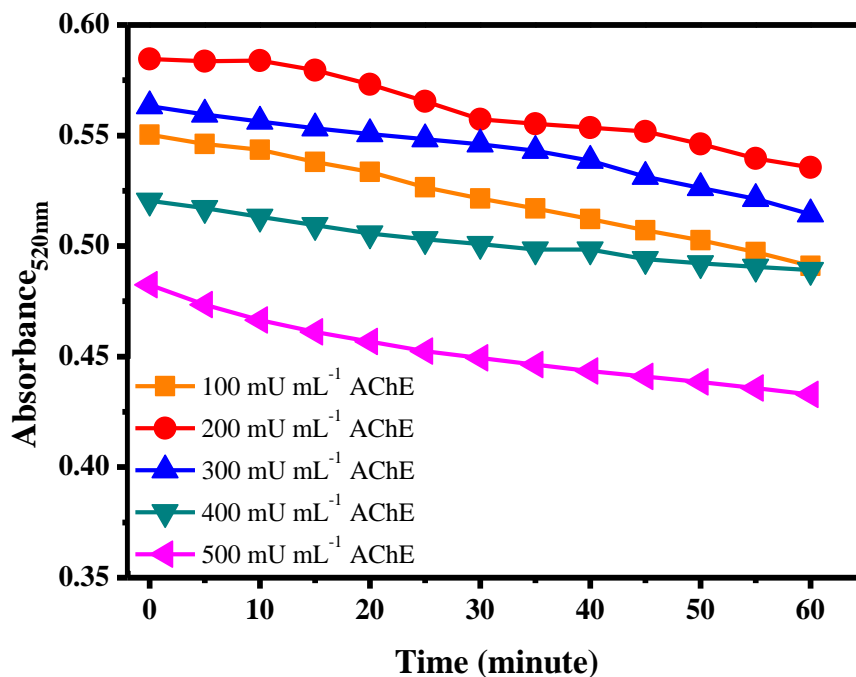


Figure 4.9 Variation of absorbance at 520 nm versus reaction time for GQDs-AuNPs in the presence of ATCh (50 μ M, pH 7.0 PBS) having different concentrations of AChE (100, 200, 300, 400 and 500 mU mL^{-1}) recorded every 5 min.

4.3.3.4 Effect of the reaction time

The influence of the reaction or incubation time was studied because it is a critical parameter for determination of chlorpyrifos with colorimetric analysis. In this study, the effect of reaction time on reaction solution was investigated over the range of 0 to 60 min. Results obtained from UV-Visible absorption spectra (Figure 4.10a) revealed that the band at 520 nm decreased with increasing reaction time. Meanwhile, a new absorption band at 650 nm increased with increasing reaction time. Figure 4.10b shows the plots of absorbance at 520 nm and 650 nm versus the reaction time. The result indicated that absorbance at 520 nm decreased with increasing reaction time. Whereas the new band at 650 nm increased with increasing reaction time from 0 to 10 min. The absorbance bands at 520 and 650 nm were gradually constant and remain stable at reaction time of 30 min. For this reason, reaction time of 30 min was chosen as the optimal reaction time in this detection system.

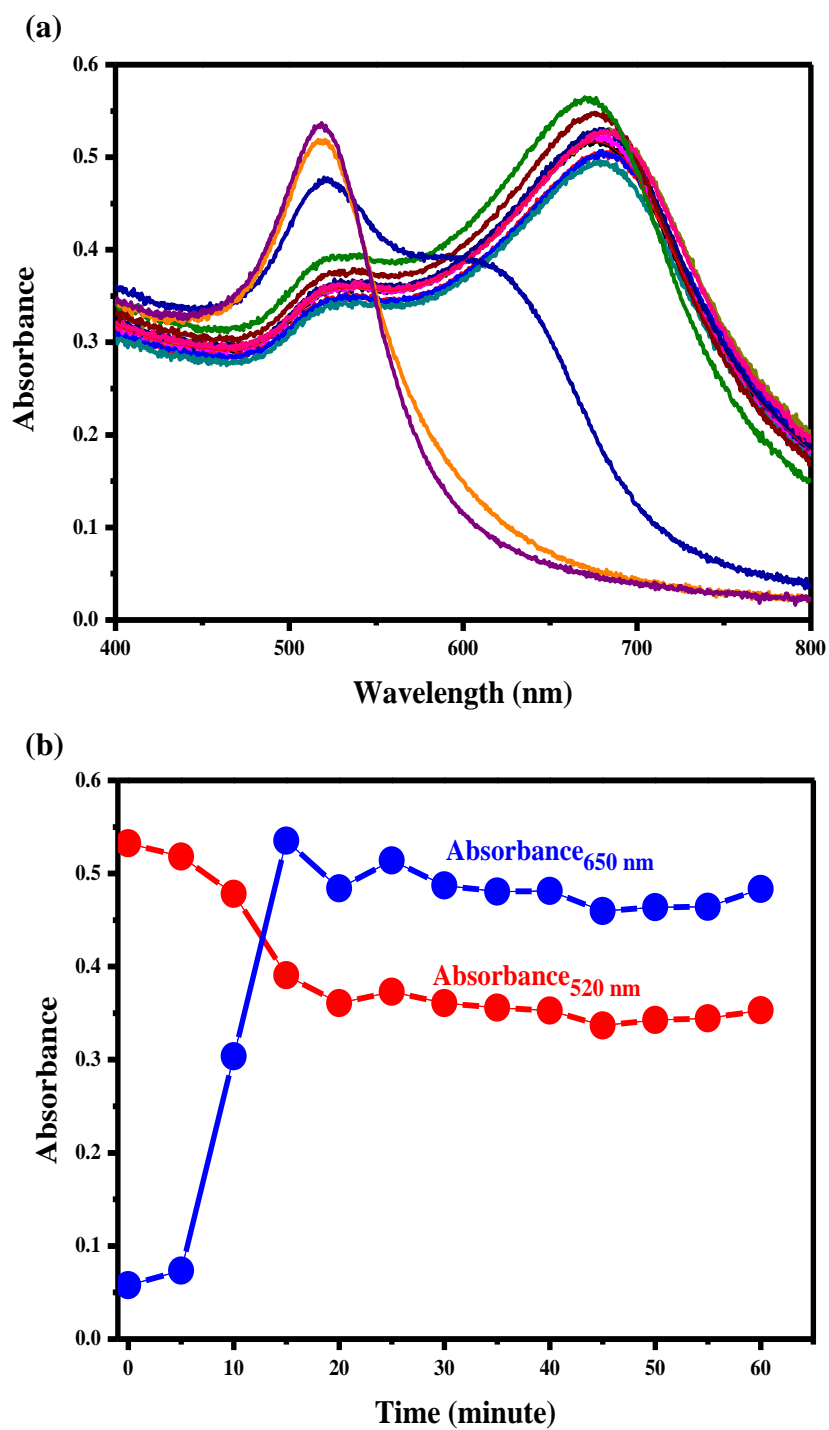


Figure 4.10 Absorption spectra of GQDs-AuNPs after addition of ATCh (50 μM , pH 7.0 PBS) and AChE (200 mU mL^{-1}) recorded every 5 min (a) and the plots of absorbance at 520 nm and 650 nm versus the reaction time (b).

4.1.4 Colorimetric method for chlorpyrifos detection

4.1.4.1 Linear concentration range of chlorpyrifos

To test the performance of the assay described in section 3.6.3.2, difference concentrations of chlorpyrifos were added into AChE and this solution was mixed with ATCh and GQDs-AuNPs. The distinctive color change (from red to blue) at $\lambda_{\max} = 520$ nm is a result of the aggregation of GQDs-AuNPs. This phenomenon provides a method for quantitative determination of chlorpyrifos. The red color at 520 nm results from reaction between GQDs-AuNPs and thiocholine and the intensity varies with chlorpyrifos concentration. As shown in Figure 4.11a, the peak at 520 nm increased with increasing concentration of chlorpyrifos due to the chlorpyrifos inhibited AChE hydrolysis of ATCh, leading to anti-aggregation of GQDs-AuNPs. The change of reaction color depends on the concentration of chlorpyrifos and the color change could be observed by naked eye as shown in the inset of Figure 4.11a. Calibration plot between A/A_0 and the concentration of chlorpyrifos, where A and A_0 were the absorbance with and without chlorpyrifos was shown in Figure 4.11b. The resulting A/A_0 calculated from absorbance band at 520 nm is linearly proportional to the concentration of chlorpyrifos over the range of 0.1-50 $\mu\text{g mL}^{-1}$. The linear equation for this curve is $y = 0.0131x + 1.0246$, with a linear correlation coefficient (r^2) of 0.996. Analytical performance of the proposed method was compared with related methods for OPs detection (Table 4.1). The proposed method exhibits the widest linearity range (0.1 to 50 $\mu\text{g mL}^{-1}$) compare to other methods [92, 93, 103-108] that 2,2'-Azino-bis(3-ethylbenzothiazoline-6-sulfonic acid) diammonium salt (ABTS²⁻) [104], silver nanoparticle (AgNPs) and molecularly imprinted polymers (MIP) [106], citrate-AuNPs treated with sodium sulfate (Na_2SO_4) (citrate-AuNPs/ Na_2SO_4) [107], and the carbon nanodots (C-dots) with Fe^{2+} - H_2O_2 system bi-enzyme (C-dot/ Fe^{2+} - H_2O_2 /AChE/ChOX) [108].

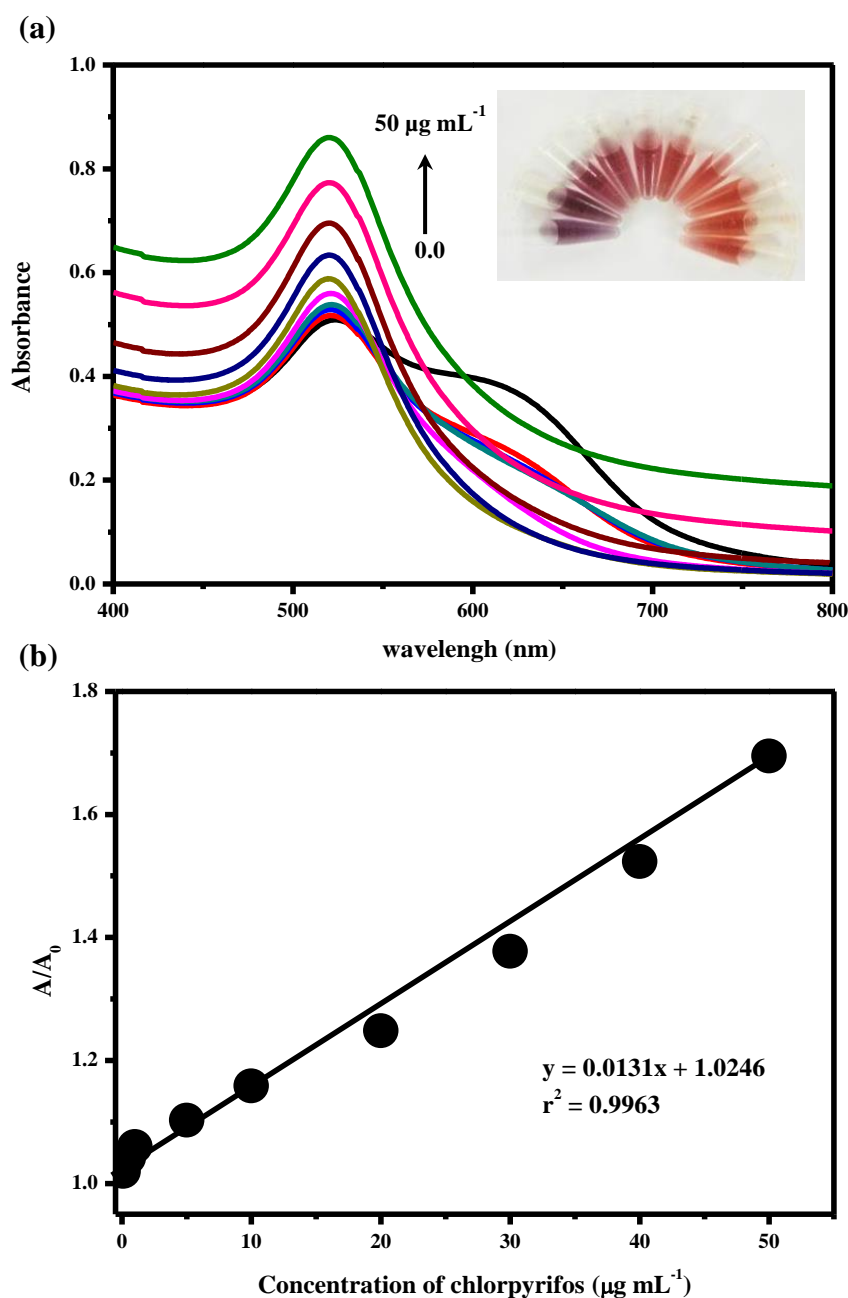


Figure 4.11 Absorption spectra of the reaction assay with different concentration of chlorpyrifos (0, 0.1, 0.5, 1.0, 5.0, 10, 20, 30, 40 and 50 $\mu\text{g mL}^{-1}$). The reaction composed of 0.9 mL of GQDs-AuNPs, 100 μL of ATCh (50 μM), 10 μL of AChE (200 mU mL^{-1}) and 290 μL of PBS (50 mM PBS, pH 7) (a). Inset is their respective images. The calibration plot between A/A_0 and the concentration of chlorpyrifos was constructed for the colorimetric detection of chlorpyrifos, where A and A_0 were the absorbance with and without chlorpyrifos ($n=3$) (b).

Table 4.1 Comparison of the developed method analytical performance with other methods for the colorimetric detection of organophosphate pesticide.

Materials	Method	Analytes	Concentration range ($\mu\text{g mL}^{-1}$)	LOD ($\mu\text{g mL}^{-1}$)	Ref.
Citrate-AuNPs	Colorimetric	Terbutylazine	0.02-0.2	0.004	[93]
Cu(I)/alkyne-Au NPs/AChE	Colorimetric	Paraoxon	0.001-0.1	0.001	[103]
AChE/H ₂ O ₂ -DNAzyme-ABTS ²⁻	Colorimetric	Chlorpyrifos	0.04-1.0	0.01	[104]
CDs-AgNPs/AChE	Colorimetric	Carbaryl	0.01-0.1	0.006	[105]
AgNPs-MIP	Colorimetric	Chlorpyrifos	0.1-10	0.02	[106]
Au@citrate/Na ₂ SO ₄	Colorimetric	Chlorpyrifos	0.1-0.25	0.02	[107]
GQDs-MnO ₂	Colorimetric	Parathion	0.001-0.04	-	[92]
C-dot/Fe ²⁺ -H ₂ O ₂ /AChE/ChOX	Colorimetric	Chlorpyrifos	0.01-1.0	0.003	[108]
GQDs-AuNPs/AChE	Colorimetric	Chlorpyrifos	0.1-50	0.046	[This work]

Citrate = sodium citrate dihydrate, AuNPs = gold nanoparticles, Cu (I) = copper (I) ion, AChE = acetylcholinesterase enzyme, DNA = deoxyribonucleic acid, ABTS = 2,2'-azino-bis(3-ethylbenzothiazoline-6-sulphonic acid), CDs = carbon dots, AgNPs = silver nanoparticles, MIP = molecularly imprinted polymers, GQDs = graphene quantum dot, and MnO₂ = Manganese (IV) oxide,

4.1.4.2 Limit of detection (LOD) for chlorpyrifos

In this study, the limit of detection (LOD) for chlorpyrifos was investigated by measurement of blank solution with ten replicates. The LOD was calculated on the basis of 3-fold of standard deviation per slope ($3S.D_{\text{blank}}/\text{slope}$). The calculated LOD was $0.046 \mu\text{g mL}^{-1}$. The simple colorimetric method provides good precision ($\%RSD = 0.03$) for chlorpyrifos detection with ten replicates. Table 4.1 summarize analytical characteristics of the proposed method compare to related methods for OPs detection. The LOD ($0.046 \mu\text{g mL}^{-1}$) for the proposed method is comparable to those methods [104, 106, 107] which used AuNPs [107], ABTS²⁻ [104] and AgNPs [106] as color probes. Outstanding feature of the developed method are simple synthesis, rapid and high stability.

4.1.5 Interference study

In this study, the effect of potential interferences that are likely present in vegetable samples, including cations, anions and compound molecules were investigated. The interference effect was evaluated by adding different amounts of competing substance into $20 \mu\text{g mL}^{-1}$ chlorpyrifos standard solution, and comparing the absorbance response to that for the initial chlorpyrifos measurement. The concentration of the interferent species that provided absorbance change greater than $\pm 5\%$ was considered as the tolerance limit. Figure 4.12 shows the tolerance limits of interfering substances. The results reveal that a 15-fold excesses of Fe^{3+} , Zn^{2+} , or Ni^{2+} produce no obvious effects on chlorpyrifos response. Twenty-five-fold excess concentrations of Mg^{2+} , or Ca^{2+} , 50-fold excess of S^{2-} , I^- , or NO_3^- , 100-fold excess of K^+ , Na^+ and compound molecules (fructose, maltose, glucose and ascorbic acid), and 250-fold PO_4^{3-} do not interfere with chlorpyrifos determination. These results indicated that this proposed method provides good selectivity for colorimetric determination of chlorpyrifos.

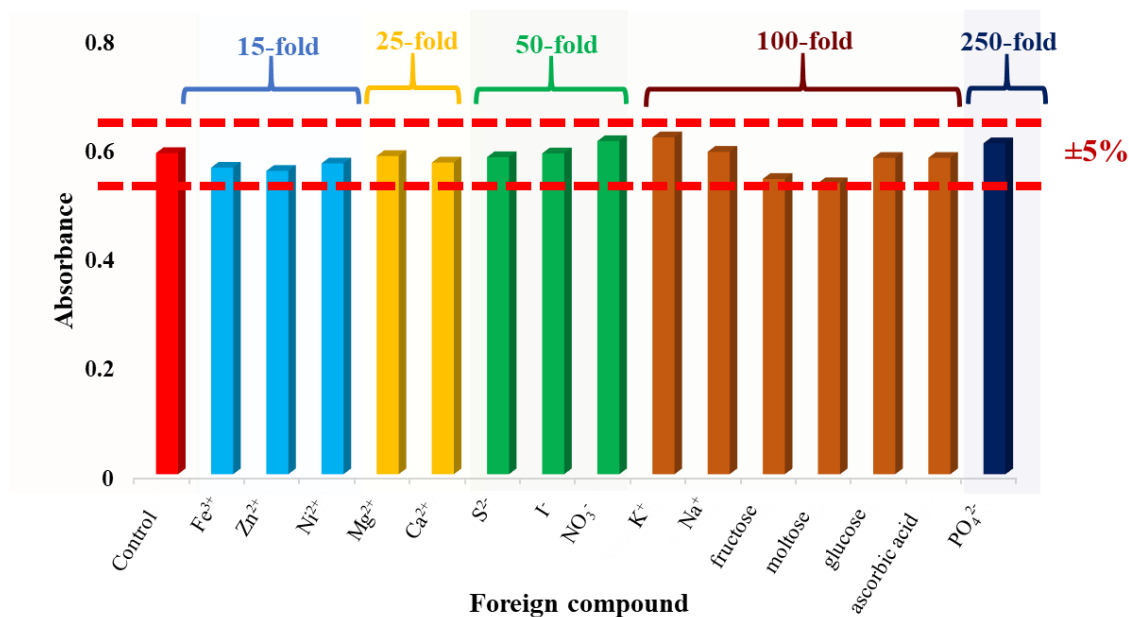


Figure 4.12 The selectivity of developed colorimetric method for chlorpyrifos detection, comparison between the absorbance band at 520 nm obtained from $20 \mu\text{g mL}^{-1}$ of chlorpyrifos and the chlorpyrifos with interfering substances such as ions (Fe^{3+} , Zn^{2+} , Ni^{2+} , Mg^{2+} , NO_3^- , I^- , Ca^{2+} , K^+ , Na^+ , S^{2-} , and PO_4^{3-}) and compound molecules (fructose, maltose, glucose and ascorbic acid). Dotted line marks the $\pm 5\%$ signal alteration range.

4.2 Part II: 3D- μ PAD for chlorpyrifos determination

4.2.1 Characterizations of 3D- μ PAD

The 3D- μ PAD for chlorpyrifos detection was characterized. Figure 4.13 shows comparison between the hydrophobic and hydrophilic zones of the fabricated 3D- μ PAD. Red ink absorbs into the paper in the hydrophilic zone, but does not absorb in the hydrophobic zone as shown in the top Figure 4.13. The photograph shows that the designed hydrophilic four circles on 3D- μ PAD had average diameter of approximate 5 ± 0.45 mm, 5 ± 0.40 mm, 5 ± 0.45 mm and 5 ± 0.50 mm ($n=5$), respectively. On the other hand, the hydrophobic dumbbell shape on the sampling sheet had average wide and length size of approximately 2 ± 0.20 mm and 8 ± 0.50 mm, respectively.

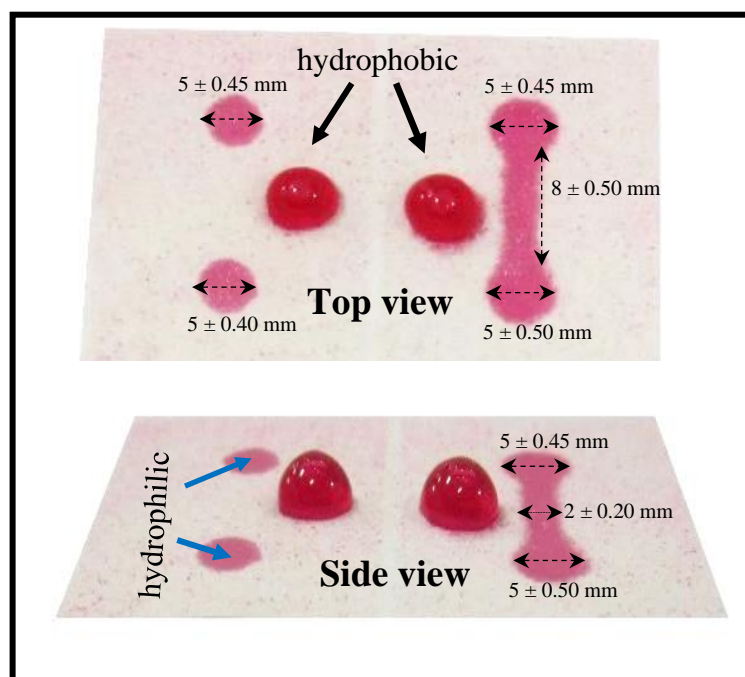


Figure 4.13 Photograph of the screen-printed 3D- μ PAD: demonstration of hydrophilic and hydrophobic zones on the paper by applying a drop of colored food dye to the surface.

4.2.2 Parameters that effect the sensitivity of the chlorpyrifos detection

4.2.2.1 Effect of the color intensity

The color intensity in RGB system obtained from the measurement using the developed 3D- μ PAD in the presence of chlorpyrifos was performed. We investigated the intensities of the red, green, blue, and R+G+B (grey) channels. The color intensity values obtained from the image processing software (ImageJ) were illustrated in Figure 4.14. Calibration curves for $[I_0-I]$ vs. chlorpyrifos concentration are plotted for all color channels of interest. In the figure, I and I_0 represent the color intensities with (I) and without (I_0) chlorpyrifos. Obviously, the green channel has the steepest slope of the calibration graph, indicating that this color provides the greatest sensitivity. It should be noted that RGB color intensities obtained from ImageJ are subtractive values, and thus, according to light spectrum theory, the dark-red color produced with increasing chlorpyrifos concentration, reflects red light and absorbs green light [60]. Therefore, the green-light channel was chosen for determination of chlorpyrifos concentration in samples.

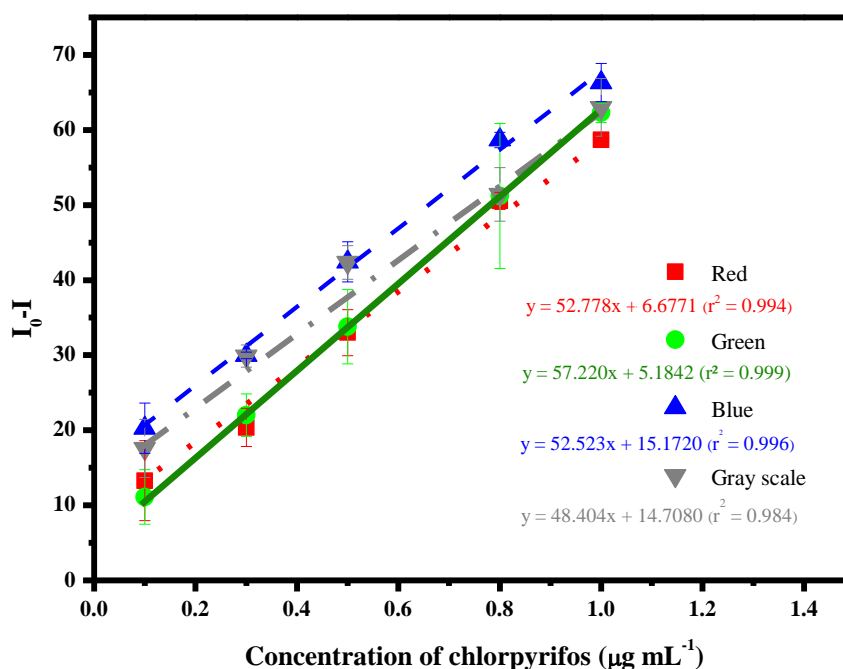


Figure 4.14 The color intensity (I_0-I) of the images was separated into red, green, blue and average grayscale $(R+G+B)/3$ intensity and plot versus concentration of chlorpyrifos ($n=3$).

4.2.2.2 Effect of pH of phosphate buffer saline

The effect of pH value for the chlorpyrifos detection in the developed 3D- μ PAD was investigated over the range of pH 6.0 to 9.0 using 50 mM PBS. During this pH tests in the developed 3D-PAD, which used chlorpyrifos, ATCh and AChE concentrations of $0.5 \mu\text{g mL}^{-1}$, 0.5 mM and 5.0 U mL^{-1} , PBS solution (8 μL , pH 7.0), and 30 minutes incubation time. As shown in Figure 4.15a, color intensity increases with pH, to a maximum at pH 7.0. Further increases of the pH result in weaker intensities. The AChE enzyme is a natural protein that is highly effective at neutral pH, but which denatures under extreme pH conditions. Thus, at pH of 7.0 of PBS (50 mM) for all further tests. The pH for in this work was similar to the result reported by A. Apilux et al [35], that at pH 7.4 of PBS (20 mM) was the optimum value for determination of OPs and carbamate insecticides using paper-based TGA-capped CdTe QDs devices.

4.2.2.3 Effect of the volume of buffer

The volume of PBS buffer loading was investigated by adding various volumes of buffer in the range of 4 to 10 μL . After applying the chlorpyrifos-ATCh mixture solution and incubation solution for 5.0 min. The variation of buffer solution was added to the buffer loading area. The buffer loading area was created to elute solution along the channel and gather to the detection zone. Figure 4.15 b shows plot of color intensity versus buffer volume. The result shows that the color intensity increase with buffer volume, from 4.0 to 8.0 μL as a consequence of the grater quantity of ATCh-Chlorpyrifos that elutes and is able to interact with enzyme in the detection zone. However, increasing buffer volume beyond 8.0 μL results in decreased color intensity because of dilution and overloading effects. Therefore, the buffer volume of 8.0 μL was chosen as the optimum volume.

4.2.2.4 Effect of the ATCh concentrations

The optimization for ATCh concentration within the range of 0.1 to 10 mM was investigated. Figure 4.15c shows that color intensity increased with ATCh concentration increasing from 0.1 to 0.5 mM. Greater quantities of ATCh produce more thiocholine, resulting in increased GQDs-AuNPs aggregation and a consequent increase in signal intensity. However, intensity remains constant at ATCh concentrations higher than of 0.5 mM. This may be due to the presence of insufficient quantities of AChE.

Thus, the ATCh concentration of 0.5 mM was chosen as optimal for further experiments, since this concentration produces the greatest color intensity. These results were in good agreement with a previous report [97,35], that at 3.0 mM and 10 mM of ATCh concentration were selected for organophosphate pesticides by using nanoceria-coated paper-based device [97] and paper-based TGA-capped CdTe QDs devices [35], respectively.

4.2.2.5 Effect of the AChE enzyme concentrations

The effect of AChE concentration on the chlorpyrifos detection response was examined in the range 0.1-20 U mL⁻¹. As shown in Figure 4.15d, the increasing AChE concentration increases the amount of thiocholine generated by hydrolysis, and therefore enhances GQDs-AuNPs aggregation. The maximal response intensity was observed for an AChE concentration of 5.0 U mL⁻¹. At the greater concentrations, the response intensity remains constant. Therefore, an AChE concentration of 5.0 U mL⁻¹ was selected for optimal sensitivity. Herein, one analysis is carried out by using only 5.0 μL of AChE (5.0 U mL⁻¹). To the best of our knowledge, however, this proposed assay required lowest amount of reagents and enzyme compared to that has been reported previously where up to 2.0 μL of 2,500 U mL⁻¹ AChE was needed for the foldable paper sheet with bi-enzymatic based fluorescent sensor [39] and 5.0 mL of AChE (16 mU mL⁻¹) was required for AChE-based test strip coupled with rhodamine-B functional AuNPs entrapped in agarose and coated with hydrogel [2].

4.2.2.6 Effect of the reaction time

The effect of incubation or reaction time between zero and 40 min on the reaction intensity was investigated. Figure 4.15e shows the plot of color intensity versus reaction time. Color intensity increased with increasing reaction time, from 0.0 to 15 min. Longer reaction times does not significant change the resulting intensity. Therefore, a reaction time of 15 min that provide the greatest sensitivity within the shortest time was chosen. The reaction time used in this work was similar to the result reported by S. Nouanthavong. et al [97], that a reaction time at 15 min was selected for organophosphate analysis.

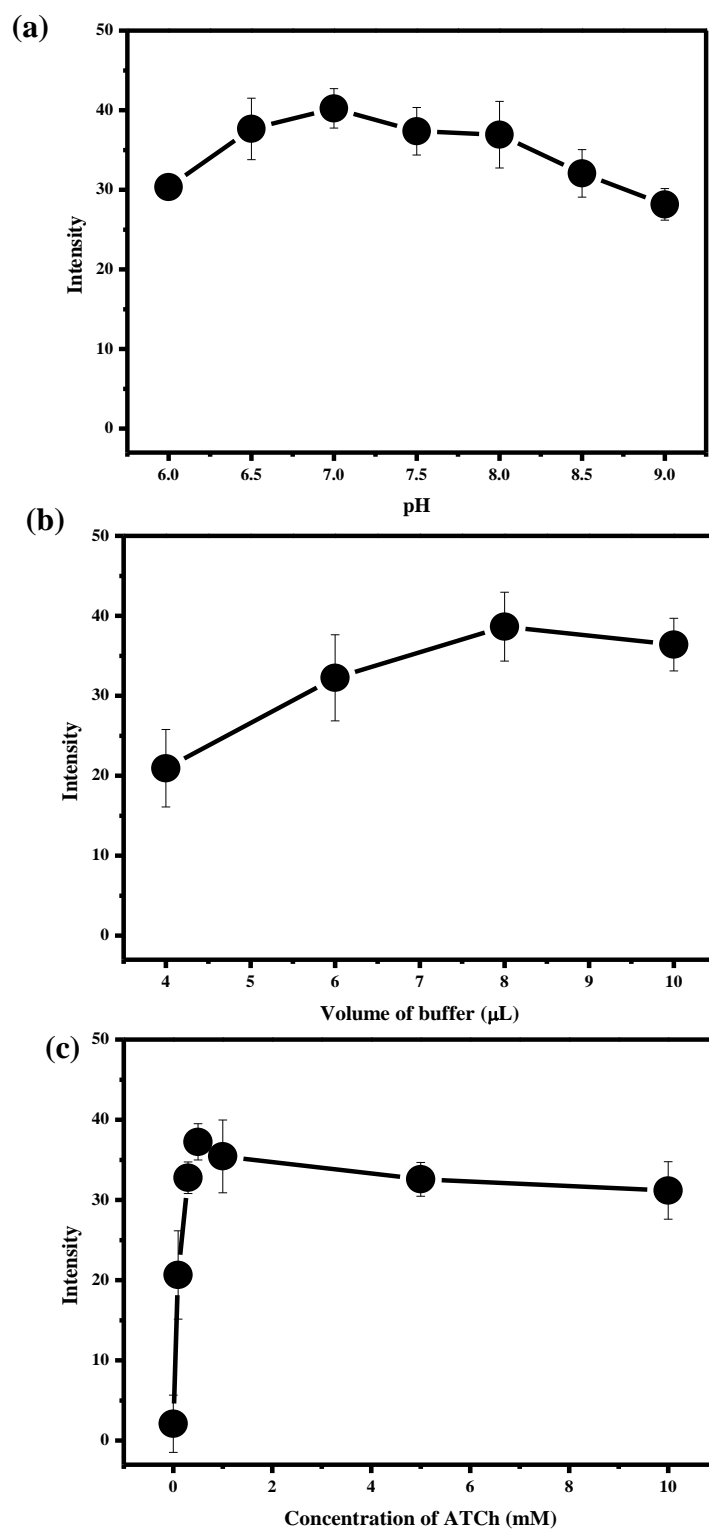


Figure 4.15 The green color intensity of 3D-μPAD for chlorpyrifos detection in fixed concentration of $0.5 \mu\text{g mL}^{-1}$ chlorpyrifos pesticide and various conditions; pH (a), volume of buffer (b), concentration of ATCh (c), concentration of AChE (d) and reaction time (e).

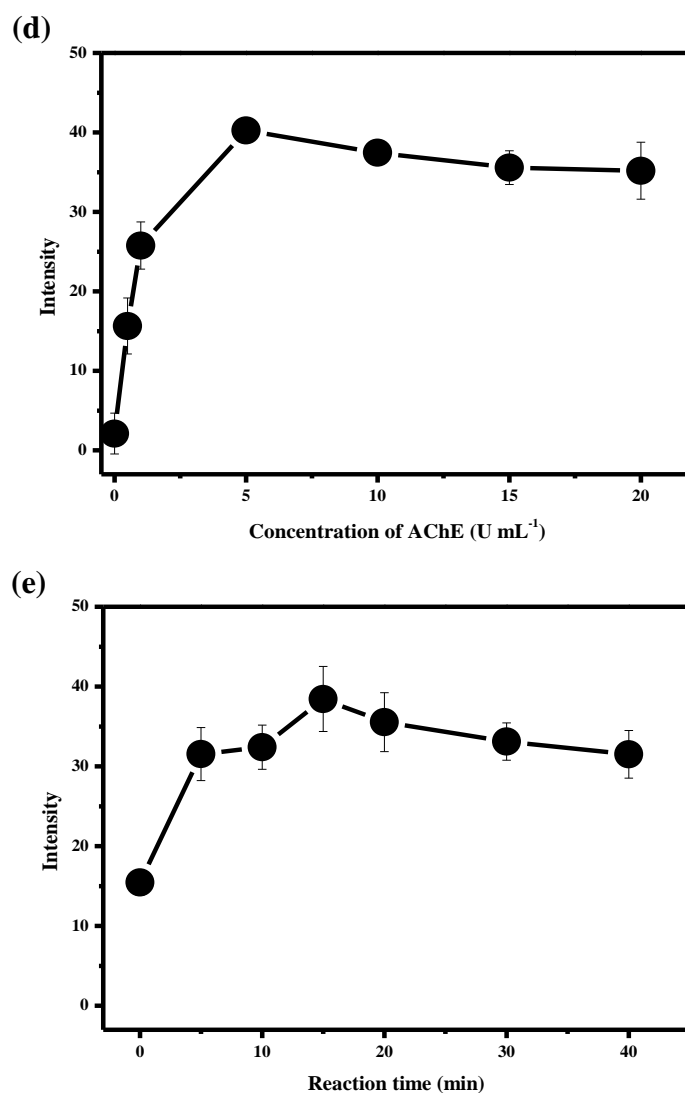


Figure 4.15 The green color intensity of 3D- μ PAD for chlorpyrifos detection in fixed concentration of $0.5 \mu\text{g mL}^{-1}$ chlorpyrifos pesticide and various conditions; pH (a), volume of buffer (b), concentration of ATCh (c), concentration of AChE (d) and reaction time (e).

4.2.3 Colorimetric method for chlorpyrifos detection

4.2.3.1 Linear concentration range of chlorpyrifos

To test the performance of 3D- μ PAD detection, linearity range for chlorpyrifos analysis was determined. Figure 4.16 shows the chlorpyrifos calibration curve for $[I_0-I]$ of green color intensity vs. chlorpyrifos concentration, where I and I_0 represent the color intensities with (I) and without (I_0) chlorpyrifos. Green color intensity increases linearly with chlorpyrifos concentration from 0.001 to 1.0 $\mu\text{g mL}^{-1}$. The calibration curve from quintuplicate analysis is given by $y = 58.4620 \pm 2.3150x + 14.3219 \pm 1.6925$, and the linear correlation coefficient (r^2) is 0.998. The photograph shows the color change of GQDs-AuNPs interaction with thiocholine. The result shows that the red color of GQDs-AuNPs increased with increasing concentration of chlorpyrifos.

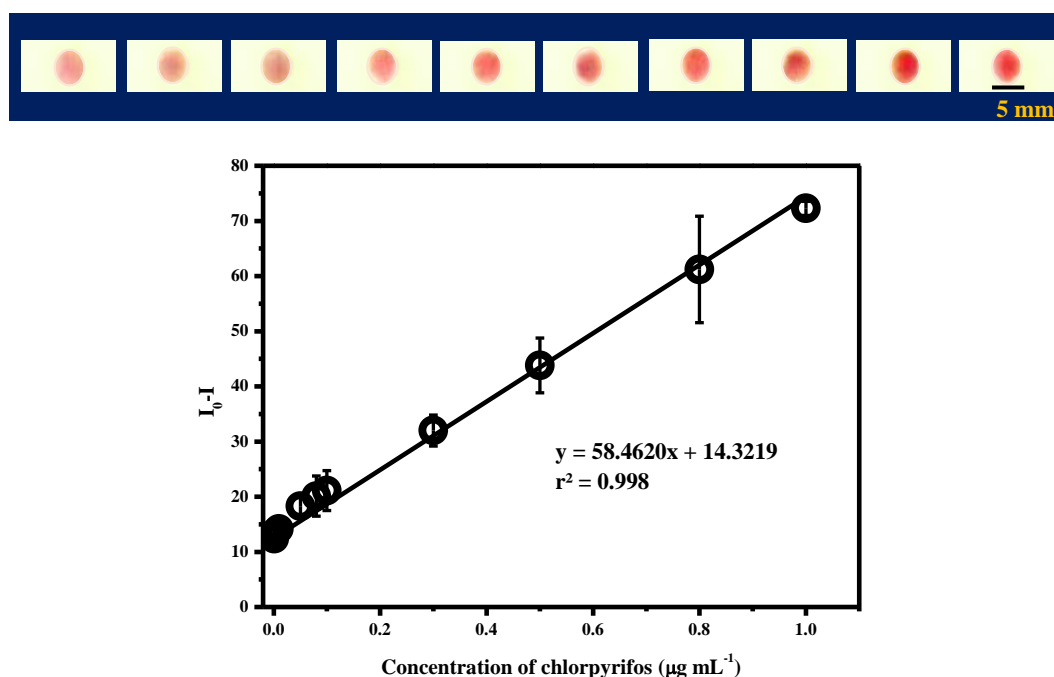


Figure 4.16 Calibration curve of chlorpyrifos using 3D- μ PAD (plot between I_0-I of green intensity and the variation of chlorpyrifos concentrations; 0.001, 0.005, 0.01, 0.05, 0.1, 0.3, 0.5, 0.8 and 1.0 $\mu\text{g mL}^{-1}$) reaction conditions; GQDs-AuNPs, ATCh (0.5 mM) and AChE (5.0 U mL^{-1}). Error bar obtained from quintuplicate ($n=5$).

4.2.3.2 Limit of detection (LOD) for chlorpyrifos

In this study, the limit of detection (LOD) for chlorpyrifos was investigated by measurement of blank solution with ten replicates. The LOD was calculated on the basis of 3-fold of standard deviation per slope ($3S.D_{\text{blank}}/\text{slope}$). The calculated LOD was $0.0007 \mu\text{g mL}^{-1}$. The simple colorimetric method provides good precision (%RSD = 0.01) for chlorpyrifos detection with ten replicates. Therefore, the detection limit of developed 3D- μ PAD ($0.0007 \mu\text{g mL}^{-1}$) is less than the codex maximum residual limit for chlorpyrifos residues, and falls in the range of $0.05\text{-}1.0 \text{ mg kg}^{-1}$ (or $0.05\text{-}1 \mu\text{g mL}^{-1}$) for several vegetable samples, indicating that the method is suitable for quantitative analysis of chlorpyrifos in food samples. Analytical performance of the proposed device was compared with related methods for chlorpyrifos detection (Table 4.2). The chlorpyrifos 3D- μ PAD exhibits the widest linearity range (0.001 to $1.0 \mu\text{g mL}^{-1}$) compare to other μ PAD methods. The LOD of $0.0007 \mu\text{g mL}^{-1}$ for the proposed method is lower than that for AChE-based colorimetric methods [2, 35, 98, 97, 100] that use rhodamine-B (RB) functional AuNPs entrapped in agarose and coated with hydrogel (polyethylene glycol diacrylate) (RB-AuNPs/hydrogel/-AChE) [2], the nanoceria coated PAD using AChE/choline oxidase (ChOX) bi-enzyme (AChE/ChOX/CeO₂) [97], and indoxyl acetate (AChE/IDA) [100]. This 3D- μ PAD detection method is as good as methods using colorimetric and chemiluminescent dual-readout immunoassay test strips based on graphitic carbon nitride/bismuth ferrite nanocomposites (g-C₃N₄/BiFeO₃ NCs-antibodies) [109] and manganese dioxide nanoflowers (MnO₂NFs-luminol-H₂O₂) [110]. It should be noted that the cited works [109, 110] report colorimetric and chemiluminescent results, while detection limits are based on chemiluminescence measurements alone. When compared to related detection techniques, the propose method is simpler to apply than the cited works [46, 47, 60]. The 3D- μ PAD provides several other advantages, for example, screen printing is a simple one-step process, allowing mass production of devices without the need for expensive equipment. The reaction test is sensitive and rapid, and the reaction can be performed in a few steps, with the results plainly visible to the naked eye.

Table 4.2 Comparison of other method for the detection of organophosphate pesticide using μ PAD.

Materials	Method	Analyte	Concentration ranges ($\mu\text{g mL}^{-1}$)	LOD ($\mu\text{g mL}^{-1}$)	Ref.
RB-AuNPs/hydrogel/AChE	Colorimetric	Chlorpyrifos	0.005-0.5	-	[2]
Au ³⁺ -CTAB/AuNPs/AChE	Colorimetric	Parathion	0.0-1.2	0.035	[98]
TGA capped CdTe QDs/AChE/ChOX	Fluorometric	Dichlorvos	0.01-10	0.01	[35]
IDA/AChE	Colorimetric	Chlorpyrifos	0.0-25	8.60	[100]
CeO ₂ /AChE/ChOX	Colorimetric	Chlorpyrifos	0.0-0.06	0.005	[97]
g-C ₃ N ₃ /BiFe ₃ NCs-antibodies	Colorimetric Luminescence	Chlorpyrifos	0.0001-0.05	0.00003	[109]
MnO ₂ NFs-luminol-H ₂ O ₂	Colorimetric Luminescence	Chlorpyrifos	0.0001-0.05	0.00007	[110]
GQDs-AuNPs/AChE	Colorimetric	Chlorpyrifos	0.001-1.0	0.0007	[This work]

RB = rhodamine-B, AuNPs = gold nanoparticles, AChE = acetylcholinesterase enzyme, Au³⁺ = aurum (III) ion, CTAB = cetyltrimethylammonium bromide, TGA = thioglycolic acid, CdTe QDs = cadmium telluride quantum dots, ChOX = choline oxidase, IDA = IDA = indoxyl acetate, g-C₃N₄ = graphitic carbon nitride, BiFe₃ NCs = bismuth ferrite nanocomposites, MnO₂NFs = manganese dioxide nanoflowers and GQDs = graphene quantum dot

4.2.4 Interference study

Interference studies were done in order to explore the specific detection of chlorpyrifos in vegetables using the proposed 3D- μ PAD. These experiments included investigation of most commonly found substances in real samples of vegetables, such as fructose, maltose, glucose, ascorbic acid, Fe^{3+} , Cu^{2+} , Zn^{2+} , Mg^{2+} , NO_3^- , I^- , Ca^{2+} , K^+ , Na^+ , S^{2-} , and PO_4^{3-} . The interference effect was evaluated by adding different amounts of competing substance into $0.05 \mu\text{g mL}^{-1}$ chlorpyrifos standard solution, and comparing the intensity response to that for the initial chlorpyrifos measurement. The tolerance limit was defined as the amount of interfering substance needed to cause intensity changes in excess of $\pm 5\%$. Figure 4.17 shows the tolerance limits of interfering substances. The results reveal that a 50-fold excesses of Fe^{3+} , Cu^{2+} , or Zn^{2+} produce no obviously effects on chlorpyrifos response. One hundred-fold excess concentrations of Mg^{2+} , NO_3^- , or I^- , 500-fold excess of Ca^{2+} , K^+ , Na^+ , S^{2-} , and compound molecules (fructose, maltose, glucose and ascorbic acid), and 1000-fold PO_4^{3-} do not interfere with chlorpyrifos determination. Moreover, this designed 3D- μ PAD provides good selectivity for colorimetric determination of chlorpyrifos.

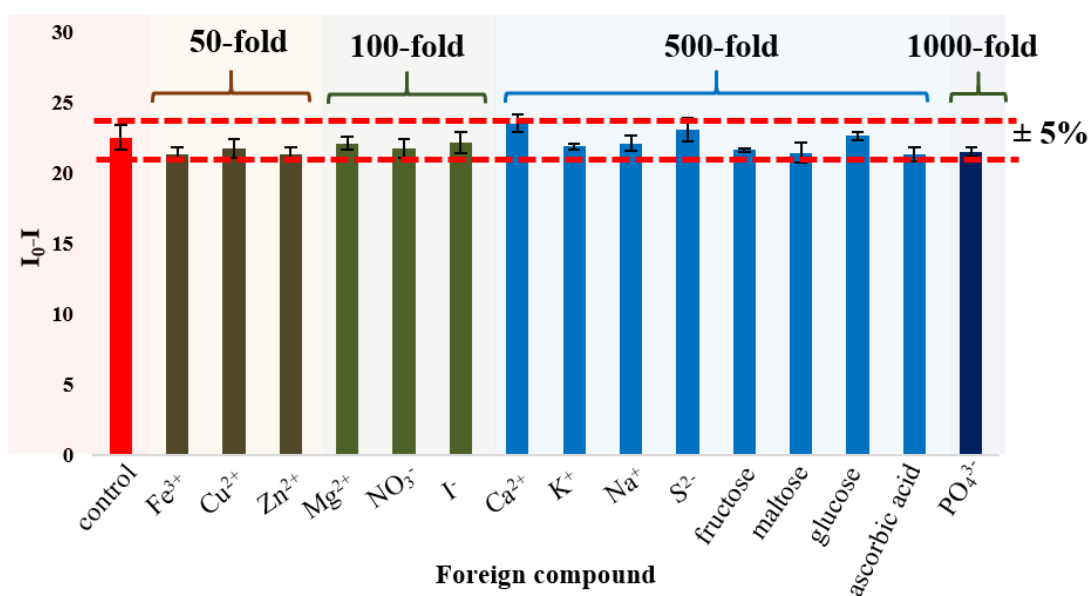


Figure 4.17 The selectivity of developed 3D- μ PAD for chlorpyrifos detection, comparison between the color intensity obtained from $0.05 \mu\text{g mL}^{-1}$ of chlorpyrifos and the chlorpyrifos with interfering substances such as ions (Fe^{3+} , Cu^{2+} , Zn^{2+} , Mg^{2+} , NO_3^- , I^- , Ca^{2+} , K^+ , Na^+ , S^{2-} , and PO_4^{3-}) and compound molecules (fructose, maltose, glucose and ascorbic acid), ($n=3$). Dotted mark the $\pm 5\%$ signal alteration range.

4.2.5 Detection of chlorpyrifos in real samples

The proposed 3D- μ PAD was applied to the determination of chlorpyrifos in vegetable samples (cucumber, radish, lettuce, carrot, cabbage, and tomato) to demonstrate a practical application. Extracted samples were quantified by the 3D- μ PAD and the results compared to those obtained using conventional HPLC. Table 4.3 summarises the results, showing added chlorpyrifos and calculated recovery values. As shown in the table, samples were either treated with chlorpyrifos concentrations below the detection limit (n.d.), or were chlorpyrifos-free. These results were confirmed by HPLC (Table 4.1). The chlorpyrifos concentrations found by the developed 3D- μ PAD are not significantly different from those found by conventional HPLC. The accuracy of the analytical process, using percent recovery data for spiked chlorpyrifos standards (0.03 and $0.1 \mu\text{g mL}^{-1}$), falls in the range of 93.0% to 104.6%. The developed method provides good precision with %RSD values ranging from 0.3 to 1.6. The percentage of relative error was calculated by comparing measured recovery values with the reference value obtained from HPLC measurements. The calculated relative error ranges, from 1.0% to 5.3%, indicate that there are no significant matrix interferences from the vegetable samples. These results indicate that the proposed 3D- μ PAD is sufficiently accurate, precise, and suitable for rapid quantitative analysis of chlorpyrifos in vegetable samples.

Table 4.3 Comparison of chlorpyrifos determination in vegetables between the developed 3D- μ PAD and the reference HPLC method (n=3).

Samples	Chlorpyrifos ($\mu\text{g mL}^{-1}$)								Relative error (%)
	HPLC method				Proposed 3D- μ PAD				
	Added	Found	Recovery (%)	RSD (%)	Added	Found	Recovery (%)	RSD (%)	
Cucumber	0	ND ^a	-		0	ND ^a	-	0.5	-
	0.03	0.0292	97.3	2.9	0.03	0.0295	96.3	0.3	-1.0
	0.1	0.0964	96.4	0.7	0.1	0.0998	99.8	0.5	3.4
Lettuce	0	ND ^a	-	5.2	0	ND ^a	-	0.9	-
	0.03	0.0295	98.3	3.2	0.03	0.0298	99.3	0.8	1.0
	0.1	0.0991	99.1	2.1	0.1	0.1044	104.4	1.6	5.3
Radish	0	ND ^a	-	1.7	0	ND ^a	-	0.6	-
	0.03	0.0291	97.0	1.0	0.03	0.0285	95.0	0.6	-2.0
	0.1	0.0983	98.3	3.0	0.1	0.1033	103.3	0.7	5.0
Tomato	0	ND ^a	-	4.5	0	ND ^a	-	0.3	-
	0.03	0.0291	97.0	0.8	0.03	0.0294	98.0	0.6	1.0
	0.1	0.0992	99.2	0.9	0.1	0.1008	100.8	0.7	1.6
Cabbage	0	ND ^a	-	0.7	0	ND ^a	-	0.6	-
	0.03	0.0291	97.0	1.1	0.03	0.0302	100.6	1.1	3.6
	0.1	0.0994	99.4	2.4	0.1	0.1046	104.6	1.0	5.2
Carrot	0	ND ^a	-	0.0	0	ND ^a	-	0.6	-
	0.03	0.0294	98.0	3.3	0.03	0.0301	100.3	0.5	2.3
	0.1	0.1004	100.4	1.3	0.1	0.0970	97.0	1.2	-3.4

CHAPTER 5

CONCLUSIONS

This research presents the development of a highly sensitive and selective colorimetric assay for chlorpyrifos pesticide in vegetable samples. Colorimetric assay was developed based on the reaction using graphene quantum dot capped with gold nanoparticles (GQDs-AuNPs) as a color probe. AuNPs were synthesized using GQDs as a reducing agent and stabilizing agent. The synthesis of GQDs-AuNPs were successfully characterized by UV-Visible spectroscopy, fluorescence spectroscopy, transmission electron microscope (TEM) and fourier transform infrared (FT-IR) spectroscopy. The TEM images of GQDs-AuNPs reveals that as prepared AuNPs has average diameter of 12 ± 0.26 nm. In addition, the figure also shows that large AuNPs were surrounded by many smaller GQDs, which has diameters of approximately 3 nm. The principle of assay was based on acetylcholinesterase (AChE) enzyme catalyzed hydrolysis of an acetylthiocholine (ATCh) substrate to produce thiol-bearing thiocholine. Thiocholine causes the aggregation of GQDs-AuNPs, to generate a purple-blue colored product. The hydrolysis step was inhibited in the presence of chlorpyrifos, resulting in anti-aggregation of red colored GQDs AuNPs. Development of colorimetric assay for chlorpyrifos determination was carried out based on two approaches; (i) chlorpyrifos detection in solution UV-Visible spectrophotometer and (ii) three-dimensional microfluidic paper-based analytical device (3D- μ PAD) for detected by ImageJ program.

UV-Visible spectrophotometer was used to monitor change in absorbance during the reaction. Chlorpyrifos inhibited AChE by binding to the active site of an enzyme. This suppresses ATCh hydrolysis, thereby blocking the generation of thiocholine. Optimal conditions were under using ATCh and AChE concentrations of 50 μ M and 200 mU mL⁻¹, PBS solution (50 mM, pH 7.0), and 30 minutes of incubation time. The distinctive color change of GQDs-AuNPs, from red to blue with the maximum absorption wavelength at 520 nm. The proposed colorimetric assay in solution exhibits linear calibration over the range of 0.1-50 μ g mL⁻¹. The linear equation for this curve is

$y = 0.0131x + 1.0246$, with a linear correlation coefficient (r^2) of 0.996. The limit of detection (LOD) calculated based on $[3 \text{ S.D.}]/\text{slope}$ is $0.046 \mu\text{g mL}^{-1}$. The simple colorimetric method provides good precision ($\% \text{RSD} = 0.03$; $n = 10$) for chlorpyrifos detection. The proposed method of detection was also tested for interference with cations, anions and compound molecules. The result shows that none of the ions or molecules led to any significant interference in the detection of chlorpyrifos. Therefore, this proposed method provides satisfied selectivity for colorimetric determination of chlorpyrifos.

Three-dimensional microfluidic paper-based analytical device (3D- μ PAD) is an alternative technology for development of affordable, portable, disposable and low-cost diagnostic tools. The 3D- μ PAD was fabricated by one-step polymer-screen-printing, using rubber latex (RL) waste as a hydrophobic reagent for low-cost and simple manufacture. 3D- μ PAD for colorimetric chlorpyrifos assay was designed by having two parts on paper in one sheet. The top-layer test sheet, consisting of two 5 mm circles; one circle forms the detection zone, for placing the GQDs-AuNPs and AChE-enzyme mixture, and the other is a loading area, with adding buffer for analyte elution. When folded, the detection zone and loading area align with a hydrophilic dumbbell-shape printed on the bottom-layer sampling sheet. The dumbbell shape features two 5.0 mm circles were connected by a straight 2×8 mm channel. The bottom circle area of the dumbbell-shape was used as sample loading by applying the mixed solution of sample/standard (chlorpyrifos) and ATCh (substrate). After loading the 3D- μ PAD, the test sheet is folded so that the circles in the upper and lower layers align. Sample then elutes from the loading area and into the detection zone, where reaction with AuNPs occurs. Under the optimized experimental conditions, using $8.0 \mu\text{L}$ of ATCh (0.5 mM) and $5.0 \mu\text{L}$ AChE (5.0 U mL^{-1}) concentrations, $8.0 \mu\text{L}$ of PBS solution ($\text{pH } 7.0$, 50 mM), and 15 minutes incubation time. Green color intensity increased linearly with chlorpyrifos concentration from 0.001 to $1.0 \mu\text{g mL}^{-1}$. The calibration curve was given by $y = 58.4620 \pm 2.3150x + 14.3219 \pm 1.6925$, and the linear correlation coefficient (r^2) is 0.998. The detection limit, calculated based on $[3\text{S.D.}]/\text{slope}$, was $0.0007 \mu\text{g mL}^{-1}$. The 3D- μ PAD provided good precision ($0.01\% \text{ RSD}$, $n = 10$). Interference study exhibited insignificant interference on the detection of chlorpyrifos. Therefore, the developed 3D- μ PAD provides a good selectivity for chlorpyrifos. The 3D- μ PAD

performance was evaluated for the analysis of chlorpyrifos in vegetable samples. Extracted samples were quantified by the 3D- μ PAD and the results compared to those obtained using conventional HPLC. The accuracy of the analytical process, using percent recovery data for spiked chlorpyrifos standards (0.03 and 0.1 $\mu\text{g mL}^{-1}$), falls in the range of 93.0% to 104.6%. The developed method provides good precision with %RSD values ranging from 0.3 to 1.6. The percentage of relative error was calculated by comparing measured recovery values with the reference value obtained from HPLC measurements. The calculated relative error ranges, from 1.0% to 5.3%, indicate that there are no significant matrix interferences from the vegetable samples. These results indicate that the proposed 3D- μ PAD is sufficiently accurate, precise, and is suitable for rapid quantitative analysis of chlorpyrifos in vegetable samples.

REFERENCES

REFERENCES

- [1] Aurbek, N. and et al. “Analysis of inhibition, reactivation and aging kinetics of highly toxic organophosphorus compounds with human and pig acetylcholinesterase”, **Toxicology**. 229(1-2): 91-99; July, 2009.
- [2] Liu, Q. and et al. “A novel test strip for organophosphorus detection”, **Sensors and Actuators B: Chemical**. 210: 803-810; April, 2015.
- [3] Nganchamung, T. Robson, M. G. and Siriwong, W. “Association between blood cholinesterase activity, organophosphate pesticide residues on hands, and health effects among chili farmers in Ubon Ratchathani Province, Northeastern Thailand”, **Roczniki Państwowego Zakładu Higieny**. 68(2): 175-183, 2017.
- [4] Thapinta, A. and Hudak, P. F. “Pesticide use and residual occurrence in Thailand”, **Environmental Monitoring and Assessment**. 60(1): 103-114; January, 2000.
- [5] Taneepanichskul, N. and et al. “Pesticide application and safety behaviour among male and female chilli-growing farmers in Hua Rua Sub-District, Ubon Ratchathani Province, Thailand”, **Journal of Health Research**. 26(4): 193-197; July-August, 2012.
- [6] Eaton, D. L. and et al. “Review of the toxicology of chlorpyrifos with an emphasis on human exposure and neurodevelopment”, **Critical Reviews in Toxicology**. 38(sup2): 1-125; October, 2008.
- [7] Phung, D. T. and et al. “Biological monitoring of chlorpyrifos exposure to rice farmers in Vietnam”, **Chemosphere**. 87(4): 294-300; April, 2012.
- [8] Yuan, Y. and et al. “Residue of chlorpyrifos and cypermethrin in vegetables and probabilistic exposure assessment for consumers in Zhejiang Province, China”, **Food Control**. 36(1): 63-68; February, 2014.
- [9] Codex Alimentarius. FAO/WHO Food Standards Programme. “Pesticide residues in food”, **Pesticides Database Search**. http://www.fao.org/fao-who-codexalimentarius/codex-texts/dbs/pestres/pesticide-detail/en/?p_id=17. July 2, 2019.

REFERENCES (CONTINUED)

- [10] Taylor, P. Camp S. and Radić, Z. “Acetylcholinesterase”, **Encyclopedia of Neuroscience**. 5–7; 2009.
- [11] Colovic, M. B. and et al. “Acetylcholinesterase Inhibitors: Pharmacology and Toxicology”, **Current Neuropharmacology**. 11(3): 315–335; May, 2013.
- [12] Hadjmohammadi, M. R. Peyrovi, M. and Biparva, P. “Comparison of C18 silica and multi-walled carbon nanotubes as the adsorbents for the solid-phase extraction of Chlorpyrifos and Phosalone in water samples using HPLC”, **Journal of separation science**. 33(8): 1044-1051; April, 2010.
- [13] Mauldin, E. R. and et al. “A simple HPLC method for the determination of chlorpyrifos in black oil sunflower seeds”, **Journal of Liquid Chromatography & Related Technologies**. 29(3): 339-348; February, 2006.
- [14] García-Valcárcel, I. A. and Tadeo, L. J. “A combination of ultrasonic assisted extraction with LC–MS/MS for the determination of organophosphorus pesticides in sludge”, **Analytica Chimica Acta**. 641(1-2): 117-123; May, 2009.
- [15] Sinha, N. S. and et al. “Effect of dissociation energy on ion formation and sensitivity of an analytical method for determination of chlorpyrifos in human blood, using gas chromatography–mass spectrometer (GC–MS in MS/MS)”, **International Journal of Mass Spectrometry**. 253(1-2): 48-57; June, 2006.
- [16] Oubiña, A. and et al. “Evaluation of a magnetic particle-based ELISA for the determination of chlorpyrifos-ethyl in natural waters and soil samples”, **Environmental Science & Technology**. 30(2): 509-512; January, 1996.
- [17] Qian, G. and et al. “A monoclonal antibody-based sensitive enzyme-linked immunosorbent assay (ELISA) for the analysis of the organophosphorous pesticides chlorpyrifos-methyl in real samples”, **Food Chemistry**. 117(2): 364-370; November, 2009.

REFERENCES (CONTINUED)

- [18] Al-Meqbali, A. S. R. El-Shahawi, M. S. and Kamal, M. M. “Differential pulse polarographic analysis of chlorpyrifos insecticide”, **Electroanalysis**. 10(11): 784-786; December, 1998.
- [19] Samet, Y. Agengui, L. and Abdelhédi, R. “Electrochemical degradation of chlorpyrifos pesticide in aqueous solutions by anodic oxidation at boron-doped diamond electrodes”, **Chemical Engineering Journal**. 161(1-2): 167-172; July, 2010.
- [20] Li, A. and et al. “Chemiluminescence determination of organophosphorus pesticides chlorpyrifos in vegetable”, **Analytical Letters**. 41(8): 1375-1386; March, 2008.
- [21] Song, Z. Hou, S. and Zhang, N. “A new green analytical procedure for monitoring sub-nanogram amounts of chlorpyrifos on fruits using flow injection chemiluminescence with immobilized reagents”, **Journal of Agricultural and Food Chemistry**. 50(16): 4468-4474; June, 2002.
- [22] Black, K. G. and Fenske, R. A. “Dislodge ability of chlorpyrifos and fluorescent tracer residues on turf: comparison of wipe and foliar wash sampling techniques”, **Archives of Environmental Contamination and Toxicology**. 31(4): 563-570; November, 1996.
- [23] Zou, Z. and et al. “Quantum dot-based immunochromatographic fluorescent biosensor for biomonitoring trichloropyridinol, a biomarker of exposure to chlorpyrifos”, **Analytical Chemistry**. 82(10): 5125-5133; June, 2010.
- [24] Martinez, A. W. and et al. “Patterned paper as a platform for inexpensive, low-volume, portable bioassays”, **Angewandte Chemie International Edition**. 46(8): 1318-1320; October, 2013.
- [25] Ge, L. and et al. “Three-dimensional paper-based electrochemiluminescence immunodevice for multiplexed measurement of biomarkers and point-of-care testing”, **Biomaterials**. 33(4): 1024-1031; November, 2012.
- [26] Y. Sameenoi, and et al. “Microfluidic paper-based analytical device for aerosol oxidative activity”, **Environmental Science & Technology**. 47(2): 932-940; December, 2013.

REFERENCES (CONTINUED)

- [27] Li, X. Tian J. and Shen, W. “Quantitative biomarker assay with microfluidic paper-based analytical devices”, **Analytical and Bioanalytical Chemistry**. 396(1): 495-501; October, 2010.
- [28] Abarghoei, S. and et al. “A colorimetric paper sensor for citrate as biomarker for early stage detection of prostate cancer based on peroxidase-like activity of cysteine-capped gold nanoclusters”, **Spectrochimica Acta Part A: Molecular and Biomolecular Spectroscopy**. 210: 251-259; March, 2019.
- [29] Martinez, A. W. and et al. “FLASH: a rapid method for prototyping paper-based microfluidic devices”, **Lab on a Chip**. 8(12): 2146-2150; August, 2008.
- [30] Bruzewicz, D. A. Reches, M. and Whitesides, G. M. “Low-cost printing of poly (dimethylsiloxane) barriers to define microchannels in paper”, **Analytical Chemistry**. 80(9): 3387-3392; May, 2008.
- [31] Fenton, E. M. and et al. “Multiplex lateral-flow test strips fabricated by two-dimensional shaping”, **ACS Applied Materials & Interfaces**. 1(1): 124-129; January, 2009.
- [32] Carrilho, E. Martinez A. W. and Whitesides, G. M. “Understanding wax printing: a simple micropatterning process for paper-based microfluidics”, **Analytical Chemistry**. 81(16): 7091-7095; July, 2009.
- [33] Li, X. and et al. “Fabrication of paper-based microfluidic sensors by printing”, **Colloids and Surfaces B: Biointerfaces**. 76(2): 564-570; April, 2010.
- [34] Duagchai, W. Chailapakul, O. and Henry, C.S. “A low-cost, simple, and rapid fabrication method for paper-based microfluidics using wax screen-printing”, **Analyst**. 136(1): 77-82; September, 2011.
- [35] Apilux, A. and et al. “Paper-based thioglycolic acid (TGA)-capped CdTe QD device for rapid screening of organophosphorus and carbamate insecticides”, **Analytical Methods**. 9(3): 519-527; December, 2017.
- [36] Apilux, A. and et al. “Paper-based acetylcholinesterase inhibition assay combining a wet system for organophosphate and carbamate pesticides detection”, **EXCLI Journal**. 14: 307-319; February, 2015.

REFERENCES (CONTINUED)

- [37] Liu, D. and et al. “A highly sensitive, dual-readout assay based on gold nanoparticles for organophosphorus and carbamate pesticides”, **Analytical Chemistry**. 84(9): 4185-4191; April, 2012.
- [38] Yue, G. and et al. “Gold nanoparticles as sensors in the colorimetric and fluorescence detection of chemical warfare agents”, **Coordination Chemistry Reviews**. 311: 75-84; March, 2016.
- [39] Bai, W. and et al. “Gold nanoparticle–based colorimetric aptasensor for rapid detection of six organophosphorous pesticides”, **Environmental Toxicology and Chemistry**. 34(10): 2244-2249; September, 2015.
- [40] Bala, R. Sharma R. K. and Wangoo, N. “Highly sensitive colorimetric detection of ethyl parathion using gold nanoprobess”, **Sensors and Actuators B Chemical**. 210(10): 425-430; April, 2015.
- [41] Li, H. and et al. Visual detection of organophosphorus pesticides represented by mathamidophos using Au nanoparticles as colorimetric probe”, **Talanta**. 87: 93-99; October, 2011.
- [42] Liu, W. and et al. “Highly sensitive and selective colorimetric detection of cartap residue in agricultural products”, **Talanta**. 101: 382-387; September, 2012.
- [43] Xie, R. and et al. “Graphene quantum dots as smart probes for biosensing”, **Analytical Methods**. 8(20): 4001-4016; April, 2016.
- [44] Sinduja, B. and John, S. A. “Ultrasensitive optical sensor for hydrogen peroxide using silver nanoparticles synthesized at room temperature by GQDs”, **Sensors and Actuators B: Chemical**. 247: 648-654; August, 2017.
- [45] Shi, J. and et al. “A fluorescence resonance energy transfer (FRET) biosensor based on graphene quantum dots (GQDs) and gold nanoparticles (AuNPs) for the detection of mecA gene sequence of Staphylococcus aureus”, **Biosensors and Bioelectronics**. 67: 595-600; May, 2015.

REFERENCES (CONTINUED)

- [46] Malahom, N. and et al. “Simple test kit based on colorimetry for quantification of magnesium content in natural rubber latex by miniaturized complexometric titration without using masking agent”, **Polymer Testing**. 59: 160-167; May, 2017.
- [47] Jarujamrus, P. and et al. “Screen-printed microfluidic paper-based analytical device (μ PAD) as a barcode sensor for magnesium detection using rubber latex waste as a novel hydrophobic reagent”, **Analytica Chimica Acta**. 2019 (accepted).
- [48] Royal Society of Chemistry (RSC). (2009). “ULTRAVIOLET-VISIBLE SPECTROSCOPY (UV)”, **Introduction to Ultraviolet-visible Spectroscopy**. http://www.rsc.org/learnchemistry/content/filerepository/-CMP/00/001/304/UV-Vis_Student_resource_pack_ENGLISH.pdf. August 15, 2019.
- [49] Cark, J. “UV-VISIBLE ABSORPTION SPECTRA”, **Instrumental Analysis**. <http://www.chemguide.co.uk/analysis/uvvisible/theory.html>. August 15, 2019.
- [50] Choodum, A and Daeid, NN. “Rapid and semi-quantitative presumptive test for opiate drugs”, **Talanta**. 86: 284-291; October, 2011.
- [51] Sharma, G. **Digital color imaging handbook: color fundamentals for digital imaging**. New York: CRC Press, 2002.
- [52] Burger, W. and Burge, MJ. **Principles of digital image processing: fundamental techniques**. London: Springer-Verlag London Limited, 2009.
- [53] Birch, NC and Stickle DF. “Example of use of a desktop scanner for data acquisition in a colorimetric assay”, **Clinica Chimica Acta**. 333: 95-96; July, 2003.
- [54] Choodum, A. and et al. “Rapid quantitative colourimetric tests for trinitrotoluene (TNT) in soil”, **Forensic Science International**. 222: 340-345; October, 2011.
- [55] Choodum, A. and et al. “Using the iPhone as a device for rapid quantitative analysis of trinitrotoluene in soil”, **Talanta**. 115: 143-149; October, 2013.

REFERENCES (CONTINUED)

- [56] Epperson, P.M. and et al. “Applications of charge transfer devices in spectroscopy”, **Analytical Chemistry**. 60: 327A-335A; March, 1998.
- [57] Suzuki, Y and et al. “Tristimulus colorimetry using a digital still camera and its application to determination of iron and residual chlorine in water samples”, **Analytical Science**. 22: 411-414; March, 2006.
- [58] Cantrell, Y and et al. “Use of the parameter of the hue, saturation, value color spaces as a quantitative analytical parameter for bitonal optical sensors”, **Analytical Chemistry**. 82: 531-542; December, 2010.
- [59] Byrne, L. and et al. “Digital imaging as a detector for generic analytical measurements”, **TrAC Trends in Analytical Chemistry**. 19: 517-522; August, 2000.
- [60] Meelapsom, R. and et al. “Chromatic analysis by monitoring unmodified silver nanoparticles reduction on double layer microfluidic paper-based analytical devices for selective and sensitive determination of mercury (II)”, **Talanta**. 155: 193-201; August, 2016.
- [61] Xia, Y. Si, J. and Li, Z. “Fabrication techniques for microfluidic paper-based analytical devices and their applications for biological testing: A review”, **Biosensors and Bioelectronics**. 77: 774-789; October, 2016.
- [62] Lu, Y. and et al. “Fabrication and characterization of paper-based microfluidics prepared in nitrocellulose membrane by wax printing”, **Analytical Chemistry**. 82(1): 329–335; December, 2010.
- [63] Cai, L.F. and et al. “A simple paper-based microfluidic device for the determination of the total amino acid content in a tea leaf extract” **Journal of Chemical Education**. 90(2): 232–234; December, 2013.
- [64] Yamada, K. and et al. “Paper-based inkjet-printed microfluidic analytical devices”, **Angewandte Chemie International Edition**. 54(18): 5294–5310; April, 2015.
- [65] Xu, C. and et al. “Low-cost and rapid prototyping of microfluidic paper-based analytical devices by inkjet printing of permanent marker ink”, **RSC Advance**. 5(7): 4770–4773, December, 2015.

REFERENCES (CONTINUED)

- [66] Yu, W.W. and White, I.M. “inkjet printed surface enhanced raman spectroscopy array on cellulose paper”, **Analytical Chemistry**. 82: 9626–9630; November, 2010.
- [67] Yamada, K. and et al. “Paper-based inkjet-printed microfluidic analytical devices”, **Angewandte Chemie International Edition**. 54(18): 5294–5310; April, 2015.
- [68] Carrilho, E. and et al. “Paper microzone plates”, **Analytical Chemistry**. 81(15): 5990–5998; July, 2009.
- [69] Olkkonen, J. Lehtinen, K. and Erho, T. “Flexographically printed fluidic structures in paper”, **Analytical Chemistry**. 84(24): 10246-10250; November, 201.
- [70] Li, X. Ballerini, D.R. and Shen, W. “A perspective on paper-based microfluidics: Current status and future trends”, **Biomicrofluidics**. 6(1): 11301–113013, March, 2012.
- [71] Li, X. and et al. “Paper-based microfluidic devices by plasma treatment”, **Analytical Chemistry**. 80(23): 9131–9134; November, 2008.
- [72] Chitnis, G. and et al. “Laser-treated hydrophobic paper: an inexpensive microfluidic platform”, **Lab on a Chip**. 11(6): 1161–1165; December, 2011.
- [73] Sones, C.L. and et al. “Laser-induced photo-polymerisation for creation of paper-based fluidic devices”, **Lab on a Chip**. 14(23): 4567–4574; September, 2014.
- [74] Spicar-Mihalic, P. and et al. “CO₂ laser cutting and ablative etching for the fabrication of paper-based devices”, **Journal of Micromechanics and Microengineering**. 23(6): 6; May, 2013.
- [75] Cai, L. and et al. “A simple paper-based sensor fabricated by selective wet etching of silanized filter paper using a paper mask”, **Biomicrofluidics**. 8(5): 056504; October, 2014.

REFERENCES (CONTINUED)

- [76] Zhang, L. and et al. "Fabrication of glass-based microfluidic devices with dry film photoresists as pattern transfer masks for wet etching", **RSC Advance**. 5(8): 5638–5646, December, 2015.
- [77] Sun, J.Y. Cheng, C.M. and Liao, Y.C. "Screen printed paper-based diagnostic devices with polymeric inks", **Analytical Sciences**. 31(3): 145–151, 2015.
- [78] Wang, S. and et al. "Paper-based chemiluminescence ELISA: Lab-on-paper based on chitosan modified paper device and wax-screen-printing", **Biosensors and Bioelectronics**. 31(1): 212–218; January, 2012.
- [79] De Souza, C. D. Nogueira, B. R. and Rostelato, M. E. C. "Review of the methodologies used in the synthesis gold nanoparticles by chemical reduction. Journal of Alloys and Compounds", **Journal of Alloys and Compounds**. 798: 714-740; August, 2019.
- [80] Zhao, P. Li, N. and Astruc, D. "State of the art in gold nanoparticle synthesis", **Coordination Chemistry Reviews**. 257(3-4): 638-665; February, 2013.
- [81] Kimling, M. and et al. "Turkevich method for gold nanoparticle synthesis revisited", **The Journal of Physical Chemistry B**. 110(32): 15700-15707; July, 2006.
- [82] Daniel M.-C. and Astruc, D. "Gold nanoparticles: assembly, supramolecular chemistry, quantum-size-related properties, and applications toward biology, catalysis, and nanotechnology", **Chemical Reviews**. 104(1): 293-346; December, 2004.
- [83] Toma, H.E. and et al. "The coordination chemistry at gold nanoparticles", **Journal of the Brazilian Chemical Society**. 21(7): 1158-1176, 2010.
- [84] Mertens, R. and Peleg, R. "Graphene quantum dot", **Graphene Quantum Dots: Introduction and Market News**. <https://www.grapheneinfo.com/graphene-quantum-dots>. August 21, 2019.
- [85] Merck. "Synthesis of graphene quantum dot", **Graphene Quantum Dots: Properties, Synthesis & Applications**. <https://www.sigmaaldrich.com/-technical/documents/articles/materials-science/graphene-quantum-dots.html>. August 21, 2019.

REFERENCES (CONTINUED)

- [86] Benítez-Martínez, S. and Valcárcel, M. “Graphene quantum dots in analytical science”, **Trends in Analytical Chemistry**. 72: 93-113; October, 2015.
- [87] Abarghoei, S. and et al. “A colorimetric paper sensor for citrate as biomarker for early stage detection of prostate cancer based on peroxidase-like activity of cysteine-capped gold nanoclusters”, **Spectrochimica Acta Part A: Molecular and Biomolecular Spectroscopy**. 210: 251-259; March, 2019.
- [89] Abdelhalim, M. A. K. Mady M. M. and Ghannam, M.M. “Physical properties of different gold nanoparticles: ultraviolet-visible and fluorescence measurements”, **Journal of Nanomedicine & Nanotechnology**. 3(3): 178-194; May, 2012.
- [90] J. Sun, and et al. “A simple, label-free AuNPs-based colorimetric ultrasensitive detection of nerve agents and highly toxic organophosphate pesticide”, **Biosensors and Bioelectronics**. 28(1): 152-157; October, 2011.
- [91] N. Li, and et al. “Graphene quantum dots for ultrasensitive detection of acetylcholinesterase and its inhibitors”, **2D Materials**. 2: 034018; September, 2015.
- [92] J. Deng, and et al. “Highly sensitive GQDs-MnO₂ based assay with turn-on fluorescence for monitoring cerebrospinal acetylcholinesterase fluctuation: A biomarker for organophosphorus pesticides poisoning and management”, **Environmental Pollution**. 224: 436-444; May, 2017.
- [93] Chen, N. and et al. “A colorimetric sensor based on citrate-stabilized AuNPs for rapid pesticide residue detection of terbuthylazine and dimethoate”, **Sensors and Actuators B: Chemical**. 255: 3093-3101; February, 2018.
- [94] Li, H. and et al. “Carbon dot-based bioplatform for dual colorimetric and fluorometric sensing of organophosphate pesticides”, **Sensors and Actuators B: Chemical**. 260: 563-570; May, 2018.
- [95] Zakir Hossain, S. M. and et al. “Reagentless bidirectional lateral flow bioactive paper sensors for detection of pesticides in beverage and food samples”, **Analytical Chemistry**. 81(21): 9055–9064; September, 2009.

REFERENCES (CONTINUED)

- [96] Badawy, M. E. and El-Aswad, A. F. “Bioactive paper sensor based on the acetylcholinesterase for the rapid detection of organophosphate and carbamate pesticides”, **Analytical Chemistry**. 2014: 536823-536829; November, 2014.
- [97] Nouanthavong, S. and et al. “Pesticide analysis using nanoceria-coated paper-based devices as a detection platform”, **Analyst**. 141(5): 1837-1846; January, 2016.
- [98] Wu, S. and et al. “Gold nanoparticles dissolution based colorimetric method for highly sensitive detection of organophosphate pesticides”, **Sensors and Actuators B: Chemical**. 238: 427-433; January, 2017.
- [99] Luo, Q. and et al. “A 3D-printed self-propelled, highly sensitive mini-motor for underwater pesticide detection”, **Talanta**. 183: 297-303; June, 2018.
- [100] Kim, H. J. and et al. “Development of colorimetric paper sensor for pesticide detection using competitive-inhibiting reaction”, **BioChip Journal**. 12(4): 326-331; December, 2018.
- [101] Harshit, D. Charmy, K. and Nrupesh, P. “Organophosphorus pesticides determination by novel HPLC and spectrophotometric method”, **Food Chemistry**. 230: 448-453; September, 2017.
- [102] Shen, Y. and et al. “A new water-soluble and colorimetric fluorescent probe for highly sensitive detection of organophosphorus pesticides”, **RSC Advances**. 6(91): 88096-88103; August, 2016.
- [103] Fu, G. and et al. “Highly sensitive colorimetric detection of organophosphate pesticides using copper catalyzed click chemistry”, **Talanta**. 103: 110-115; January, 2013.
- [104] Liu, T. and et al. “acetylcholinesterase-free colorimetric detection of chlorpyrifos in fruit juice based on the oxidation reaction of H₂O₂ with chlorpyrifos and ABTS²⁻ Catalyzed by Hemin/G-Quadruplex DNAzyme”, **Food Analytical Methods**. 8(6): 1556-1564; November, 2015.

REFERENCES (CONTINUED)

- [105] Zhao, D. and et al. “Carbon dots-assisted colorimetric and fluorometric dual-mode protocol for acetylcholinesterase activity and inhibitors screening based on the inner filter effect of silver nanoparticles”, **Analyst**. 141(11): 3280-3288; April, 2016.
- [106] Feng, S. and et al. “Development of molecularly imprinted polymers-surface-enhanced Raman spectroscopy/colorimetric dual sensor for determination of chlorpyrifos in apple juice”, **Sensors and Actuators B: Chemical**. 241: 750-757; March, 2017.
- [107] Lisha, K. P. and Pradeep, T. “Enhanced visual detection of pesticides using gold nanoparticles”, **Journal of Environmental Science and Health Part B**. 44(7): 697-705; September, 2009.
- [108] Lin, B. and et al. “Modification-free carbon dots as turn-on fluorescence probe for detection of organophosphorus pesticides”, **Food Chemistry**. 245: 1176-1182; April, 2018.
- [109] Kim, H. J. and et al. “development of colorimetric paper sensor for pesticide detection using competitive-inhibiting reaction”, **BioChip Journal**. 12(4): 326-331; December, 2018.
- [110] Ouyang, H. and et al. “Colorimetric and chemiluminescent dual-readout immunochromatographic assay for detection of pesticide residues utilizing g-C₃N₄/BiFeO₃ nanocomposites”, **Biosensors and Bioelectronics**. 106: 43-49; May, 2018.

APPENDICES

APPENDIX A

A Part I: Spectrophotometric method for chlorpyrifos determination

Synthesis of GQDs-AuNPs

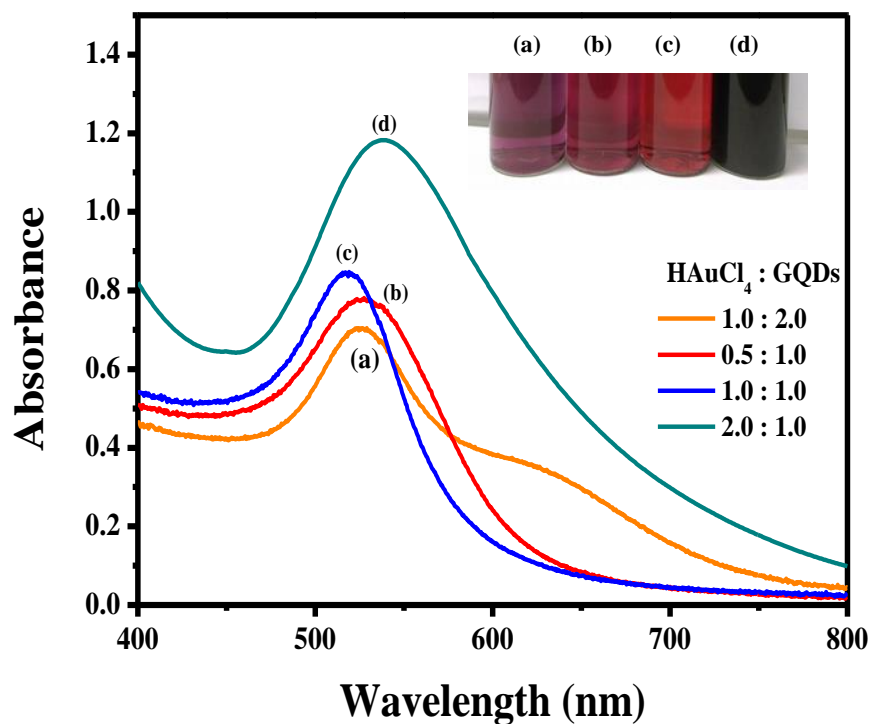


Figure A.1 Absorption spectra of various volume ratio of HAuCl₄ (0.4 mM): GQDs (0.4 mg mL⁻¹) at and for synthesis GQDs-AuNPs. Inset is their respective images.

Fluorescence spectroscopy

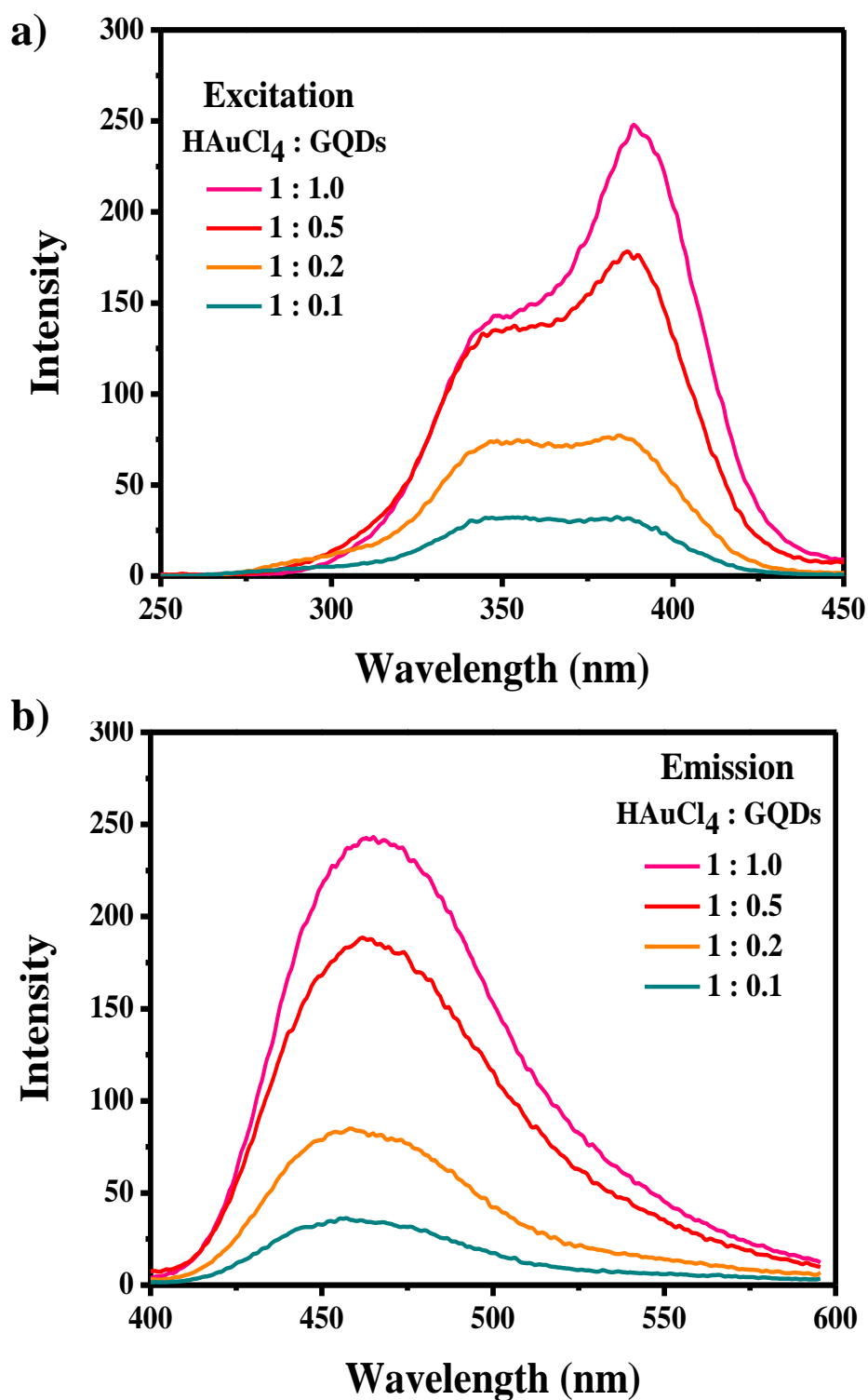


Figure A.2 Fluorescence spectra of various volume ratio of HAuCl₄ (0.4 mM): GQDs (0.4 mg mL⁻¹) for synthesis GQDs-AuNPs, a) excitation and b) emission spectra.

Effect of the ATCh concentrations

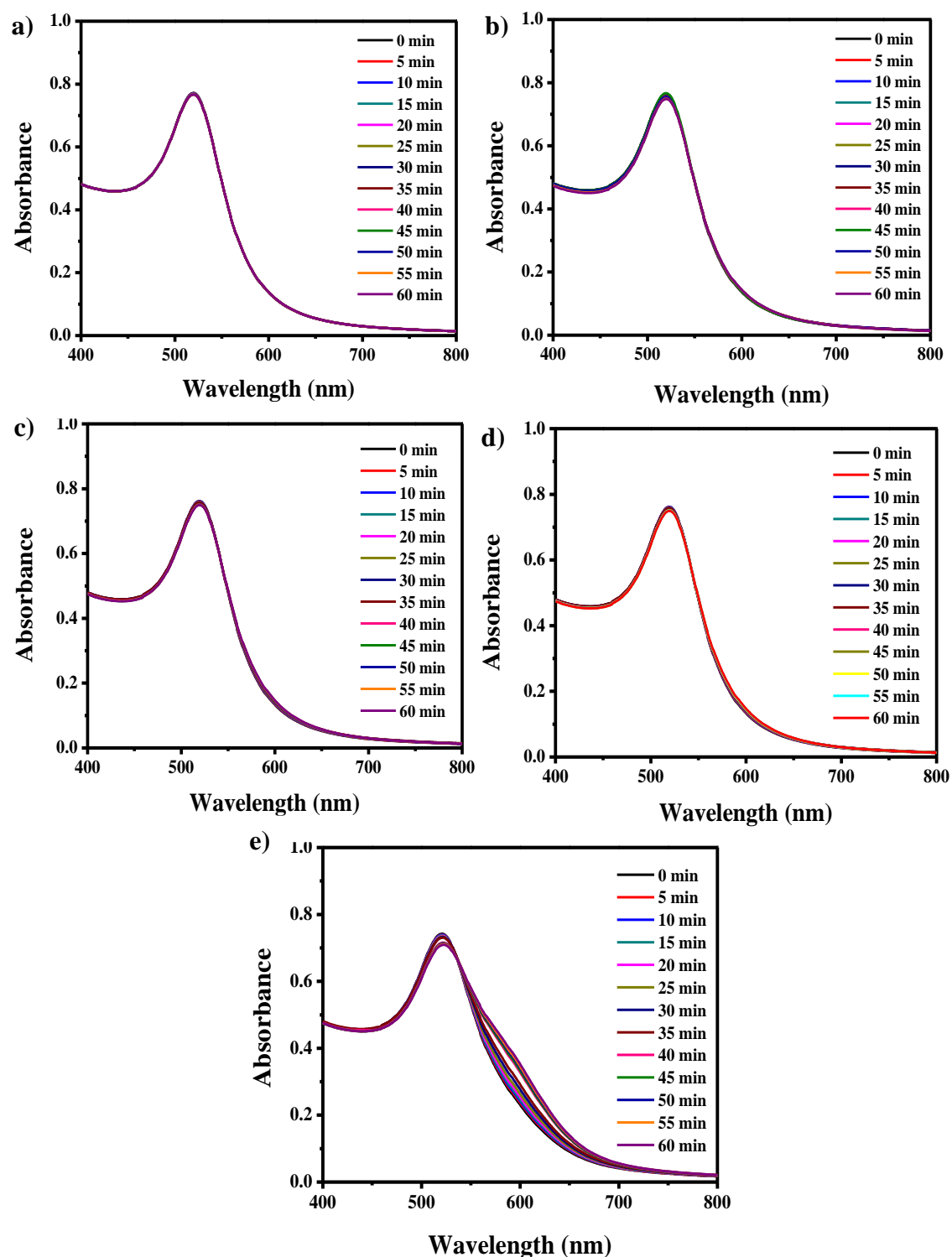


Figure A.3 Absorption spectra of GQDs-AuNPs after addition of various concentration of ATCh recorded every 5 min, a) 50 μM , b) 100 μM , c) 200 μM , d) 300 μM and e) 500 μM .

Effect of the AChE concentration

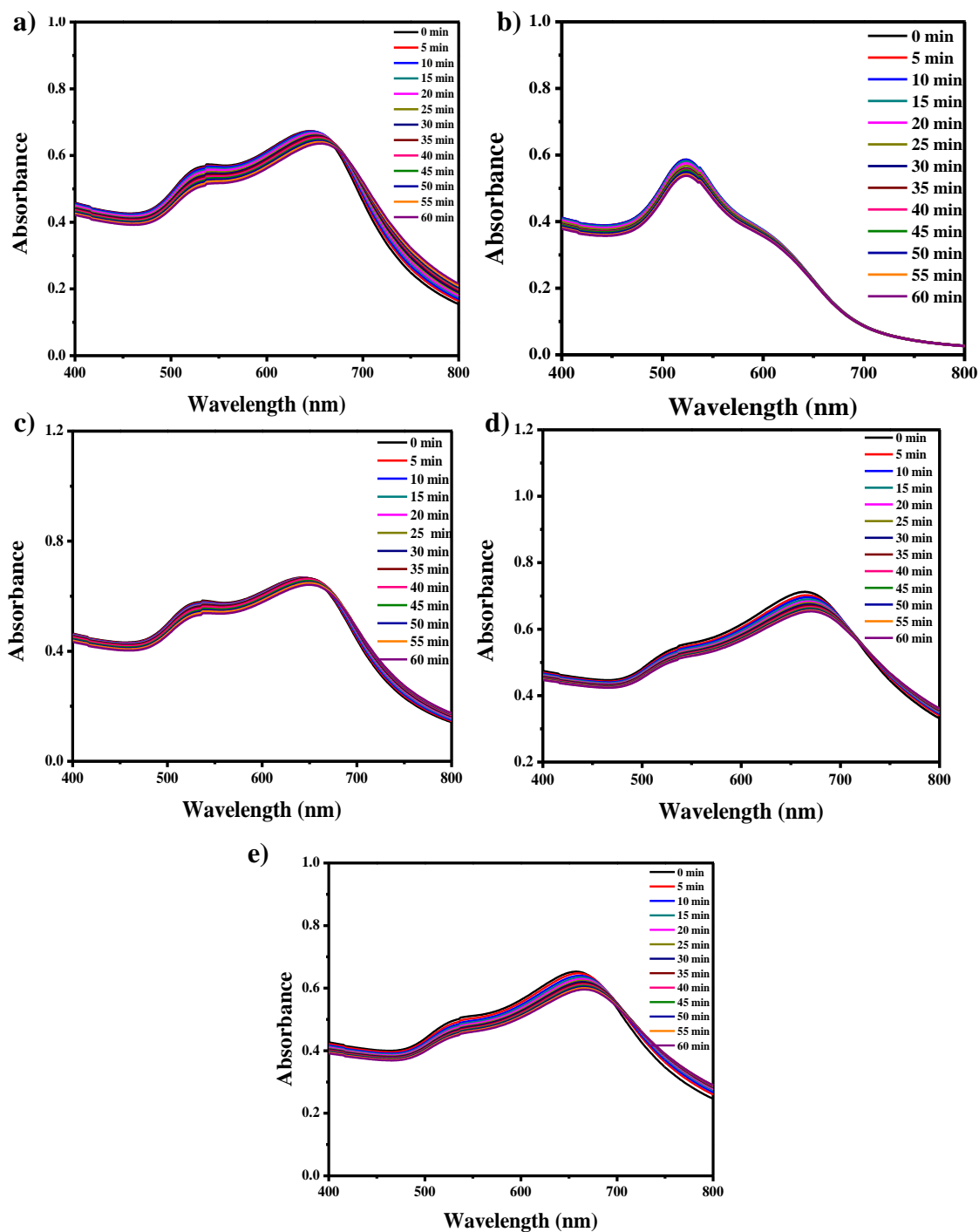
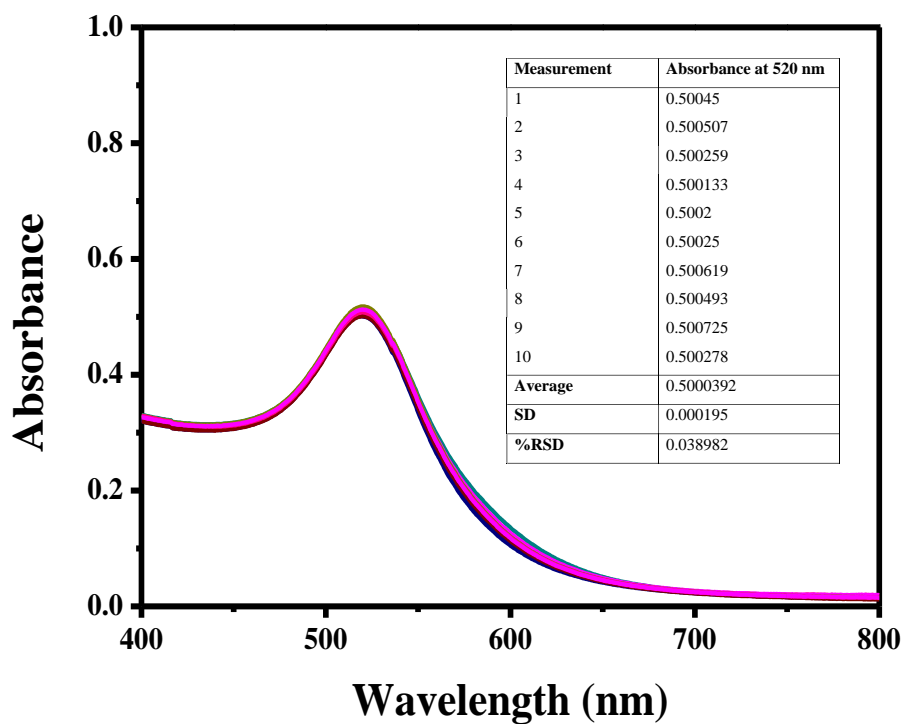


Figure A.4 Absorption spectra of GQDs-AuNPs after addition of ATCh (50 μM , pH 7.0 PBS) and difference concentration of AChE recorded every 5 min, a) 100 mU mL^{-1} , b) 200 mU mL^{-1} , c) 300 mU mL^{-1} , d) 400 mU mL^{-1} and e) 500 mU mL^{-1} .

Limit of detection (LOD) for chlorpyrifos**Figure A.5 Absorption spectra for bank signal in reaction solution (ten replicated).**

Interference study

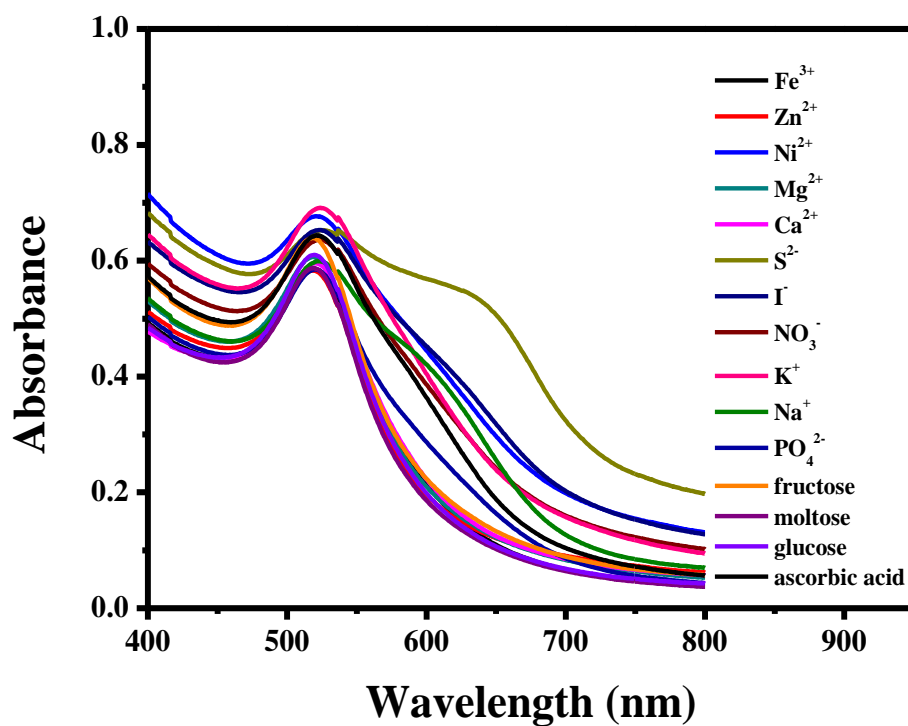


Figure A.6 Absorption spectra of interference study for chlorpyrifos detection.

APPENDIX B

B Part II: 3D- μ PAD for chlorpyrifos determination

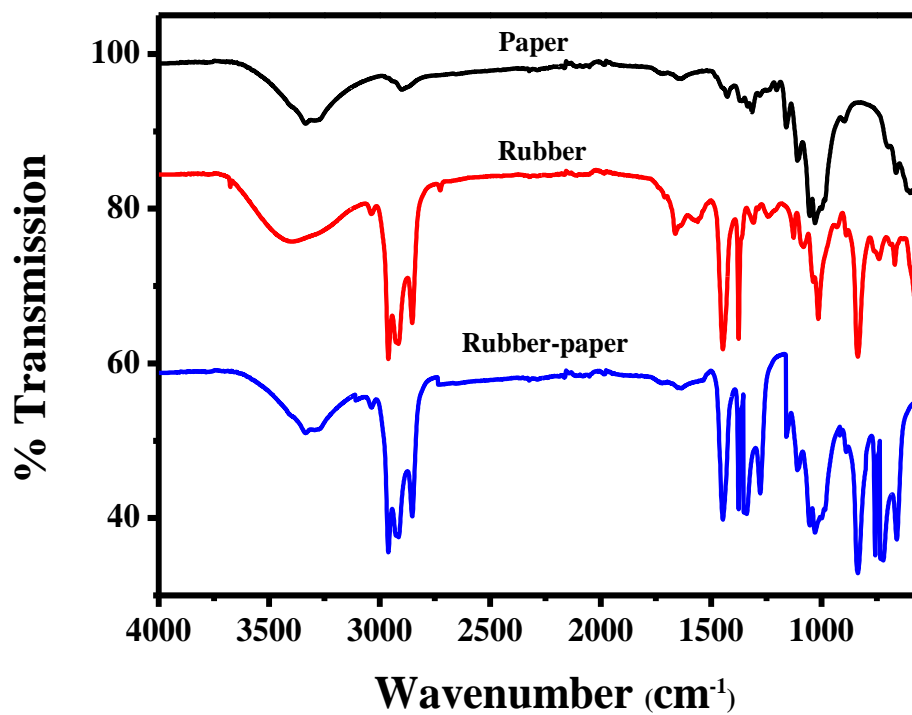
Fourier-transform infrared spectroscopy (FTIR)

Figure B.1 FT-IR spectra of paper, rubber, and rubber-paper.

Method validation

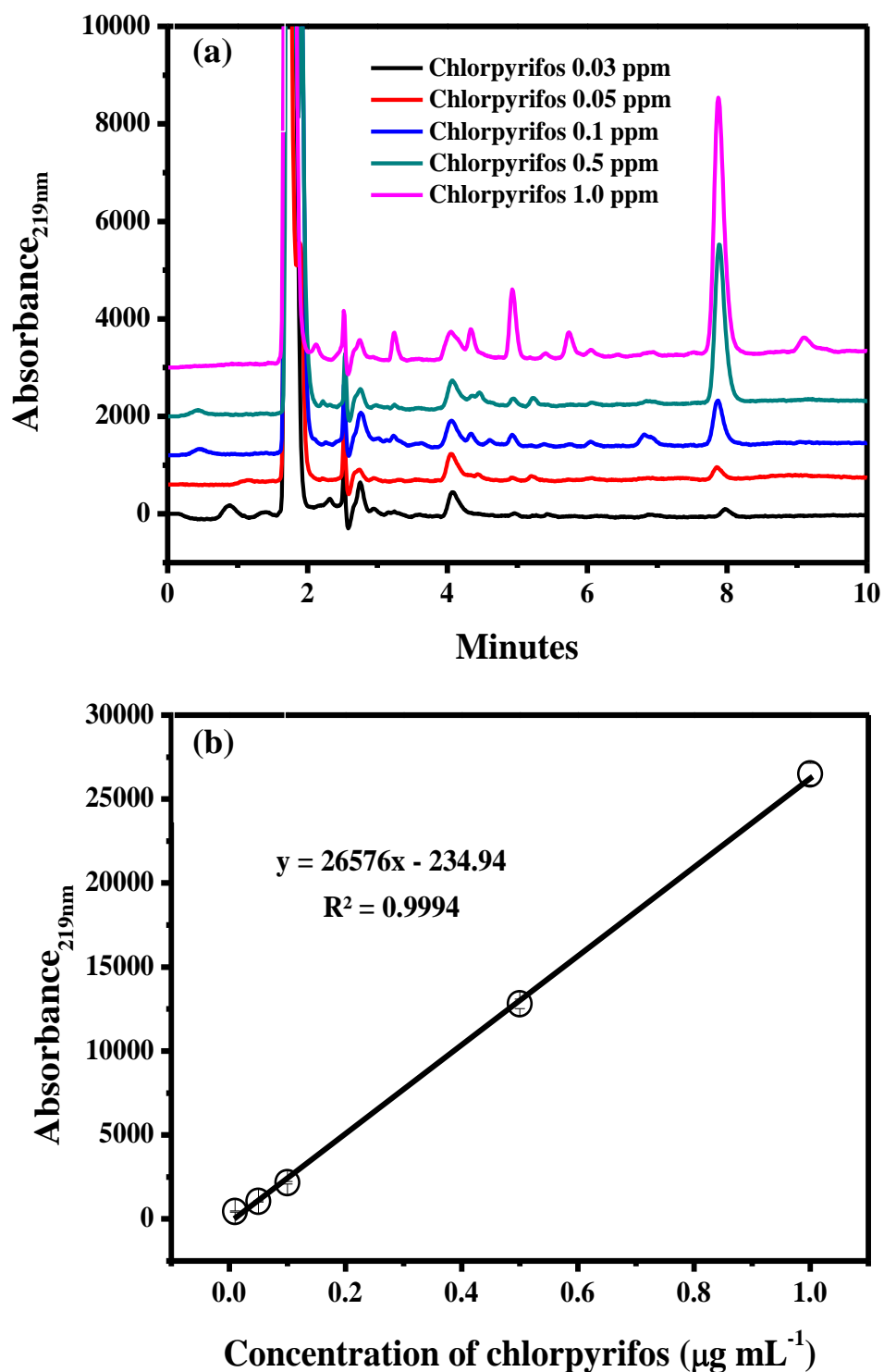


Figure B.2 HPLC chromatogram at 219 nm of various chlorpyrifos concentration (a), and calibration plot between absorbance at 219 nm and concentration of chlorpyrifos.

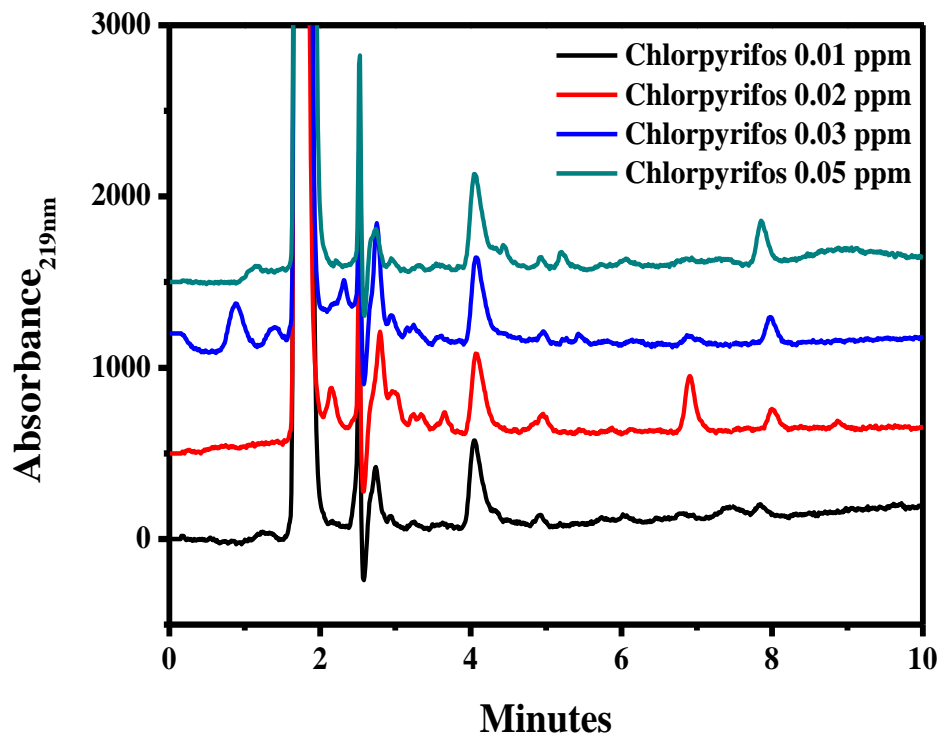
Method validation**Limit of detection (LOD) for method validation**

Figure B.3 HPLC chromatogram at 219 nm of various chlorpyrifos concentration.

Method validation

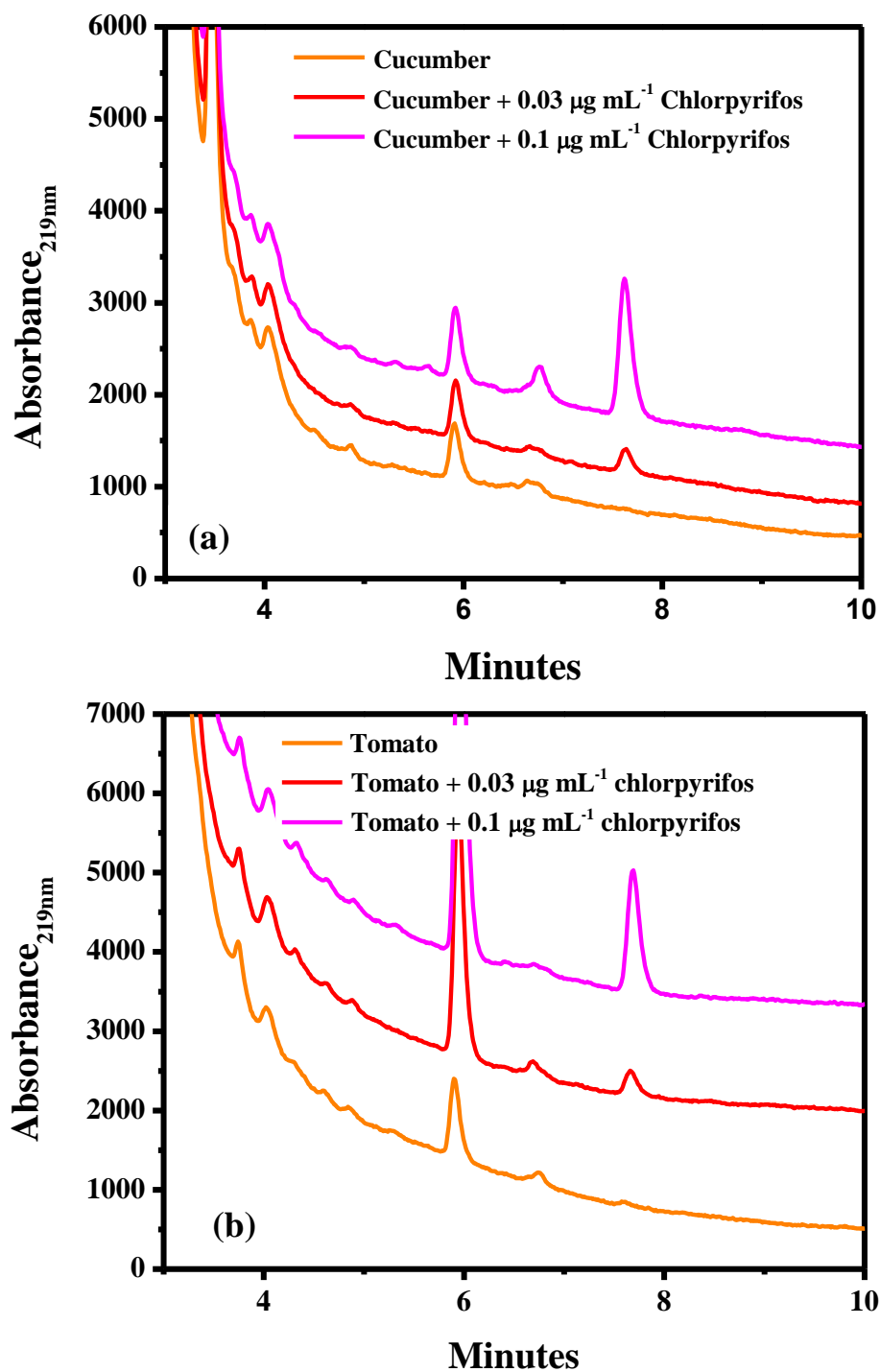


Figure B.4 HPLC chromatogram at 219 nm for chlorpyrifos detection in fixed concentration of standard chlorpyrifos (0.0, 0.03 and 0.1 $\mu\text{g mL}^{-1}$) and various real sample; cucumber (a), tomato (b), lettuce (c), cabbage (d), carrot (e), and radish (f).

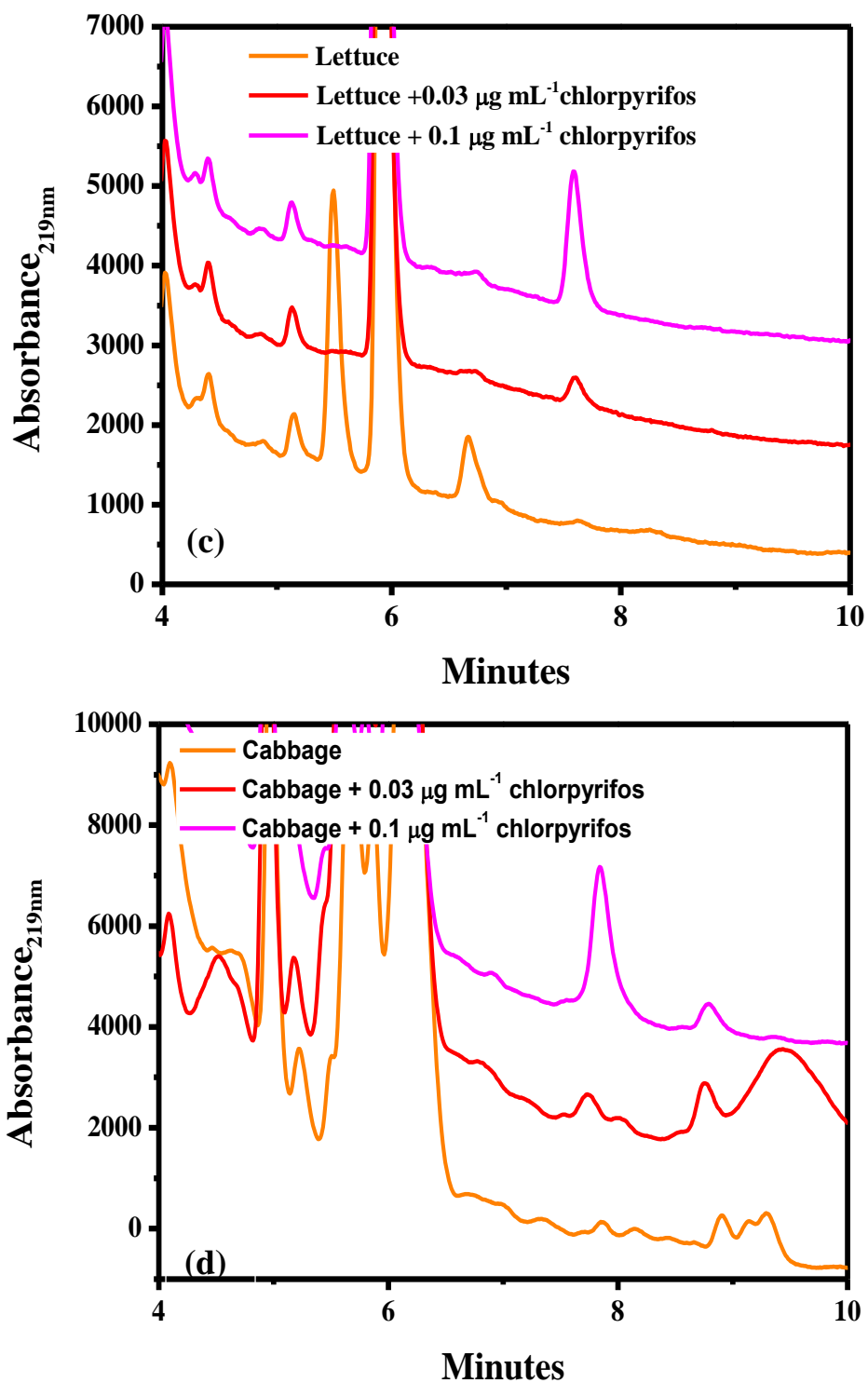


Figure B.4 HPLC chromatogram at 219 nm for chlorpyrifos detection in fixed concentration of standard chlorpyrifos (0.0, 0.03 and 0.1 $\mu\text{g mL}^{-1}$) and various real sample; cucumber (a), tomato (b), lettuce (c), cabbage (d), carrot (e), and radish (f) (Continued).

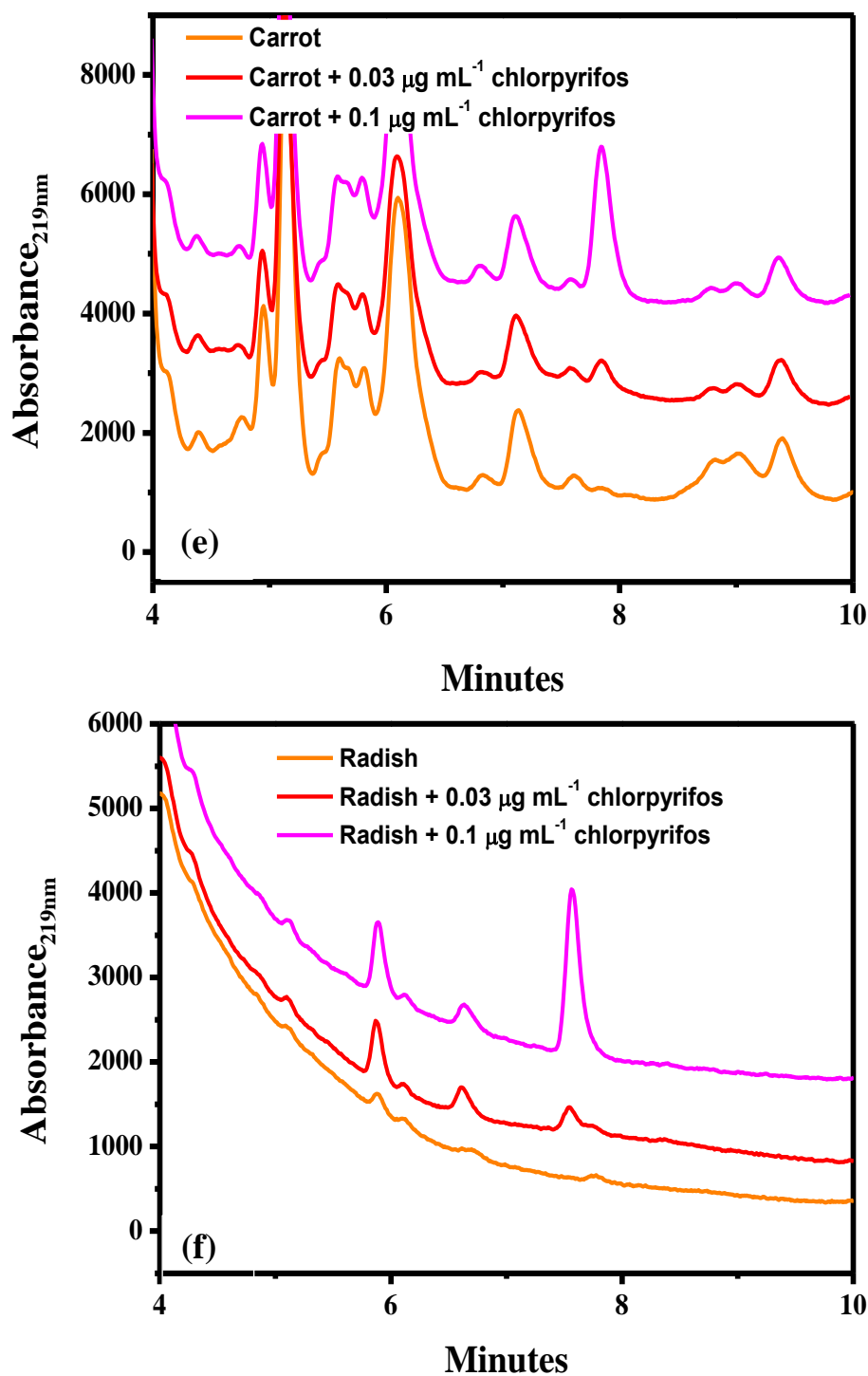


Figure B.4 HPLC chromatogram at 219 nm for chlorpyrifos detection in fixed concentration of standard chlorpyrifos (0.0, 0.03 and 0.1 $\mu\text{g mL}^{-1}$) and various real sample; cucumber (a), tomato (b), lettuce (c), cabbage (d), carrot (e), and radish (f) (Continued).

APPENDIX C
CONFERENCES

CONFERENCES

Poster presentation

1. Warinporn Chungchai, Purim Jarujamrus, Sanoe Chiaram, and Maliwan Amatatongchai* “Highly sensitive colorimetric detection of organophosphate pesticides using L-cysteine modified gold nanoparticles” **The 2018 Pure and Applied Chemistry International Conference (PACCON 2018)**, 7-9 February 2018, Prince of Songkla University, Thailand.

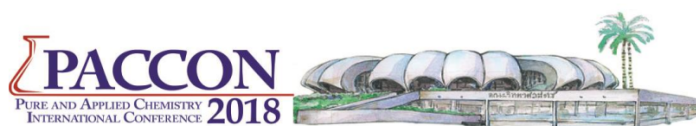
2. W. Chungchai, P. Jarujamrus, S. Chiaram, and M. Amatatongchai* “Development of a novel colorimetric sensor for organophosphate pesticides” **2018 International Congress for Innovation in Chemistry (PERCH-CIC Congress X)**. 4-7 July 2018, Jomtien Palm Beach Hotel & Resort in Pattaya, Thailand.

Oral presentation

1. Warinporn Chungchai “Development of a novel colorimetric sensor for organophosphate pesticides” **2018 International Congress for Innovation in Chemistry (PERCH-CIC Congress X)**. 4-7 July 2018, Jomtien Palm Beach Hotel & Resort in Pattaya, Thailand.

Publication

1. Warinporn Chungchai, Maliwan Amatatongchai, Rattapol Meelapsom, Ketsarin Seebunrueng, Saksri Suparsorn & Purim Jarujamrus. “Development of a novel three-dimensional microfluidic paper-based analytical device (3D- μ PAD) for chlorpyrifos detection using graphene quantum-dot capped gold nanocomposite for colorimetric assay” **International Journal of Environmental Analytical Chemistry**. (2019), Published online: 07 Aug 2019.



Highly sensitive colorimetric detection of organophosphate pesticides using L-cysteine modified gold nanoparticles

Warinporn Chungchai, Purim Jarujamrus, Sanoë Chiaram,
Maliwan Amatongchai*

*Department of Chemistry and Center of Excellence for Innovation in Chemistry, Faculty of Science,
Ubon Ratchathani University, Ubon Ratchathani 34190, Thailand.*

**E-mail: maliwan.a@ubu.ac.th.*

Abstract: This research presents the development of highly sensitive colorimetric technique for detection of organophosphate pesticides. L-cysteine used to modify the gold nanoparticles (Cys-AuNPs) surface, exhibiting extremely high selectivity towards thiocholine under optimized conditions. The principle of the assay based on enzymatic hydrolysis of acetylthiocholine (ATCh) into positively charged thiocholine by acetylcholinesterase (AChE). A distinctive color changed from red to blue could be firstly observed by naked eyes and UV-Visible spectrophotometric measurement at maximum wavelength of 580 nm as a result of the aggregation of AuNPs induced by the interaction between thiocholine and Cys-AuNPs. Upon addition of chlorpyrifos and profenofos as organophosphate pesticides, the inhibition of enzymatic hydrolysis of AChE was occurred, leading to anti-aggregation of Cys-AuNPs. The increasing of red color of Cys-AuNPs at 520 nm was proportionally observed to the concentration of pesticides. The parameters affecting the pesticides quantification including pH, reaction time, concentration of AChE and ATCh were investigated. The linearity of developed method was established in the range of 0–400 ppt ($r^2=0.9940$ and 0.9980) with the detection limit was 0.704 and 0.713 ppt for chlorpyrifos and profenofos, respectively. This work demonstrates alternative approach which is simple, rapid, sensitive and selective detection of organophosphate pesticides.

Keywords: Cysteine-Gold nanoparticles (Cys-AuNPs), Acetylthiocholine, Chlorpyrifos, Profenofos, Acetylcholinesterase enzyme, Thiocholine, Colorimetry



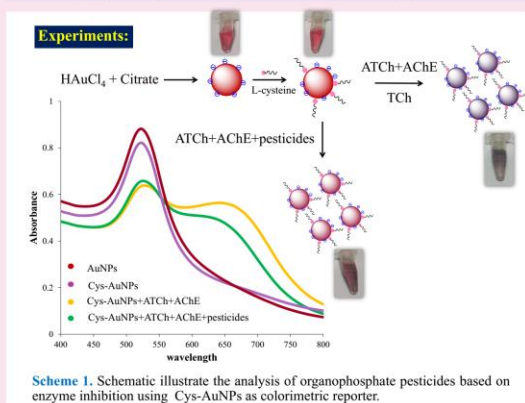
Highly sensitive colorimetric detection of organophosphate pesticides using L-cysteine modified gold nanoparticles

Warinporn Chungchai, Purim Jarujamrus, Sanoe Chiaram, Maliwan Amatongchai*
Department of Chemistry and Center of Excellence for Innovation in Chemistry, Faculty of Science,
Ubon Ratchathani University, Ubon Ratchathani 34190, Thailand.

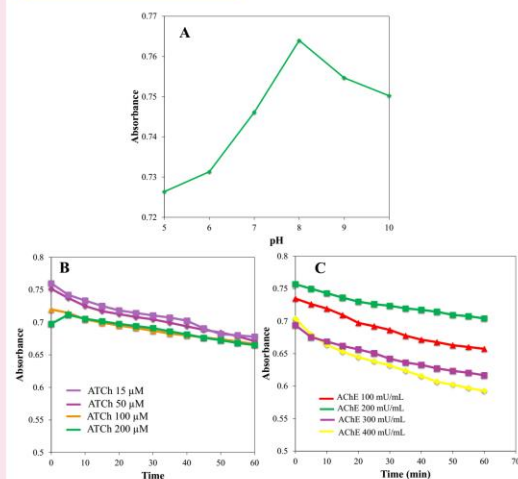
*E-mail: maliwan.a@ubu.ac.th



Abstract: This research presents the development of highly sensitive colorimetric technique for detection of organophosphate pesticides. L-cysteine was used to modify the gold nanoparticles (Cys-AuNPs) surface, exhibiting extremely high selectivity towards thiocholine under optimized conditions. The principle of the assay based on enzymatic hydrolysis of acetylthiocholine (ATCh) into positively charged thiocholine by acetylcholinesterase (AChE). A distinctive color changed from red to blue could be firstly observed by naked eyes and UV-Visible spectrophotometric measurement at maximum wavelength of 580 nm as a result of the aggregation of AuNPs induced by the interaction between thiocholine and Cys-AuNPs. Upon addition of chlorpyrifos and profenofos as organophosphate pesticides, the inhibition of enzymatic hydrolysis of AChE was occurred, leading to anti-aggregation of Cys-AuNPs. The increasing of red color of Cys-AuNPs at 520 nm was proportionally observed to the concentration of pesticides. The parameters affecting the pesticides quantification including pH, reaction time, concentration of AChE and ATCh were investigated. The linearity of developed method was established in the range of 0-1000 μM ($r^2=0.9940$ and 0.9980) with the detection limit was 2.0 μM and 0.96 μM for chlorpyrifos and profenofos, respectively. This work demonstrates alternative approach which is simple, rapid, sensitive and selective detection of organophosphate pesticides.



Optimization of conditions :



References :

Sun, J.; Guo, L.; Bao, Y.; Xie, J. *Biosensors and Bioelectronics* **2011**, *21*, 151-157.
Liu, D. B.; Chen, W. W.; Wei, J. H.; Li, X. B.; Wang, Z.; Jiang, X. Y. *Analytical Chemistry* **2012**, *84*, 4185-4191.
Li, H.; Gao, J.; Ping, H.; Liu, L.; Zhang, M.; Guan, F.; Sun, C.; Zhang, Q. *Talanta* **2011**, *87*, 93-99.

Linearity:

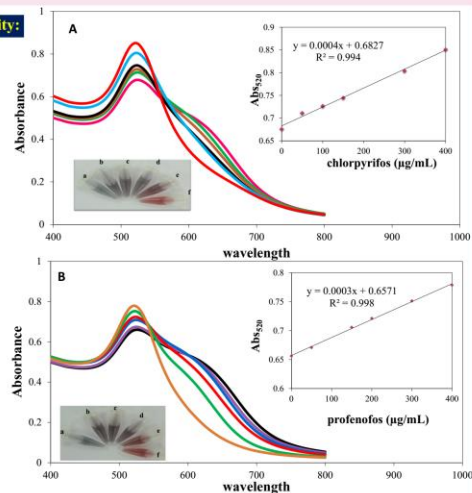


Table 1. Effect of foreign ions on the absorbance at 520 nm (A_{520}) obtained from standard 200 $\mu\text{g/mL}$ chlorpyrifos and profenofos.

Interference	Tolerance limit (mg/mL)	
	Chlorpyrifos	Profenofos
Na^+ , K^+	50	50
CO_3^{2-}	40	40
Cu^{2+} , Mg^{2+} , I^-	30	35
PO_4^{3-} , Br^- , SO_4^{2-} , SO_3^{2-} , NO_3^-	20	25
S^{2-}	15	20
Cl^-	10	10
Ca^{2+}	5	5
Fe^{3+} , Co^{2+} , Ni^{2+}	1	2

*Investigated concentration 0-100 mg/mL

Conclusions :

We developed highly sensitive colorimetric technique for detection of organophosphate pesticides. The detection was based on the aggregation of L-cysteine coated gold nanoparticles (Cys-AuNPs) when reacted with thiocholine leading to color change from red to blue. This reaction was applied for determination of profenofos and chlorpyrifos. The developed method shows a widely linear range with acceptable low detection limit. This method provides a simply, rapidly, sensitivity and selectivity for detection of organophosphate pesticides.

Acknowledgements :



S1-P8

Development of a novel colorimetric sensor for organophosphate pesticides

Warinporn Chungchai, Purim Jarujamrus, Sanoee Chiaram, and Maliwan Amatatongchai*

Department of Chemistry and Center of Excellence for Innovation in Chemistry (PERCH-CIC), Faculty of Science, Ubon Ratchathani University, Ubon Ratchathani 34190, Thailand.

maliwan.a@ubu.ac.th

This research presents the development of a highly sensitive colorimetric assay for chlorpyrifos organophosphate pesticide in vegetable and fruit samples. The graphene quantum dot (GQDs) capped with gold nanoparticles (AuNPs) (GQDs-AuNPs) was synthesized and exhibited extremely high selective activity towards thiocholine under the optimized conditions. The assay was based on enzymatic hydrolysis of acetylthiocholine (ATCh) into positively charged thiocholine by acetylcholinesterase (AChE). A distinctive color changed from red to blue could be observed by naked eyes and UV-Visible spectrophotometric measurement either at the maximum wavelength of 520 nm (red) and 650 nm (blue) as a result of the aggregation of GQDs-AuNPs induced by the interaction between thiocholine and GQDs-AuNPs. Upon addition of chlorpyrifos, the inhibition of enzymatic hydrolysis of AChE was occurred, leading to anti-aggregation of GQDs-AuNPs. The increasing of red color of AuNPs at 520 nm was proportionally observed to the concentration of chlorpyrifos. The parameters affecting the chlorpyrifos quantification including pH, reaction time, concentration of AChE and ATCh were investigated. The linearity of developed method was established in the range of 0.1-50 $\mu\text{g/mL}$ ($r^2=0.9910$) with the detection limit of 0.046 $\mu\text{g/mL}$. This work demonstrates alternative approach which is simple, rapid, sensitive and selective detection of organophosphate pesticide.

Keywords: graphene quantum dot capped gold nanoparticles (GQDs-AuNPs), thiocholine, chlorpyrifos, acetylthiocholine (ATCh), colorimetry, acetylcholinesterase (AChE)

References:

1. Nouanthavong,; Nacapricha, D.; Henry, C. S.; Sameenoi, Y. *Analyst* **2016**, *141*(5), 1837.
2. Sharma, S.; Singh, S.; Ganguli, A. K.; Shanmugam, V. *Carbon* **2017**, *115*, 781.
3. Meng, X.; Schultz, C. W.; Cui, C., *Sensor. Actuat. B Chem.* **2015**, *215*, 577.
4. Su, X.; Chan, C.; Shi, J.; Tsang, M. K.; Pan, Y.; Cheng, C.; Gerile, O.; Yang, M. *Biosens. Bioelectron.* **2017**, *92*, 489.



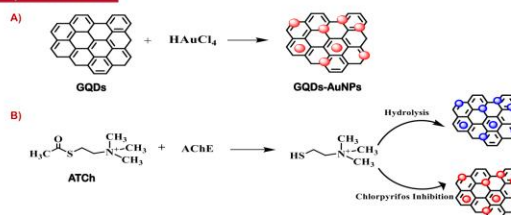
Development of a novel colorimetric sensor for organophosphate pesticides

W. Chungchai, P. Jarujamrus, S. Chiaram, M. Amatongchai*

Department of Chemistry and Center of Excellence for Innovation in Chemistry (PERCH-CIC),
Faculty of Science, Ubon Ratchathani University, Ubon Ratchathani 34190, Thailand.
*E-mail: maliwan.a@ubu.ac.th

Abstract : This research presents the development of a highly sensitive colorimetric assay for chlorpyrifos organophosphate pesticide in vegetable and fruit samples. The graphene quantum dot (GQDs) capped with gold nanoparticles (AuNPs) (GQDs-AuNPs) was synthesized and exhibited extremely high selective activity towards thiocholine under the optimized conditions. The assay was based on enzymatic hydrolysis of acetylthiocholine (ATCh) into positively charged thiocholine by acetylcholinesterase (AChE). A distinctive color change from red to blue could be observed by naked eyes and UV-Visible spectrophotometric measurement either at the maximum wavelength of 520 nm (red) and 650 nm (blue) as a result of the aggregation of GQDs-AuNPs induced by the interaction between thiocholine and GQDs-AuNPs. Upon addition of chlorpyrifos, the inhibition of enzymatic hydrolysis of AChE was occurred, leading to anti-aggregation of GQDs-AuNPs. The increasing of red color of AuNPs at 520 nm was proportionally observed to the concentration of chlorpyrifos. The parameters affecting the chlorpyrifos quantification including pH, reaction time, concentration of AChE and ATCh were investigated. The linearity of developed method was established in the range of 0.1-50 µg/mL ($r^2=0.9910$) with the detection limit of 0.046 µg/mL. This work demonstrates alternative approach which is simple, rapid, sensitive and selective detection of organophosphate pesticide.

Experimental :



Scheme 1. Schematic illustration of chlorpyrifos colorimetric detection based on GQDs-AuNPs reaction (A). The synthesis reaction of GQDs-AuNPs (B) detection mechanism of chlorpyrifos.

Result :

Optimization of assay condition :

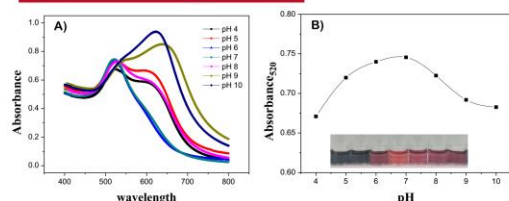


Fig. 1. (A) Spectra of GQDs-AuNPs in the presence of ATCh prepared at different pHs after incubation at 37°C for 20 min and (B) the variation of A_{520} with pHs obtained from GQDs-AuNPs and ATCh reaction.

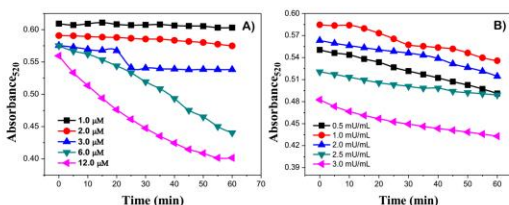


Fig. 2 Variation of A_{520} versus time for the reactions of GQDs-AuNPs in the presence of different concentrations of (A) ATCh and (B) AChE.

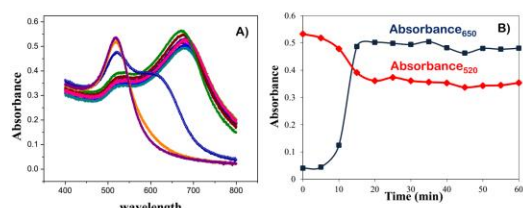


Fig. 3. (A) Absorption spectra of GQDs-AuNPs after addition of ATCh (1.0 µM, pH 7.0 PBS) and AChE (1.0 mU/mL) recorded every 5 min.

References:

- 1) Nounthavong, Nacpricha, D.; Henry, C. S.; Samcenoi, Y., *The Analyst*, **2016**, 141 (5), 1837-1846.
- 2) Sharma, S.; Singh, S.; Ganguli, A. K.; Sharmugam, V., *Carbon*, **2017**, 115, 781-790.
- 3) Meng, X.; Schultz, C. W.; Cui, C., *Sensors and Actuators B: Chemical*, **2015**, 215, 577-583.
- 4) Su, X.; Chan, C.; Shi, J.; Tsang, M. K.; Pan, Y.; Cheng, C.; Gerlie, O.; Yang, M., *Biosensors & bioelectronics*, **2017**, 92, 489-495.

Colorimetric detection of chlorpyrifos :

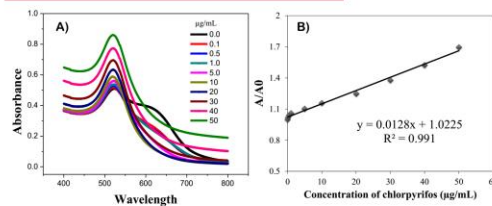


Fig. 4. (A) Absorption spectra of the detection reactions with the variation of chlorpyrifos concentrations and (B) The corresponded calibration plot of chlorpyrifos-AuNPs (0.4 mM), ATCh (1.0 µM) and AChE (1.0 mU/mL) in 0.05 M PBS.

Kinetic analysis :

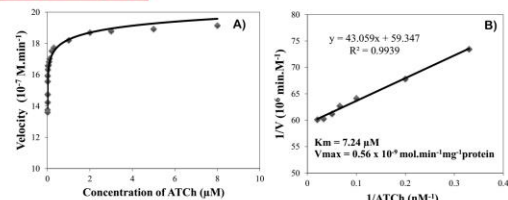


Fig. 5. (A) Plot of the initial velocities for an increasing concentration of ATCh at a constant amount of AChE, and the data were fitted by the Michaelis-Menten equation. (B) The data were fitted by Lineweaver-Burk equation.

Conclusion :

- Highly sensitive colorimetry for chlorpyrifos detection was developed based on the aggregation of GQDs-AuNPs when reacted with thiocholine generated from enzymatic hydrolysis of ATCh by AChE.
- The developed method provided a linearity ranged from 0.1-50 µg/mL with (r^2) of 0.991.
- The LOD for chlorpyrifos was 0.046 µg/mL.
- This work demonstrates alternative approach which is simple, rapid, sensitive and selective detection of organophosphate pesticides.

Acknowledgements :

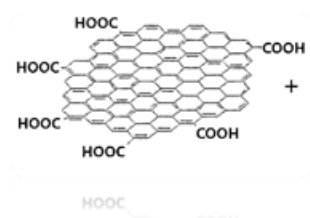
This work is supported by research grants from Chemistry and Center of Excellence for Innovation in Chemistry (PERCH-CIC).

The research scholarships and instrumental facilities of the Department of Chemistry, Faculty of Science, Ubon Ratchathani University are also gratefully acknowledged.

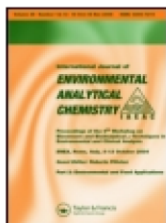


Development of a novel colorimetric sensor for Organophosphate pesticides

Warinporn Chungchai
Department of Chemistry
Ubon Ratchathani University



Asst. Prof. Dr. Maliwan Amatatongchai (advisor)



International Journal of Environmental Analytical Chemistry



ISSN: 0306-7319 (Print) 1029-0397 (Online) Journal homepage: <https://www.tandfonline.com/loi/geac20>

Development of a novel three-dimensional microfluidic paper-based analytical device (3D- μ PAD) for chlorpyrifos detection using graphene quantum-dot capped gold nanocomposite for colorimetric assay

Warinporn Chungchai, Maliwan Amatatongchai, Rattapol Meelapsom, Ketsarin Seebunrueng, Saksri Suparsorn & Purim Jarujamrus

To cite this article: Warinporn Chungchai, Maliwan Amatatongchai, Rattapol Meelapsom, Ketsarin Seebunrueng, Saksri Suparsorn & Purim Jarujamrus (2019): Development of a novel three-dimensional microfluidic paper-based analytical device (3D- μ PAD) for chlorpyrifos detection using graphene quantum-dot capped gold nanocomposite for colorimetric assay, International Journal of Environmental Analytical Chemistry, DOI: [10.1080/03067319.2019.1650921](https://doi.org/10.1080/03067319.2019.1650921)

To link to this article: <https://doi.org/10.1080/03067319.2019.1650921>

 View supplementary material [↗](#)

 Published online: 07 Aug 2019.

 Submit your article to this journal [↗](#)

 Article views: 7

 View Crossmark data [↗](#)

Full Terms & Conditions of access and use can be found at
<https://www.tandfonline.com/action/journalInformation?journalCode=geac20>

Development of a novel three-dimensional microfluidic paper-based analytical device (3D- μ PAD) for chlorpyrifos detection using graphene quantum-dot capped gold nanocomposite for colorimetric assay

Warinporn Chungchai^{a,b}, Maliwan Amatatongchai^{a,b}, Rattapol Meelapsom^{b,c}, Ketsarin Seebunrueng^a, Saksri Suparsorn^{a,b} and Purim Jarujamrus^{a,b}

^aDepartment of Chemistry and Center of Excellence for Innovation in Chemistry, Faculty of Science, Ubon Ratchathani University, Ubon Ratchathani, Thailand; ^bNanomaterials Science, Sensors & Catalysis for Problem-Based Projects, Faculty of science, Ubon Ratchathani University, Ubon Ratchathani, Thailand; ^cDepartment of Science and Mathematics, Faculty of Science and Health Technology, Kalasin University, Kalasin, Thailand

ABSTRACT

This report presents a three-dimensional microfluidic paper-based analytical device (3D- μ PAD) with colorimetric assay, for chlorpyrifos organophosphate pesticide detection in vegetable samples. The 3D- μ PAD was fabricated by one-step polymer-screen-printing, using rubber latex (RL) waste as a hydrophobic reagent for low-cost and simple manufacture. The 3D- μ PAD design comprises two sheets; a testing sheet containing two circular zones, and a sampling sheet in the shape of a dumbbell design. Assay involves the acetylcholinesterase (AChE)-catalysed hydrolysis of an acetylthiocholine (ATCh) substrate to produce thiocholine. Thiocholine causes the aggregation of graphene-quantum-dot capped gold-nanocomposite particles (GQD-AuNPs) to give a purple-blue-coloured solution. Incubation with chlorpyrifos inhibits the hydrolysis reaction, resulting in anti-aggregation of red-coloured GQD-AuNPs. The assay can determine chlorpyrifos by ImageJ detection, over a linear range of 0.001 to 1.0 $\mu\text{g mL}^{-1}$, with a detection limit of 0.0007 $\mu\text{g mL}^{-1}$, without sophisticated instrumentation. The developed 3D- μ PAD was applied to detect chlorpyrifos in spiked vegetable samples, with per cent recoveries ranging from 93.0% to 104.6%. Our developed device provides good precision (%RSD ranges from 0.3 to 1.6). The calculated relative error comparison with HPLC ranges from 1.0% to 5.2%, indicating a high degree of accuracy. The 3D- μ PAD exhibits good sensitivity and selectivity for a low-cost and rapid-screening test for the presence of insecticides, and might be useful for on-site applications.

ARTICLE HISTORY

Received 1 July 2019
Accepted 26 July 2019

KEYWORDS

Graphene quantum dot (GQDs); gold nanoparticles (AuNPs); chlorpyrifos; acetylcholinesterase; three-dimensional microfluidic paper-based analytical device (3D- μ PAD)

1. Introduction

Organophosphate pesticides (OPs), consist of phosphate ester compound derivatives ($\text{O} = \text{P}(\text{OR})_3$). OPs are most widely used in environmental and agricultural pest-control applications. These compounds are highly toxic to humans and animals because they

CONTACT Maliwan Amatatongchai  amaliwan@gmail.com

 Supplemental data for this article can be accessed here.

© 2019 Informa UK Limited, trading as Taylor & Francis Group

inhibit acetylcholinesterase (AChE) enzyme activity on the nervous system [1,2], resulting in physical responses including sweating, diarrhoea, headache, muscle tremors, and in more severe cases, breathing difficulties, convulsions, and death. Chlorpyrifos (*O*, *O*-diethyl *O*-(3,5,6-trichloropyridin-2-yl)-phosphorothioate) is one of the most widely used OPs in many countries, including Thailand, Vietnam, China, and the United States [3,4], and is also common in other countries. Chlorpyrifos has low solubility in water and readily partitions from aqueous to organic phases in the environment, thus there is a significant hazard for human exposure. The Codex maximum residue limits for chlorpyrifos residues for various commodities range from 0.05 to 1 mg kg⁻¹ [5]. Thus, sensitive and selective methods for chlorpyrifos detection are highly desirable due to environmental protection requirements and concerns over the safety of human health. Conventional methods for determination of chlorpyrifos include high-performance liquid-chromatography (HPLC) [6,7], liquid chromatography/mass spectrometry (LC-MS) [8], gas chromatography/mass spectrometry (GC-MS) [9], enzyme-linked immunosorbent assay (ELISA) [10,11], and electrochemical [12,13], chemiluminescence [14,15], and fluorescence spectroscopies [16,17]. Although these methods provide high sensitivity, high selectivity, and detection limits at the nanomolar level, they still require expensive instrumentation, time-consuming analytic procedures, and large quantities of reagents or samples. Furthermore, the requirements for extensive instrumentation limit their practical applications to laboratory settings, and thus these methods are not well suited to remote applications.

These problems are addressed by a recently developed microfluidic paper-based analytical device (μ PAD). Since its introduction by the Whitesides group in 2007 [18], the μ PAD has provided an alternative method for medical diagnostic and chemical analysis in areas such as disease diagnosis [19], environmental analysis [20], and biochemical analysis [21]. The μ PAD is simple to use, low-cost, lightweight, easy to fabricate, disposable, and provides quick results. The white paper used is well suited to colorimetric methods, while the hydrophilic cellulose fibres that comprise the paper are a suitable material for the capillary flow of aqueous fluids. A flow channel is easily formed on the paper by printing hydrophobic barriers to confine a fluid to the desired area [22]. A number of established μ PAD fabrication techniques exist, including photolithography [18], plotting [23], cutting [24], wax printing [25], inkjet printing [26], and screen printing [27]. Each method has its own advantages and drawbacks. Among these printing methods, screen printing has generally been the standard choice for μ PAD fabrication owing to its high speed, simplicity, versatility, and cost-effectiveness [27]. Specifically, many μ PAD devices can be quickly produced by screen printing.

Herein, we report the development of a novel three-dimensional microfluidic paper-based analytical device (3D- μ PAD) for colorimetric chlorpyrifos determination in vegetable samples. The 3D- μ PAD is fabricated by a one-step polymer-screen-printing process, without the need to heat or bake the device, and by using recycled rubber latex (RL) waste as an eco-friendly hydrophobic reagent [28]. The simple fabrication method produces a foldable device that includes both testing and sampling sheets. The testing sheet consists of two circular zones and a dumbbell-shaped sampling sheet (Figure 1(a)). Acetylcholinesterase (AChE) enzyme-catalysed hydrolysis of acetylthiocholine (ATCh) substrate produces thiocholine, which then interacts with aggregated graphene quantum-dot-capped gold nanoparticles (GQDs-AuNPs). Colorimetric assay is based on the colour change that occurs in GQDs-AuNPs upon interaction with thiocholine. AuNPs are synthesised, using graphene quantum dots (GQDs) as reducing

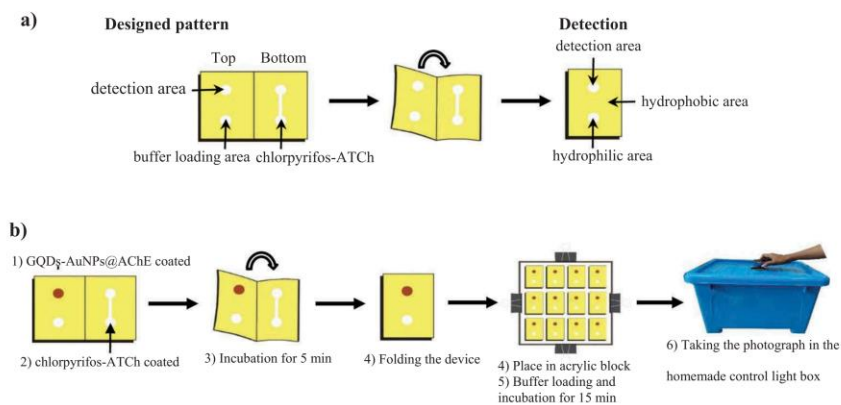
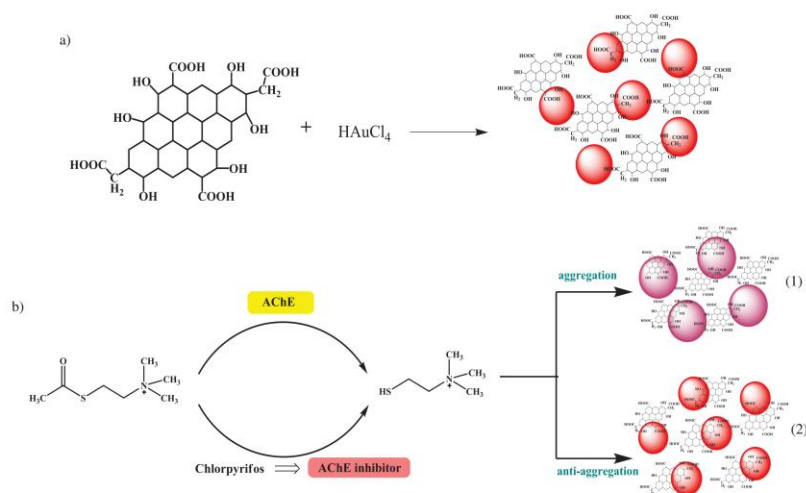


Figure 1. (a) The designed three-dimension microfluidic paper-based analytical device (3D-μPAD) for chlorpyrifos detection using a foldable sheet consisting of two parts (top/bottom layer). (b) The typical procedure for chlorpyrifos determination on 3D-μPAD.

and capping agents (Scheme 1(a)). Scheme 1(b) illustrates the analytical principle for determination of chlorpyrifos. AChE catalyses ATCh hydrolysis to produce thiocholine, which contains a thiol group (-SH). The presence of the thiol causes formation of a purple-blue-coloured GQDs-AuNPs aggregate (1). Chlorpyrifos inhibits AChE catalysis of ATCh, producing the red-coloured anti-aggregation GQDs-AuNPs product (2). Quantification of chlorpyrifos is carried out by detection of the red colour produced when performing the assay reaction within the 3D-μPAD detection zone. Our 3D-μPAD-based detection platform is simple, cost-effective,



Scheme 1. (a) The synthesis reaction of GQDs-AuNPs and (b) mechanism of chlorpyrifos colorimetric detection based on GQDs-AuNPs reaction.

rapid, sensitive, and selective for chlorpyrifos detection. The device would be an effective tool for food-quality monitoring and for on-site applications, including environmental monitoring. We were able to find only a few literature reports of using wax printing [29] and cutting technique covered with plastic sheet [30]. An alternative quantum-dot-based process uses a bienzymatic system of AChE and Choline oxidase, reacted with thioglycolic acid-capped CdTe quantum dots [29]. Another approach is an AChE-based indoxyl acetate (IDA) reaction [30]. However, these methods are either more expensive because of the use of two enzymes, or more toxic because of the use of a probe made from heavy metals.

2. Experimental

2.1. Chemicals and materials

All chemicals were of analytical grade. Deionised water (WaterPro Ps, USA) was used for reagent preparation. Hydrogen tetrachloroauric (III) acid trihydrate ($\text{HAuCl}_4 \cdot 3\text{H}_2\text{O}$, 99.99%) was purchased from Acros Organic (Geel, Belgium). Citric acid ($\text{C}_6\text{H}_8\text{O}_4$), iron (III) chloride, copper (II) sulphate pentahydrate, zinc sulphate, magnesium sulphate, potassium iodide, sodium sulphide nonahydrate were purchased from Carlo Erba (Milan, Italy). Acetylcholinesterase (AChE, E.C.3.1.1.7; type V-S, ≥ 1000 units mg^{-1} protein), acetylthio-choline chloride (ATCh, 99.9%) and chlorpyrifos ($\text{C}_9\text{H}_{11}\text{Cl}_3\text{NO}_3\text{PS}$) were purchased from Sigma-Aldrich (St. Louis, USA). Whatman No.4 (thickness 205 μm , pore size 20–25 μm) filter paper was purchased from Whatman International Ltd. (Maidstone, England). A ready to use wooden-framed woven mesh screen (888.32 mesh, 60T) made from nylon was obtained from a local screen shop (Ubon Ratchathani, Thailand). Solid RL residue was obtained from the Rubber Science and Technology Program, Department of Chemistry, Faculty of Science, Ubon Ratchathani University. Gasoline was purchased from a gas station in Ubon Ratchathani, Thailand (PTT PLC.). Toluene was obtained from Carlo Erba, Italy. All glassware was cleaned with aqua regia (1:3 volume ratio of HNO_3 : HCl) and immersed in HNO_3 10%, v/v for 24 h.

2.2. Instruments

UV-Visible absorption spectra were collected using a double beam, spectrophotometer (UV-2600, Shimadzu, Japan) with a 10 mm quartz cell (45 × 12.5 × 12.5 mm; volume 1500 μL). The morphology and sizes of the QDs-AuNPs were investigated by using a JEM-1230 transmission electron microscope (TEM; JEOL, Japan) at an accelerating voltage of 200 kV. Fourier transformed infrared (FTIR) spectroscopy was performed using a spectrum II FTIR spectrometer (Perkin Elmer, USA), to investigate nanoparticle structure and composition. Images were acquired using a digital camera (Canon IXUS 105; 12.1 MP, 4x Optical Zoom) at a shooting distance of 10 cm. We used HPLC, model CTO-10AC (Shimadzu, Japan), coupled to an SPD-20A UV/Vis detector, to perform chlorpyrifos quantification in vegetable extracts, for method validation.

2.3. Synthesis of QDs

QDs were synthesised by a pyrolysing method adopted from Sinduja et al. [31]. Briefly, 2 g of citric acid was heated to 200°C on a magnetic stirrer-hotplate for 30 min. The

solution colour changed from yellow to orange. The resulting orange liquid (1 g) was added dropwise to a 0.25 M NaOH solution (100 mL) under continuous stirring, to provide the QDs product (10 mg mL^{-1}) as a yellow solution.

2.4. Preparation of QDs capped AuNPs

The preparation of QDs capped AuNPs was carried out by mixing HAuCl_4 (10 mL, 0.4 mM), QDs ($10 \text{ mL } 0.4 \text{ mg mL}^{-1}$), and deionised water (5 mL) in a 250-mL round-bottomed flask and heating to 100°C under continuous stirring. Stirring was continued a further 30 min until the colourless solution had turned red. Stirring continued for 1 h to ensure completion of the reaction. After cooling, the QDs-AuNPs were separated by centrifugation at 10,000 rpm for 30 min. The prepared QDs-AuNPs were then re-dispersed in DI water and stored at 4°C , ready for use.

2.5. Chlorpyrifos detection based on ache inhibition activity using QDs-AuNPs as the reporter

Detection of chlorpyrifos is based on AChE-enzyme-catalysed hydrolysis of an ATCh substrate to produce thiol-bearing thiocholine, which causes the aggregation of QDs-AuNPs, to generate a purple–blue-coloured product. The hydrolysis step is inhibited in the presence of chlorpyrifos, resulting in anti-aggregation of QDs-AuNPs, a red-coloured product. To investigate the chlorpyrifos concentration dependence of the reaction, we performed catalytic hydrolysis of the AChE substrate, ATCh, in the presence of QDs-AuNPs and chlorpyrifos. In a typical experiment, AChE ($10 \text{ } \mu\text{L}, 200 \text{ mU mL}^{-1}$) and ATCh ($100 \text{ } \mu\text{L}, 50 \text{ } \mu\text{M}$) were added into a 2 mL centrifuge tube. Then, $200 \text{ } \mu\text{L}$ of chlorpyrifos standard was added to the mixture and the resulting solution was incubated for 30 min at 25°C . Finally, 0.9 mL of QDs-AuNPs and $290 \text{ } \mu\text{L}$ of 50 mM PBS (phosphate buffer solution, pH 7.0) was added to make the final volume up to 1.5 mL. The UV-Vis absorption spectrum was taken. The effect of chlorpyrifos concentration ($0\text{--}50 \text{ } \mu\text{g mL}^{-1}$) was investigated by plotting a calibration graph of monitored differences in absorbance at 520 nm.

2.6. Fabrication of chlorpyrifos 3D- μPAD

The chlorpyrifos 3D- μPAD was fabricated by using a paper sheet, folded to form upper and lower layers (Figure 1(a)). The pattern on the chlorpyrifos 3D- μPAD was fabricated by one-step polymer-screen printing, using RL as the hydrophobic barrier. Briefly, 3.8 g of finely chopped RL was placed in a 250-mL glass-beaker. Toluene (200 mL) was added and mixed to form a homogeneous RL solution. The solution was incubated at room temperature overnight. The resulting solution (80 mL) was added into gasoline (20 mL) using RL solution and gasoline in a 4:1 volume ratio. The mixture was shaken until homogeneous (~ 5 min) and the resulting solution screened on Whatman No.4 filter paper under a wooden-framed woven mesh screen (888.32 mesh, 60T), which was designed and patterned as shown in Figure. S1a. First, the patterned screen was placed directly on a sheet of No. 4 Whatman paper, and the RL solution was forced through the screen by using a squeegee. The RL solution created a patterned hydrophobic barrier as it penetrated to the bottom of the paper. The patterned paper was ready for use after removal from the screen. Finally, the fabricated device was cut out from the

patterned sheet. Our designed 3D- μ PAD for colorimetric chlorpyrifos assay comprises two parts. The top-layer test sheet, consisting of two 5-mm circles; one circle forms the detection zone, for placing the GQDs-AuNPs and AChE-enzyme mixture, and the other is a loading area, for adding buffer for analyte elution. When folded, the detection zone and loading area align with a hydrophilic dumbbell-shape printed on the bottom-layer sampling sheet. The dumbbell-shape features two 5 mm circles connected by a straight 2×8 mm channel. The bottom circle area of the dumbbell-shape was used as sample loading by applying the mixed solution of sample/standard (chlorpyrifos) and ATCh (substrate). After loading the 3D- μ PAD, the test sheet is folded so that the circles in the upper and lower layers align. Sample then elutes from the loading area and into the detection zone, where reaction with AuNPs occurs (Figure 1(a)). Sample then elutes from the loading area and into the detection zone, where reaction with AuNPs occurs (Figure 1(a)).

2.7. Detection of chlorpyrifos using the designed 3D- μ PAD

Figure 1(b) shows the chlorpyrifos-analysis procedure using the 3D- μ PAD. Five hundred microlitres of GQDs-AuNPs and AChE (5.0 U mL^{-1}) solutions are added to a 1 mL microcentrifuge tube and mixed using a vortex mixer for 2 min. The resulting mixture ($5 \mu\text{L}$) is applied to the detection zone. After combining ATCh ($400 \mu\text{L}$, 0.5 mM), chlorpyrifos standard ($200 \mu\text{L}$), and PBS ($400 \mu\text{L}$) in a 1 mL micro-centrifugal tube, the ATCh-chlorpyrifos mixture ($8 \mu\text{L}$) is applied to the loading area at one end of the dumbbell, and incubated for 5 min at room temperature. The upper and lower layers are folded together and the 3D- μ PAD is placed on an acrylic block (Figure 1(b)) to perfectly align the top and the bottom layers, and so clip them together. Details for the acrylic block are shown in supplementary materials as Figure. S2. Finally, PBS ($8 \mu\text{L}$, 50 mM , $\text{pH } 7$) is dropped onto the loading area. The PBS buffer elutes the chlorpyrifos-ATCh mixture along the channel and gather to the detection area. The elution process is allowed to proceed for 15 min at room temperature. Detection of chlorpyrifos is based on inhibition of AChE-enzyme-catalysed hydrolysis of ATCh, resulting in anti-aggregation of GQDs-AuNPs and the formation of a coloured product. Images of the detection zone are then captured in a homemade lightbox (Figure. S3) by using a digital camera set to automatic mode. The colour changes in the detection area are analysed by using ImageJ software (<https://imagej.nih.gov/ij/>).

2.8. Application to vegetable samples

To evaluate the practical applicability of the designed 3D- μ PAD, vegetable samples were assayed using a spiked recovery experiment. Cucumber, radish, lettuce, carrot, cabbage, celery, and tomato were purchased from a local market in Ubon Ratchathani Province, Thailand. We used a method for extracting OPs in vegetable samples described by Harshit et al. [32]. Briefly, finely cut and chopped 25 g samples of various vegetables were weighed, and 50 mL of acetonitrile was added to each sample. Samples were homogenised in a blender for 3 min, then centrifuged at 4000 rpm for 10 min, and supernatants from the centrifuge tubes were collected. Finally, solution samples were filtered through a PTFE syringe filter ($33 \times 0.22 \mu\text{m}$) prior to chlorpyrifos determination. We compared chlorpyrifos concentrations acquired from the 3D- μ PAD assay to those

obtained by HPLC. Separation was performed using a separation column; C-18 column (VertiSep™ UPS, 4.6 × 250 mm, 5.0 μm), isocratic elution with an acetonitrile: water mobile phase (90:10 v/v), 1.0 mL min⁻¹ flow rate, 20 μL injection volume, detection at 219 nm absorbance.

3. Results and discussion

3.1. Characterisation of GQDs-AuNPs

The most commonly used reducing agent for the synthesis of AuNPs is tri-sodium citrate. However, AuNPs prepared in this way have a tendency to aggregate, can be instable, have low sensitivity, and exhibit poor selectivity [33]. However, rhodamine B [34] or the amino acid, cysteine [35] interact more strongly with the AuNPs surface, and the resulting nanoparticles show improved performance.

We propose the use of graphene-quantum-dot capped gold-nanoparticles (GQDs-AuNPs) for chlorpyrifos sensing by colorimetric assay. GQDs-AuNPs were prepared using GQDs as the reducing agent and stabiliser. UV-Visible spectroscopy was used to investigate the absorption spectra of GQDs, GQDs-AuNPs, and cit-AuNPs nanocomposite materials (results are shown in Figure. S4). GQDs prepared by pyrolysis (Figure. S4 curve (a), yellow product) do not produce an absorption band. Whereas AuNPs prepared using tri-sodium citrate with GQDs as reducing agents (cit-AuNPs and GQDs-AuNPs) show unique surface plasmon bands at 520 nm, attributed to monodispersed particles (Figure. S4 curves b and c). The red colour and the maximum absorbance at 520 nm obtained from GQDs-AuNPs indicates their effectiveness as reducing agent and stabiliser. FT-IR spectra of the as-prepared nanocomposites are shown in Fig S5. Citrate-stabilised AuNPs (Figure. S5, curve a) shows absorption bands at 1690 cm⁻¹ and 3542 cm⁻¹, attributed to citrate carboxylate ion (COO⁻) and -OH stretching modes, respectively. GQDs (curve b) produce -OH and COO⁻ absorption bands at 1386 and 1690 cm⁻¹, due to bending vibrations, and an -OH stretching absorption at 3427 cm⁻¹. GQDs-AuNPs (Figure. S5, curve c) exhibits all three characteristic GQDs bands, together with the AuNPs absorption bands. These results indicate the successful preparation of GQDs-AuNPs. We used TEM to investigate the shape and size of the synthesised GQDs-AuNPs. Figure 2 shows that GQDs-AuNPs have round shapes and uniform sizes, with an average diameter of 12 ± 0.26 nm (n = 20). The inset figure shows that large AuNPs are surrounded by many smaller GQDs, forming a satellite-type structure. The TEM image also shows that the well-dispersed GQDs have diameters of approximately 3 nm. Our results are in good agreement with a previous report [36], that AuNPs synthesised by using citrate as the reducing agent have diameters of approximately 15 nm and GQDs synthesised by pyrolysis have smaller average diameters, of 3 ± 1 nm. In our work, GQDs are used as a reducing agent and as a stabiliser by capping the AuNPs surface.

3.2. Chlorpyrifos detection based on competitive-inhibition reaction

OPs inhibit AChE by binding to the active site of an enzyme. This suppresses ATCh hydrolysis, thereby blocking the generation of thiocholine [35]. In this study, detection of chlorpyrifos is based on competitive inhibition between chlorpyrifos and the GQDs-AuNPs-AChE-ATCh reagent. We used UV-VIS spectroscopy to monitor changes in absorbance

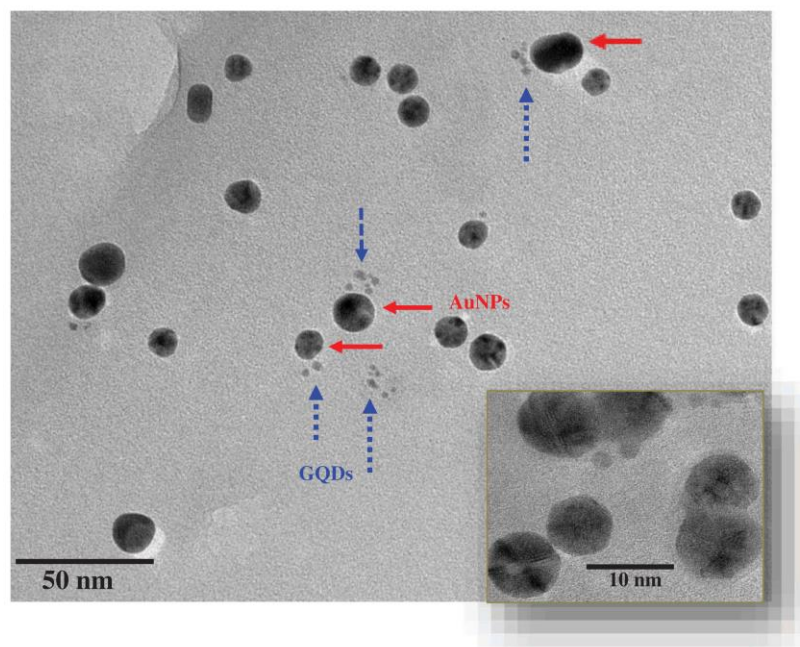


Figure 2. TEM images of well-dispersed GQDs-AuNPs nanocomposites. Inset is enlarge nanocomposite image.

during reaction. The GQDs-AuNPs absorption spectrum exhibits a characteristic peak at 520 nm (Figure 3, curve a). Addition of ATCh (50 μM , pH 7.0 PBS) does not result in any colour change (curve b), revealing that ATCh does not affect the absorption properties of the reaction solution. After addition of AChE (200 mU mL^{-1}) to the reaction solution and incubating for 30 min, the absorbance at 520 nm decreases and a new absorbance band appears at 650 nm (curve c). The solution colour change, from red, to purple-blue, is clearly visible to the naked eye (inset, Figure 3). Enzymatic hydrolysis of ATCh by AChE releases thiocholine. The thiol group in thiocholine interacts with the AuNPs to cause aggregation of the nanoparticles, and this is the cause of the colour change [35]. Addition of chlorpyrifos (curve d) inhibits ATCh hydrolysis of ATCh, leading to anti-aggregation of GQDs-AuNPs. This detection mechanism is illustrated in detail in Scheme 1.

The distinctive colour change, from red to blue, and the appearance of a maximum absorption wavelength at 520 nm (A_{520}) (Figure 4(a), red curve) as a result of the aggregation of GQDs-AuNPs, provides a method for quantitative determination of chlorpyrifos. The red colour at 520 nm results from reaction between GQDs-AuNPs and thiocholine. The intensity of the A_{520} band varies with chlorpyrifos concentration. Thus, we first tested the effect of chlorpyrifos concentration (0–50 $\mu\text{g mL}^{-1}$) on the A_{520} band intensity. Figure 4 shows that A_{520} intensity is linearly proportional to the concentration of chlorpyrifos over the range of 0.1–50 $\mu\text{g mL}^{-1}$. The linear equation for this

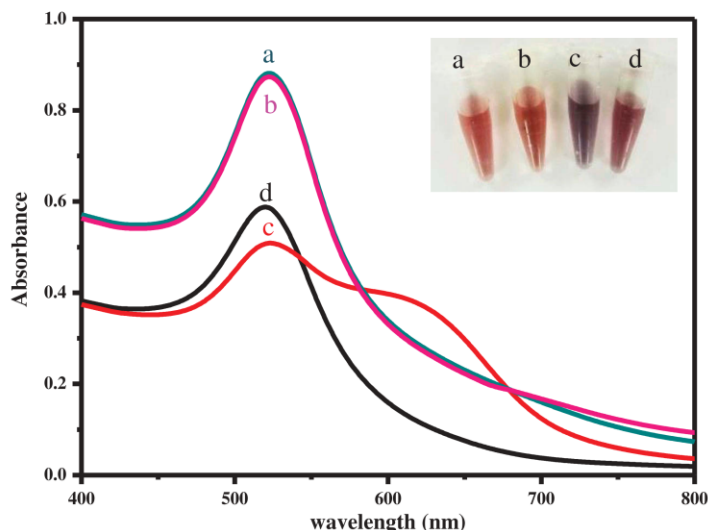


Figure 3. Absorbance spectra of GQDs-AuNPs (a), GQDs-AuNPs after the addition of ATCh (50 μM , pH 7.0 PBS) (b), GQDs-AuNPs after the addition of ATCh (50 μM , pH 7.0 PBS) and AChE (200 mU mL^{-1}) (c), GQDs-AuNPs after the addition of ATCh (50 μM , pH 7.0 PBS), AChE (200 mU mL^{-1}) and chlorpyrifos (5.0 $\mu\text{g mL}^{-1}$) (d). Incubation was performed at 25°C for 30 min.

curve is $y = 0.0131x + 1.0246$, with a linear correlation coefficient (r^2) of 0.996. The limit of detection (LOD) calculated based on $[3S.D.]/\text{slope}$ is 0.046 $\mu\text{g mL}^{-1}$.

3.3. Chlorpyrifos 3D- μPAD optimisation

The 3D- μPAD for chlorpyrifos detection was fabricated by a one-step polymer screen-printing technique using RL as the hydrophobic barrier. Fig S1b compares the hydrophobic zone of the 3D- μPAD to the hydrophilic zone. Red ink absorbs into the paper in the hydrophilic zone, but does not absorb in the hydrophobic zone. 3D- μPAD detection of chlorpyrifos was performed in a homemade lightbox. Images of the detection zone with different chlorpyrifos concentrations were captured by using a digital camera to find the most suitable colour to use. We investigated the intensities of the red, green, blue, and R + G + B (grey) channels. The colour intensity values obtained from the image processing software (ImageJ) are illustrated in Figure 5. Calibration curves for $[I - I_0]$ vs. chlorpyrifos concentration are plotted for all colour channels of interest. In the figure, I and I_0 represent the colour intensities with (I) and without (I_0) chlorpyrifos. The Green channel has the steepest slope of the calibration graph, indicating that this colour provides the greatest sensitivity. It should be noted that RGB colour intensities obtained from ImageJ are subtractive values, and thus, according to light spectrum theory, the dark-red colour produced with increasing chlorpyrifos concentration, reflects red light and absorbs green light [37]. Therefore, we chose the green-light channel for determination of chlorpyrifos concentration in samples. To maximise chlorpyrifos detection

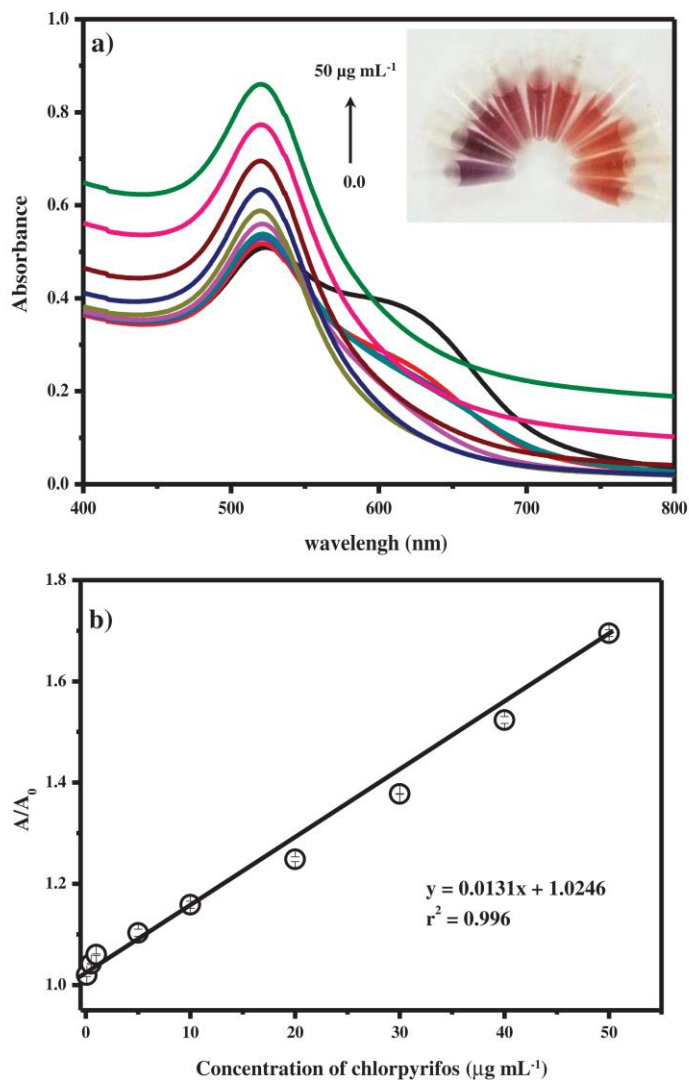


Figure 4. (a) Absorption spectra of the reaction assay with different concentrations of chlorpyrifos (0, 0.1, 0.5, 1.0, 5.0, 10, 20, 30, 40 and $50 \mu\text{g mL}^{-1}$). The reaction composed of 0.9 mL of QDs-AuNPs, 100 μL of ATCh (50 μM), 10 μL of AChE (200 mU mL^{-1}) and 290 μL of PBS (50 mM phosphate buffer, pH 7). Inset is their respective images. (b) the calibration plot between A/A_0 and the concentration of chlorpyrifos was constructed for the colorimetric detection of chlorpyrifos, where A and A_0 were the absorbance with and without chlorpyrifos ($n = 3$).

sensitivity, we optimised the reaction pH, buffer volume, ATCh and AChE concentrations, and reaction time. Reaction pH is a critical parameter affecting enzyme activity, and we

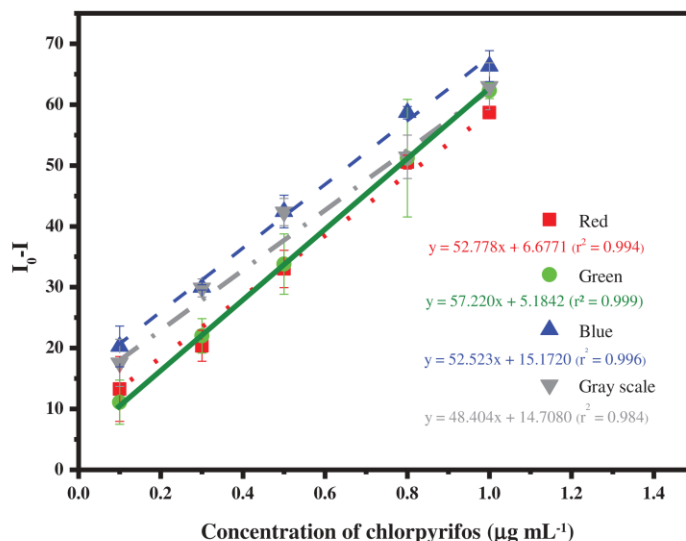


Figure 5. The colour intensity (I_0-I) of the images was separated into red, green, blue and R + G + B intensity and plot versus concentration of chlorpyrifos ($n = 3$).

therefore investigated the optimal pH for the reaction solution. As shown in [Figure 6\(a\)](#), colour intensity increases with pH, to a maximum at pH 7.0. Further increases result in weaker intensities. The AChE enzyme is a natural protein that is highly effective at neutral pH, but which denatures under extreme pH conditions. Thus, we used phosphate buffer at pH of 7.0 for all further tests.

We optimised the buffer volume for elution of chlorpyrifos-ATCh from the loading area to the detection zone. [Figure 6\(b\)](#) shows plots of colour intensity versus buffer volume. Colour intensity increases with buffer volume, from 4.0 to 8.0 μL as a consequence of the greater quantity of ATCh-Chlorpyrifos that elutes and is able to interact with enzyme in the detection zone. However, increasing buffer volume beyond 8.0 μL results in decreased colour intensity because of dilution and overloading effects. Therefore, we chose a buffer volume of 8.0 μL as optimal.

Next, we found an optimal concentration for ATCh within the range of 0.1 to 10 mM. [Figure 6\(c\)](#) shows that colour intensity increases with ATCh concentration from 0.1 to 0.5 mM. Greater quantities of ATCh produce more thiocholine, resulting in increased GQDs-AuNPs aggregation and a consequent increase in signal intensity. However, intensity remains constant at ATCh concentrations in excess of 0.5 mM. This may be due to the presence of insufficient quantities of AChE. Thus, we chose an ATCh concentration of 0.5 mM as optimal for further experiments, since this concentration produces the greatest colour intensity.

We examined the effect of AChE concentration on the chlorpyrifos detection response for concentrations in the range 0.1–20 U mL^{-1} . As shown in [Figure 6\(d\)](#), Increasing AChE concentration increases the amount of thiocholine generated by hydrolysis, and therefore

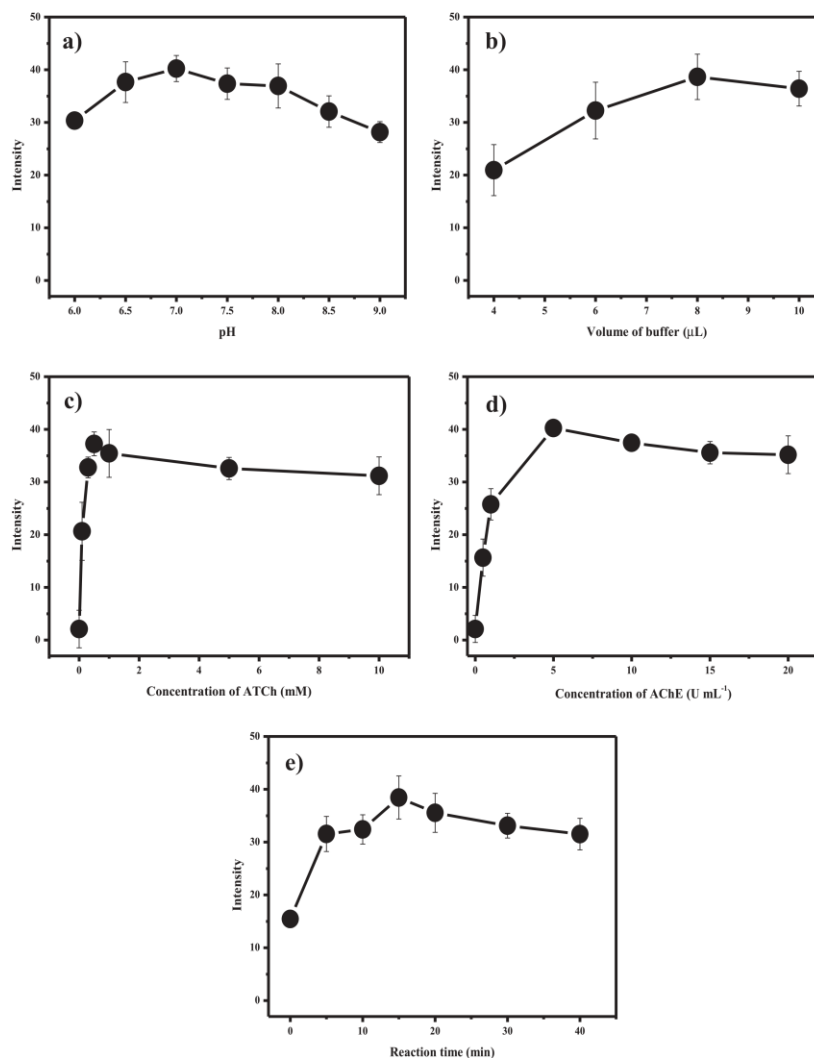


Figure 6. The green colour intensity of 3D-μPAD for chlorpyrifos detection in fixed concentration of $0.5 \mu\text{g mL}^{-1}$ chlorpyrifos pesticide and various conditions (a) pH, (b) volume of buffer, (c) concentration of ATCh, (d) concentration of AChE and (e) reaction time.

enhances QDs-AuNPs aggregation. The maximal response intensity was observed for an AChE concentration of 5 U mL^{-1} . At greater concentrations, the response intensity remains constant. Therefore, we used an AChE concentration of 5.0 U mL^{-1} for optimal sensitivity. Herein, one analysis is carried out by using only $5 \mu\text{L}$ of AChE (5 U mL^{-1}). To the best of our knowledge, however, this proposed assay required lowest amount of reagents and enzyme

compared to that has been reported previously where up to 2 μL of AChE ($2,500 \text{ U mL}^{-1}$) was needed for the foldable paper sheet with bi-enzymatic based fluorescent sensor [29] and 5 mL of AChE (16 mU mL^{-1}) was required for AChE-based test strip coupled with rhodamine-B functional AuNPs entrapped in agarose and coated with hydrogel [2].

We investigated the incubation, or reaction time between zero and 40 min. Figure 6(e) shows plots of colour intensity versus reaction time. Colour intensity increases with increasing reaction time, from 0.0 to 15 min. Longer reaction times do not result in significant changes in intensity. Therefore, we chose a reaction time of 15 min to provide the greatest sensitivity within the shortest time.

3.4. Chlorpyrifos analysis using 3D- μPAD

To test the performance of 3D- μPAD detection, we determined chlorpyrifos samples at concentrations between 0.001 and $1.0 \mu\text{g mL}^{-1}$. During these tests, we applied our optimised experimental conditions, using ATCh and AChE concentrations of 0.5 mM and 5.0 U mL^{-1} , PBS solution (8 μL , pH 7.0), and 15-min incubation time. Figure 7 shows the chlorpyrifos calibration curve. Green colour intensity increases linearly with chlorpyrifos concentration from 0.001 to $1.0 \mu\text{g mL}^{-1}$. The calibration curve is given by $y = 58.4620x + 14.3219 \pm 1.6925$, and the linear correlation coefficient (r^2) is 0.998. The detection limit, calculated based on $[3\text{S.D.}]/\text{slope}$, is $0.0007 \mu\text{g mL}^{-1}$. The 3D- μPAD provides good precision (0.01% RSD, based on 10 analyses). Analytical performance of the proposed device was compared with related methods for chlorpyrifos detection (Table 1). The performance of the 3D- μPAD is comparable to those of the AgNPs-MIP [38] and AuNPs-citrate/ Na_2SO_4 [39] systems. The chlorpyrifos 3D- μPAD exhibits the widest linearity range (0.001 to $1.0 \mu\text{g mL}^{-1}$) compare to other μPAD methods. The LOD of $0.0007 \mu\text{g mL}^{-1}$ for the proposed method is lower than that for AChE-

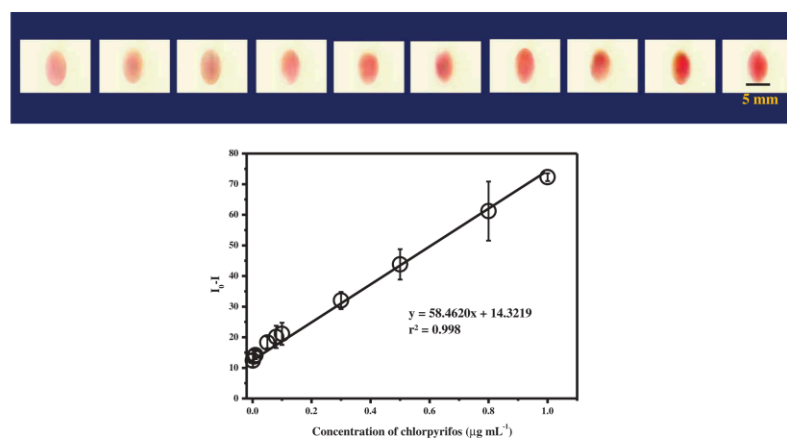


Figure 7. Calibration curve of chlorpyrifos using 3D- μPAD (plot between $I_0 - I$ of green intensity and the variation of chlorpyrifos concentrations; 0.001, 0.005, 0.01, 0.05, 0.1, 0.3, 0.5, 0.8 and $1.0 \mu\text{g mL}^{-1}$) reaction conditions; GQDs-AuNPs, ATCh (0.5 mM) and AChE (5.0 U mL^{-1}). Error bar obtained from quintuplicate ($n = 5$).

Table 1. Comparison of colorimetric method for the detection of chlorpyrifos pesticide.

Method	System	Concentration ranges ($\mu\text{g mL}^{-1}$)	LOD ($\mu\text{g mL}^{-1}$)	Ref.
Batch (solution)	AChE/H ₂ O ₂ -DNAzyme-ABTS ²⁻	0.04–1.0	0.01	[44]
	AgNPs-MIP	0.1–10	0.01	[38]
	AuNP-citrate/Na ₂ SO ₄	0.1–0.25	0.02	[39]
	C-dot/Fe ²⁺ -H ₂ O ₂ /AChE/ChOX	0.01–1.0	0.003	[45]
	AChE/GQDs-AuNPs	0.1–50	0.046	[This work]
μ PAD	RB-AuNPs/hydrogel/AChE	0.005–0.5	-	[2]
	AChE/ChOX/CeO ₂	0.0–0.12	0.005	[40]
	AChE/IDA	0.0–25.0	8.60	[41]
	g-C ₃ N ₄ /BiFeO ₃ NCs-antibodies	*0.0001–0.06	*0.00003	[42]
	MnO ₂ NFs-luminol-H ₂ O ₂	*0.0001–0.05	*0.00003	[43]
	AChE/GQDs-AuNPs	0.001–1.0	0.0007	[This work]

AChE = acetylcholinesterase, DNA = deoxyribonucleic acid, ABTS = 2,2'-azino-bis (3-ethylbenzothiazoline-6-sulphonic acid), AgNPs = silver nanoparticles, MIP = molecularly imprinted polymer, AuNPs = gold nanoparticles, C-dot = carbon dot, ChOX = choline oxidase, RB = rhodamine-B, IDA = indoxyl acetate, g-C₃N₄ = graphitic carbon nitride, BiFeO₃ NCs = bismuth ferrite nanocomposites, MnO₂NFs = manganese dioxide nanoflowers, GQDs = graphene quantum dot

*Colorimetric-chemiluminescent (CL) system, readout with CL immunochromatographic.

based colorimetric methods [2,40,41] that use rhodamine-B (RB) functional AuNPs entrapped in agarose and coated with hydrogel (polyethylene glycol diacrylate) (RB-AuNPs/hydrogel/AChE) [2], the nanoceria coated PAD using AChE/choline oxidase (ChOX) bi-enzyme (AChE/ChOX/CeO₂) [40], and indoxyl acetate (AChE/IDA) [41]. Our 3D- μ PAD detection method is as good as methods using colorimetric and chemiluminescent dual-readout immunoassay test strips based on graphitic carbon nitride/bismuth ferrite nanocomposites (g-C₃N₄/BiFeO₃ NCs-antibodies) [42] and manganese dioxide nanoflowers (MnO₂NFs-luminol-H₂O₂) [43]. It should be noted that the cited works [42,43] report colorimetric and chemiluminescent results, while detection limits are based on chemiluminescence measurements alone. When compared to related detection techniques, our method is more simple to apply than the cited works [28,37]. Our 3D- μ PAD provides several other advantages, for example, screen printing is a simple one-step process, allowing mass production of devices without the need for expensive equipment. Our fabrication material for creating hydrophobic barriers uses RL waste, and so is economical to use and is environmentally friendly. The reaction test is sensitive and rapid, and the reaction can be performed in a few steps, with the results plainly visible to the naked eye. We conclude that our chlorpyrifos 3D- μ PAD is well suited for food-quality control and onsite applications.

3.5. Interference studies

We investigated selectivity by determining the effect of potential interferences that are likely present in vegetable samples, including cations (K⁺, Na⁺, Fe³⁺, Ca²⁺, Cu²⁺, Zn²⁺, and Mg²⁺), anions (NO₃⁻, I⁻, S²⁻, and PO₄³⁻) and compound molecules (fructose, maltose, glucose and ascorbic acid). The interference effect was evaluated by adding different amounts of competing substance into 0.05 $\mu\text{g mL}^{-1}$ chlorpyrifos standard solution, and comparing the intensity response to that for the initial chlorpyrifos measurement. The tolerance limit was defined as the amount of interfering substance needed to cause intensity changes in excess of $\pm 5\%$. Figure 8 shows the tolerance limits of interfering substances. The results reveal that a 50-fold excesses of Fe³⁺, Cu²⁺, or Zn²⁺ produce no obvious effects on chlorpyrifos response. One hundred-fold excess concentrations

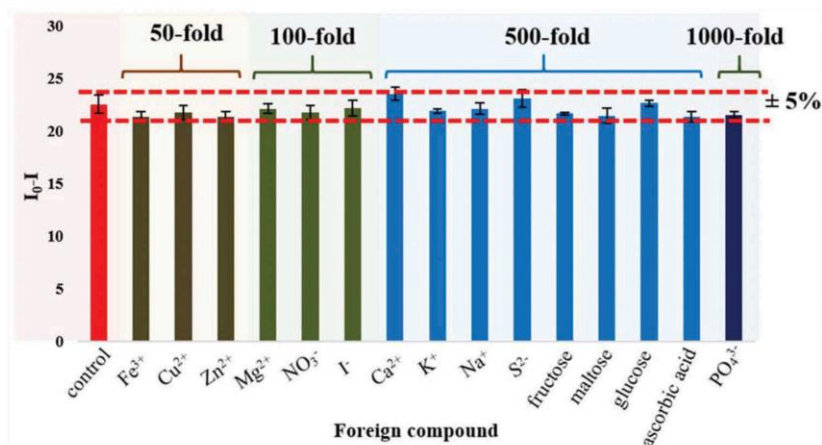


Figure 8. The selectivity of developed 3D- μ PAD for chlorpyrifos detection, comparison between the colour intensity obtained from $0.05 \mu\text{g mL}^{-1}$ of chlorpyrifos and the chlorpyrifos with interfering substances such as ions (Fe^{3+} , Cu^{2+} , Zn^{2+} , Mg^{2+} , NO_3^- , I^- , Ca^{2+} , K^+ , Na^+ , S^{2-} , and PO_4^{3-}) and compound molecules (fructose, maltose, glucose and ascorbic acid), ($n = 3$). Dotted mark the $\pm 5\%$ signal alteration range.

of Mg^{2+} , NO_3^- , or I^- , 500-fold excess of Ca^{2+} , K^+ , Na^+ , S^{2-} , and compound molecules (fructose, maltose, glucose and ascorbic acid), and 1000-fold PO_4^{3-} do not interfere with chlorpyrifos determination. We conclude that our designed 3D- μ PAD provides good selectivity for colorimetric determination of chlorpyrifos.

3.6. Detection of chlorpyrifos in real samples

The 3D- μ PAD performance was evaluated for the analysis of chlorpyrifos in vegetable samples. Extracted samples were quantified by the 3D- μ PAD and the results compared to those obtained using conventional HPLC. Table 2 summarises the results, showing added chlorpyrifos and calculated recovery values. As shown in the table, samples were either treated with chlorpyrifos concentrations below the detection limit (n.d.), or were chlorpyrifos-free. The detection limit of our 3D- μ PAD ($0.0007 \mu\text{g mL}^{-1}$) is less than the Codex maximum residual limit for chlorpyrifos residues, and falls in the range of $0.05\text{--}1.0 \text{ mg kg}^{-1}$ (or $0.05\text{--}1 \mu\text{g mL}^{-1}$) for several vegetable samples, indicating that the method is suitable for quantitative analysis of chlorpyrifos in food samples. These results were confirmed by HPLC (Table 2). Figure S6 illustrates the results of non-contamination of chlorpyrifos in the samples confirmed by HPLC. The chlorpyrifos concentrations found by the developed 3D- μ PAD are not significantly different from those found by conventional HPLC. The accuracy of the analytical process, using per cent recovery data for spiked chlorpyrifos standards (0.03 and $0.1 \mu\text{g mL}^{-1}$), falls in the range of 93.0% to 104.6%. The developed method provides good precision with %RSD values ranging from 0.3 to 1.6. The percentage of relative error was calculated by comparing measured recovery values with the reference value obtained from HPLC measurements. The calculated relative error ranges, from 1.0% to 5.3%, indicate that

Table 2. Comparison of chlorpyrifos determination in vegetables between the developed 3D- μ PAD and the reference HPLC method ($n = 3$).

Samples	Chlorpyrifos ($\mu\text{g mL}^{-1}$)								Relative error (%)
	HPLC method				Proposed 3D- μ PAD				
	Added	Found	Recovery (%)	RSD (%)	Added	Found	Recovery (%)	RSD (%)	
Cucumber	0	ND ^a	-	-	0	ND ^a	-	0.5	-
	0.03	0.0292	97.3	2.9	0.03	0.0295	96.3	0.3	-1.0
	0.1	0.0964	96.4	0.7	0.1	0.0998	99.8	0.5	3.4
Lettuce	0	ND ^a	-	5.2	0	ND ^a	-	-	0.9
	0.03	0.0295	98.3	3.2	0.03	0.0298	99.3	0.8	1.0
	0.1	0.0991	99.1	2.1	0.1	0.1044	104.4	1.6	5.3
Radish	0	ND ^a	-	1.7	0	ND ^a	-	-	0.6
	0.03	0.0291	97.0	1.0	0.03	0.0285	95.0	0.6	-2.0
	0.1	0.0983	98.3	3.0	0.1	0.1033	103.3	0.7	5.0
Tomato	0	ND ^a	-	4.5	0	ND ^a	-	0.3	-
	0.03	0.0291	97.0	0.8	0.03	0.0294	98.0	0.6	1.0
	0.1	0.0992	99.2	0.9	0.1	0.1008	100.8	0.7	1.6
Celery	0	ND ^a	-	2.6	0	ND ^a	-	1.3	-
	0.03	0.0294	98.0	4.1	0.03	0.0279	93.0	1.2	-5.0
	0.1	0.1018	101.8	1.4	0.1	0.0968	96.8	1.6	-5.0
Cabbage	0	ND ^a	-	0.7	0	ND ^a	-	0.6	-
	0.03	0.0291	97.0	1.1	0.03	0.0302	100.6	1.1	3.6
	0.1	0.0994	99.4	2.4	0.1	0.1046	104.6	1.0	5.2
Carrot	0	ND ^a	-	0.0	0	ND ^a	-	0.6	-
	0.03	0.0294	98.0	3.3	0.03	0.0301	100.3	0.5	2.3
	0.1	0.1004	100.4	1.3	0.1	0.0970	97.0	1.2	-3.4

ND^a = not detection or the samples were contaminated with concentration below LOD.

there are no significant matrix interferences from the vegetable samples. These results indicate that the proposed 3D- μ PAD is sufficiently accurate, precise, and is suitable for rapid quantitative analysis of chlorpyrifos in vegetable samples.

4. Conclusions

In this study, we demonstrated a novel colorimetric assay based on the colour change that GQDs-AuNPs undergo as they interact with thiocholine, generated by AChE-enzyme-catalysed hydrolysis of ATCh. The presence of chlorpyrifos inhibits the blue colour produced by aggregation of the AuNPs. The chlorpyrifos 3D- μ PAD is a foldable sheet consisting of loading and detection zones. The μ PAD is produced by a one-step screen-printing method, using RL to create hydrophobic barriers. Sample and reagent volumes are approximately 8 μL each. Under optimal conditions, the reaction time is reduced from 30 min in solution, to 15 min. The 3D- μ PAD exhibits linearity between 0.001 and 1.0 $\mu\text{g mL}^{-1}$, with a LOD for chlorpyrifos of 0.0007 $\mu\text{g mL}^{-1}$. We validated the proposed 3D- μ PAD by comparison with HPLC results for the analysis of chlorpyrifos in vegetable samples and in spiked samples. Both methods provided similar measured chlorpyrifos concentrations, indicating that the 3D- μ PAD provides a high degree of accuracy. Our developed 3D- μ PAD is simple to operate, cost-effective, rapid, sensitive, and highly selective for chlorpyrifos detection. This detection platform is well suited to food-quality control and onsite environmental-monitoring applications.

Acknowledgments

Financial support from the Center of Excellence for Innovation in Chemistry (PERCH-CIC), Ministry of Higher Education, Science, Research and Innovation is gratefully acknowledged. Use of the instrumental facilities at the Department of Chemistry, Faculty of Science, Ubon Ratchathani University, is also gratefully acknowledged.

Disclosure statement

No potential conflict of interest was reported by the authors.

Funding

This work is supported by research grants from the Center of Excellence for Innovation in Chemistry (PERCH-CIC).

ORCID

Maliwan Amatongchai  <http://orcid.org/0000-0002-5156-6480>

Purim Jarujamrus  <http://orcid.org/0000-0002-0666-150X>

References

- [1] N. Aurbek, H. Thiermann, L. Szinicz, P. Eyer and F. Worek, *J. Toxicol.* **224**, 91 (2006). doi:10.1016/j.tox.2006.04.030.
- [2] Q. Liu, X. Jiang, Y. Zhang, L. Zheng, W. Jing, S. Liu and G. Sui, *Sens. Actuators B Chem.* **210**, 803 (2015). doi:10.1016/j.snb.2014.12.048.
- [3] T.D. Phung, D. Connell, G. Miller, M. Hodge, R. Patel, R. Cheng and C. Chu, *Chemosphere* **87**, 294 (2012). doi:10.1016/j.chemosphere.2011.11.075.
- [4] Y. Yuan, C. Chen, C. Zheng, X. Wang, G. Yang, Q. Wang and Z. Zhang, *Food Control* **36**, 63 (2014). doi:10.1016/j.foodcont.2013.08.008.
- [5] Codex Alimentarius, *Pesticide Residues in Food* (FAO/WHO Food Standards Programme, 2000). <http://www.fao.org/tempref/codex/Reports/Alinorm03/al0324ae.pdf>
- [6] R.M. Hadjmohammadi, M. Peyrovi and P. Biparva, *J. Sep. Sci.* **33**, 1044 (2010). doi:10.1002/jssc.200900494.
- [7] E.R. Mauldin, M.T. Primus, A.T. Buettgenbach, J.J. Johnston and M.G. Linz, *J. Liq. Chromatogr. Relat. Technol.* **29**, 339 (2006). doi:10.1080/10826070500451863.
- [8] I.A. García-Valcárcel and L.J. Tadeo, *Anal. Chim. Acta.* **641**, 117 (2009). doi:10.1016/j.aca.2009.03.046.
- [9] N.S. Sinha, R. Pal, A. Dewan, M.M. Mansuri and N.H. Saiyed, *Int. J. Mass. Spectrom.* **253**, 48 (2006). doi:10.1016/j.ijms.2006.02.020.
- [10] A. Oubiña, J. Gascón, I. Ferrer and D. Barceló, *Environ. Sci. Technol.* **30**, 509 (1996). doi:10.1021/es950245p.
- [11] G. Qian, L. Wang, Y. Wu, Q. Zhang, Q. Sun, Y. Liu and F. Liu, *Food Chem.* **117**, 364 (2009). doi:10.1016/j.foodchem.2009.03.097.
- [12] R.A.S. Al-Meqbali, S.M. El-Shahawi and M.M. Kamal, *Electroanalysis* **10**, 784 (1998). doi:10.1002/(SICI)1521-4109(199809)10:11<784::AID-ELAN784>3.0.CO;2-9.
- [13] Y. Samet, L. Agengui and R. Abdelhédi, *Chem. Eng. J.* **161**, 167 (2010). doi:10.1016/j.cej.2010.04.060.
- [14] A. Li, X. Liu, J. Kong, R. Huang and C. Wu, *Anal. Lett.* **41**, 1375 (2008). doi:10.1080/00032710802119228.

- [15] Z. Song, S. Hou and N. Zhang, *J. Agric. Food Chem.* **50**, 4468 (2002). doi:10.1021/jf025589v.
- [16] G.K. Black and A.R. Fenske, *Arch. Environ. Contam. Toxicol.* **31**, 563 (1996). doi:10.1007/s002449900145.
- [17] Z. Zou, D. Du, J. Wang, N.J. Smith, C. Timchalk, Y. Li and Y. Lin, *Anal. Chem.* **82**, 5125 (2010). doi:10.1021/ac100260m.
- [18] A.W. Martinez, S.T. Phillips, M.J. Butte and G.M. Whitesides, *Angew. Chem. Int. Ed. Engl.* **46**, 1318 (2007). doi:10.1002/anie.200603817.
- [19] L. Ge, J. Yan, X. Song, M. Yan, S. Ge and J. Yu, *Biomaterials* **33**, 1024 (2012). doi:10.1016/j.biomaterials.2011.10.065.
- [20] Y. Sameenoi, P. Panymeesamer, N. Supalakorn, K. Koehler, O. Chailapakul, C.S. Henry and J. Volckens, *Environ. Sci. Technol.* **47**, 932 (2012). doi:10.1021/es304662w.
- [21] X. Li, J. Tian and W. Shen, *Anal. Bio. Anal. Chem.* **396**, 495 (2010). doi:10.1007/s00216-009-3195-9.
- [22] S. Abarghoei, N. Fakhri, Y.S. Borghei, M. Hosseini and M.R. Ganjali, *Spectrochim. Acta. A Mol. Biomol. Spectrosc.* **210**, 251 (2019). doi:10.1016/j.saa.2018.11.026.
- [23] D.A. Bruzewicz, M. Reches and G.M. Whitesides, *Anal. Chem.* **80**, 3387 (2008). doi:10.1021/ac702605a.
- [24] E.M. Fenton, M.R. Mascarenas, G.P. López and S.S. Sibbett, *ACS Appl. Mater. Interfaces* **1**, 124 (2008). doi:10.1021/am800043z.
- [25] E. Carrilho, A.W. Martinez and G.M. Whitesides, *Anal. Chem.* **81**, 7091 (2009). doi:10.1021/ac901071p.
- [26] X. Li, J. Tian, G. Garnier and W. Shen, *Colloids Surf. B* **76**, 564 (2010). doi:10.1016/j.colsurfb.2009.12.023.
- [27] W. Duagchai, O. Chailapakul and C.S. Henry, *Analyst* **136**, 77 (2011). doi:10.1039/C0AN00406E.
- [28] N. Malahom, P. Jarujamrus, R. Meelapsom, A. Siripinyanond, M. Amatatongchai and S. Chairam, *Polym. Test* **59**, 160 (2017). doi:10.1016/j.polymertesting.2017.01.023.
- [29] A. Apilux, W. Siangproh, N. Insin, O. Chailapakul and V. Prachayasittikul, *Anal. Methods* **9**, 519 (2017). doi:10.1039/C6AY02883G.
- [30] A. Apilux, C. Isarankura-Na-Ayudhya, T. Tantimongcolwat and V. Prachayasittikul, *EXCLI J.* **14**, 307 (2015). doi:10.17179/excli2014-684.
- [31] B. Sinduja and S.A. John, *Sens. Actuators B* **247**, 648 (2017). doi:10.1016/j.snb.2017.03.056.
- [32] D. Harshit, K. Charmy and P. Nrupesh, *Food Chem.* **230**, 448 (2017). doi:10.1016/j.foodchem.2017.03.083.
- [33] H. Li, J. Guo, H. Ping, L. Liu, M. Zhang, F. Guan and Q. Zhang, *Talanta* **87**, 93 (2011). doi:10.1016/j.talanta.2011.09.046.
- [34] D. Liu, W. Chen, J. Wei, X. Li, Z. Wang and X. Jiang, *Anal. Chem.* **84**, 4185 (2012). doi:10.1021/ac300545p.
- [35] W. Liu, D. Zhang, Y. Tang, Y. Wang, F. Yan, Z. Li and H.S. Zhou, *Talanta* **101**, 382 (2012). doi:10.1016/j.talanta.2012.09.045.
- [36] J. Shi, C. Chan, Y. Pang, W. Ye, F. Tian, J. Lyu and M. Yang, *Biosens. Bioelectron.* **67**, 595 (2015). doi:10.1016/j.bios.2014.09.059.
- [37] R. Meelapsom, P. Jarujamrus, M. Amatatongchai, S. Chairam, C. Kulsing and W. Shen, *Talanta* **155**, 193 (2016). doi:10.1016/j.talanta.2016.04.037.
- [38] S. Feng, Y. Hu, L. Ma and X. Lu, *Sens. Actuators B Chem.* **241**, 750 (2017). doi:10.1016/j.snb.2016.10.131.
- [39] P.K. Lisha, Anshup and T. Pradeep, *J. Environ. Sci. Health B* **44**, 697 (2009). doi:10.1080/03601230903163814.
- [40] S. Nouanthavong, D. Nacapricha, S.C. Henry and Y. Sameenoi, *Analyst* **141**, 1837 (2016). doi:10.1039/C5AN02403J.
- [41] J.H. Kim, Y. Kim, J.S. Park, C. Kwon and H. Noh, *BioChip J.* **12**, 326 (2018). doi:10.1007/s13206-018-2404-z.
- [42] H. Ouyang, X. Tu, Z. Fu, W. Wang, S. Fu, C. Zhu and Y. Lin, *Biosens. Bioelectron.* **106**, 43 (2018). doi:10.1016/j.bios.2018.01.033.

- [43] H. Ouyang, Q. Lu, W. Wang, Y. Song, X. Tu, C. Zhu and Y. Lin, *Anal. Chem.* **90**, 5147 (2018). doi:10.1021/acs.analchem.7b05247.
- [44] T. Liu, X. Zhang, J. Hao, W. Zhu, W. Liu, D. Zhang and J. Wang, *Food Anal. Methods* **8**, 1556 (2015). doi:10.1007/s12161-014-0042-1.
- [45] B. Lin, Y. Yan, M. Guo, Y. Cao, Y. Yu, T. Zhang and D. Wu, *Food Chem.* **245**, 1176 (2018). doi:10.1016/j.foodchem.2017.11.038.

CURRICURUM VITAE

NAME	Miss Warinporn Chungchai
DATE OF BIRTH	16 March 1995, Ubon Ratchathani, Thailand
EDUCATION	Bachelor's Degree of Science, Chemistry, Ubon Ratchathani University, 2016.
SCHOLARSHIP	The Center of Excellence for Innovation in Chemistry (PERCH-CIC), Ministry of Higher Education, Science, Research and Innovation
WORK EXPERIENCE	Department of Chemistry, Faculty of Science, Ubon Ratchathani University, Thailand